Preparation and Reactivity of Sigma-Complexes

Samantha J. Connelly

A dissertation submitted in partial fulfillment
of the requirements for the degree of

Doctor of Philosophy

University of Washington

2014

Reading Committee:

Dennis Michael Heinekey, Chair

Daniel Gamelin

Karen I. Goldberg

Program Authorized to Offer Degree:

Chemistry

University of Washington

Abstract

Preparation and Reactivity of Sigma-Complexes

Samantha J. Connelly

Chair of the Supervisory Committee:
Professor Dennis Michael Heinekey
Chemistry

Ligation of molecular hydrogen to transition metal complexes was first observed by Kubas and co-workers in 1984. In this work, three-coordinate pincer ligands were employed in the preparation of square-planar d^8 nickel and palladium dihydrogen complexes. The synthesis, isolation, characterization, and reactivity of these hydrogen-ligated group 10 complexes is reported. Solution nuclear magnetic resonance (NMR) spectroscopy was used to accurately determine the H-H distance in the ligand based on measurements of both T_1 and $^1J_{HD}$. Relevant to understanding the degree of bond activation occurring at a transition metal, these dihydrogen complexes can be models for important intermediates in homogeneous catalytic processes. Additionally, silylium (silyl arenium) cations were synthesized, characterized, and employed in the synthesis of the dihydrogen complexes. A crystal structure of the triethylsilane-bound triethylsilylium ion, $[(Et_3Si)_2H]^+$ is included.

Table of Contents

Acknowledgements.

So very many people deserve entire pages of thanks for their kindness, support, friendship and assistance. I could not have completed this without their encouragement.

First, sincere gratitude to Prof. Mike Heinekey. Mike is an incredibly patient advisor, who knows when to push, when to encourage, and just when to make sure your ego hasn't gotten too big (subway tokens, anyone?). While I don't think I'm "famous" yet, I have come a long way & learned a lot. Thank you. An additional note of thanks to Mike's wife, Maureen – thank you for taking the group into your home. Your kindness (and baked goodies for the lab) are greatly appreciated.

Thank you to Prof. Daniel Gamelin, Prof. Karen Goldberg, Prof. Gojko Lalic, Prof. Christine Luscombe, and Prof. Marco Rolandi for offering kind guidance throughout this process as committee members. I appreciate your thoughtful questions and critiques. Additional thanks to Prof. Jim Mayer, Prof. Brandi Coissart, and Prof. Julie Kovacs for rounding out the inorganic faculty. I would argue that UW's inorganic division is so successful is because it is collaborative and inclusive. I have loved my time here.

Next, recognition for my labmates: I am eternally indebted to Dr. Steve Matthews for teaching me when the silicon cation was "primo", how to run the magnet, and generally do decent science. I've spent a lot of time over the years contemplating "What would Steve do?" and it hasn't let me down yet. To Dr. Kate Schultz, Dr. Joe Meredith, Dr. Tony St. John, & Mike Rak: thank you for leading the way, showing me how to both have fun and work hard, and putting up with my endless questions. I also can't thank you enough for making it the norm to ditch out when you weren't being productive. Wasting time in lab is a major waste of time. Thank you to Sophia Tran for drawing me a map to climb "Ph.D. Mountain". I fear I may have gotten lost along the way without it. Amanda Zimmerman started the nickel dihydrogen chemistry, and I'd like to acknowledge her hard work on the project. It was wonderful discussing science (and non-science) with her over hot tea. Dr. Tim Brewster has been full of kind, thoughtful scientific and career advice. Specific thank yous to Jon Goldberg and Dr. Gene Wong for sharing ligands, expertise, and good times. To those I haven't mentioned, you've made the Heinekey lab a warm, friendly place to work. I've thoroughly enjoyed my time in the lab.

There are approximately zero people on the third floor (and beyond) in CHB who won't happily share their time and expertise to help you get ahead. A few people to thank specifically: Dr. Kate Allen, Wilson Bailey, Dr. Shoshanna Barnett, Dr. Miriam Bowring, Liam Bradshaw, Miles Braten, Dr. Michael Coggins, Megan Duda, Dr. Rebecca

Hayoun, Dr. Erica Ingalls, Audra Johansen, Dr. David Lao, Ben Leipzig, Dr. Elizabeth Mader, Dr. Alicia McGee, Prof. Alex Miller, Tom Porter, Jason Prantner, Julian Rees, Dr. Margaret Scheuermann, Prof. Caroline Saouma, Tyler Stevens, Dr. Adam Tenderholt, Dr. Tristan Tronic, Carolyn Valdez, and Jessica Wittman.

The UW Chemistry Department is full of people who do really great work and keep the place running smoothly: Jerrie Dickie in the stockroom, for always knowing how to find whatever we needed and send us on our way with a jolly smile. Andrea Carroll, for being an excellent guiding light and friend. You made more than one required teaching assistant assignment fun. The front office: Angie, Susan, Kim, Diana, & Ashley. On the technical side: thank you to Dr. Paul Miller, Dr. Adrienne Roehrich, and Dr. Rajan Paranji for their efforts in the NMR facility.

I feel I had a great undergraduate chemistry education at the University of Iowa. I must individually thank Prof. Darrel Eyman and Prof. Lou Messerle for introducing me to inorganic chemistry. Thank you to Dr. David Rotsch, my undergraduate research mentor, for sharing your lab space, time, expertise and friendship.

I have several scientific mentors and role models to thank: Mr. Troy Schwemm, my first chemistry teacher; was endlessly encouraging and handed the big ideas of chemistry to me in small, bite-size bits. Mrs. Sally "Sal, Sal, the Science Gal" Kriegel taught seventh grade science. There was never a doubt in my mind that girls could be awesome scientists, and I think that stems from how enthusiastic Mrs. Kriegel was about her job. She made it "cool" to enjoy science class. Mrs. Chellie Wilkins made high school biology come alive, and encouraged me to press forward. Last, but certainly not least, Sesame Street – because as soon as you can read, the world awaits.

A special thank you to Dr. Steve & Barbara Connelly for having met me once when I was young, and then opening your home to me when I moved across the country. Thanks for sharing your home at the holidays, and your garden and many dinners throughout the years.

My friends have supported me, encouraged me, loved me, laughed with me, and lived with me every step of the way.

University of Iowa

Adriane Downs
Jessica "Little J" Petruzzello
Dr. Laura (Maschmann) Rogers
Dr. Amanda (Steimel) Gilles
Dr. Wanakee Carr
Haleigh (Stahlecker) Reitz
Heidi (Quenzer) Bowman
Casey Frank

Special, heartfelt thanks
to Brooke (Gant) Morrison
and her family

Iowa Chem. Dept.

Dr. Anna Reissen
Dr. Brie Nardy
Sarah Ernst
Dr. Brian Kim
Tyler Mouw
Jen Augello
Dr. David Rotsch
Jessica (Jewett) Reed
Dr. Thomas Heineman
Todd Domeyer
Mike Moriarty

University of Washington

Liam (and Rachel) Bradshaw
Jennifer Brookes
Ben (and Kadie) Burrone
Derek Church
Megan Duda
Carrie Gower
Chelsea Hess
Audra Johansen
Phil Pierce
Tom Porter
Julian Rees & Ellen Hayes
Mike Roberto
Jessica Wittman

Seattle Area

Collin Anderson
James Bronoske
Spencer & Jenna Glushak
Onel Martinez
Kevin McGuire
Blair Scott & Carly Nations
Eric Olson
Kyrie Peterson
Liz Redmond
Rex & Lydia Thompson
Ann Watson
Jennifer Carroll

To Tom, Colleen, & Matt Robinson: thank you for welcoming me into your home and giving me a place to feel at home. The kindness, support, and encouragement you have offered over the years has been wonderful. A note of thanks to the extended Kelly family for welcoming me for holidays, weekends, and fun. I've had a blast getting to know you.

To Patrick: You have made this journey what it is. I would not have made it without you by my side: encouraging me, teasing me, cutting me slack, and pushing me forward. I can't wait to see what the world has in store for us next.

I must thank my family for their ceaseless support. To my aunt Cathi, for keeping everyone in line – and making sure no one was ever (even remotely) hungry. To my cousins Christine, Maria, and Lindsey, for giggling with me, gossiping with me, and most of all, coming to visit me during my time here in Seattle.

To my sister, Jenna, for keeping me grounded and my mom, for always being my biggest fan.

In memory of Gary D. Connelly

1957-2005

Chapter 1: Introduction to Dihydrogen Complexes

1.1 Impetus for Investigation of Dihydrogen Complexes. Annual US production of hydrogen is currently around 9 billion kilograms, primarily from the steam-reforming of methane.[1] In this process, steam and methane (CH_4, the primary component of natural gas) are heated to high temperatures (700 – 1100 °C) over a nickel-based catalyst. The highly endothermic reaction produces carbon monoxide and hydrogen (Figure 1-1: Summarized in Reaction 1). The carbon monoxide can then be combined with additional steam in a lower temperature exothermic water-gas shift reaction to produce more hydrogen (Summarized in Reaction 2).[2]

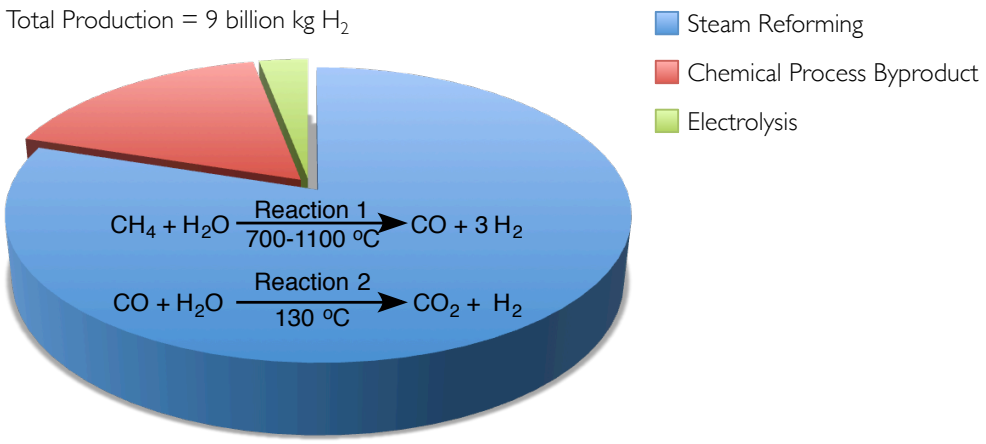

Figure 1-1. Primary methods for the production of hydrogen in the United States, 2005.

The energy-intensive steam-reforming process consumes non-renewable fossil fuels and produces the greenhouse gas carbon dioxide. The production of hydrogen comprises 1.5% of annual global energy usage.[3] Understanding the coordination and activation of hydrogen to transition metals has huge implications for the development and design of catalytic systems for the renewable and efficient production of hydrogen. Two primary desirable outcomes drive our research to better understand how small molecules, such as hydrogen, interact with transition metal centers:

(1) Hydrogen is a clean chemical fuel that produces only water as a byproduct of combustion

$$H_2 + O_2 \longrightarrow 2\,H_2O$$

As such, incorporating hydrogen into our energy landscape is a way to avoid use of carbon-based fuels that produce the greenhouse gas carbon dioxide (CO_2) upon consumption. Moving toward a "hydrogen economy" requires having the capability to produce, store, transport, use, and regenerate the fuel from a renewable source.

(2) The formation and cleavage of chemical bonds is at the heart of catalysis research. Dihydrogen, a molecule with two electrons shared between two hydrogen nuclei, is the simplest possible molecule. As a result, it is an interesting model for strong bond activation and formation studies. Learning to control the binding and activation of the H-H bond in dihydrogen complexes may result in fundamental knowledge applicable to systems with heavier elements (*i.e.*, C-H or C-O, required for the preparation of fine chemicals from renewable chemical feedstocks, functionalization of hydrocarbons, and the defunctionalization of carbohydrates derived from biomass). Understanding the coordination of dihydrogen is fundamental to our understanding of the mechanism of bond activation at a transition metal center.

1.2 Initial discovery of dihydrogen complexes. The first dihydrogen complexes were isolated and characterized by Kubas and co-workers in 1984.[4] These complexes were characterized by X-ray diffraction, neutron diffraction, IR spectroscopy, and NMR spectroscopy. *mer-trans*-$M(CO)_3(PR_3)_2(H_2)$ (M = Mo, W; R = Cy, ^{i}Pr) (Figure 1-2) were definitively determined to contain intact hydrogen molecules as ligands through location of the H atoms by neutron diffraction and observation of strong HD coupling in the partially-deuterated complex.

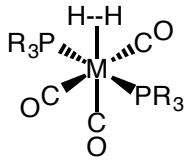

Figure 1-2. Original "Kubas Complexes". M = Mo, W; R = Cyclohexyl, *iso*-propyl.

Since Kubas' initial work, hundreds of dihydrogen complexes have been synthesized and identified. The vast majority of the known dihydrogen complexes have been observed at d^6 metal centers (Mo^0, W^0, Fe^{2+}, Ru^{2+}, Os^{2+}, Rh^{3+}, Ir^{3+}). This thesis concentrates on the less-studied d^8 metal dihydrogen complexes.

1.3 Description of dihydrogen coordination. Dihydrogen coordinates to a transition metal center to form a 3-center, 2-electron interaction between the metal and two hydrogen atoms. The orbitals involved in σ-complexation can be depicted by a model similar to the Dewar-Chatt-Duncanson description of alkene coordination (Figure 1-3).[5] Specifically, electron density from the bonding σ_{1s} orbital of the hydrogen ligand is donated to the metal center. Back-donation of electron density from the metal d-orbitals into the σ^*_{1s} anti-bonding orbital can also occur. Both of these interactions serve to lengthen the H-H distance (d_{HH}).

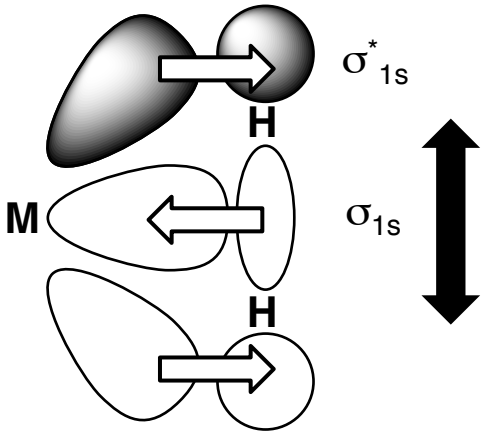

Figure 1-3. Orbital description of σ- coordination of an H_2 molecule to a transition metal. Electrons from the σ_{1s} orbital of the ligand are donated to a metal orbital. The metal donates electron density into the σ^*_{1s} orbital on the ligand. Both of these interactions lengthen d_{HH}.

With variation of the electronic properties of the metal center, these complexes can be placed on a continuum of lengthening H-H bonds, ranging from dihydrogen complexes to dihydride complexes (Figure 1-4). True dihydrogen complexes ("Kubas complexes") exhibit d_{HH} < 1.0 Angstrom, where the H-H bond is still intact (a). Complexes with longer d_{HH} may be perceived as an arrested oxidative addition of the H_2 molecule to the metal center (resulting in elongated dihydrogen (b) or compressed dihydride (c) complexes). Complete oxidative addition of the ligand to the metal center results in a formation of a dihydride complex (d).

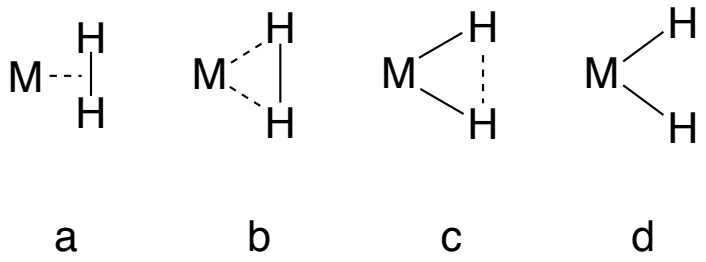

Figure 1-4. Continuum from dihydrogen complex to a dihydride complex. (a) dihydrogen complex (b) elongated dihydrogen complex (c) compressed dihydride complex (d) dihydride complex

1.4 Determination of the internuclear distance in a dihydrogen complex. The interaction between the metal and the dihydrogen ligand is an important parameter to understand when rationally designing transition metal catalysts. d_{HH} is an indication of the degree of activation of the bound ligand, but does not directly correlate to the thermodynamic acidity of the molecule.[6] d_{HH} can be estimated by a variety of methods described below.

1.4.1 Crystal diffraction techniques.

1.4.1a Single Crystal X-ray Diffraction. While generally an excellent tool for describing the structure of a molecule, X-ray diffraction is not a reliable method for determining d_{HH} in a dihydrogen complex. The method relies on interpreting the pattern produced when X-rays are diffracted by the electrons in a molecule. The large amount of electron density of the transition metal center obscures and distorts the location of the electron density between the two hydrogen nuclei in all but the best data sets and does not provide accurate description of the hydrogen atom location.[7] Further, anisotropic molecular motion and disorder in the ligand can impede correct interpretation of the results.[4]

1.4.1b Neutron Diffraction. The location of the hydrogen nuclei can be accurately determined in a neutron diffraction experiment. The nuclei, not the electrons between them, diffract the neutron beam. This method provides definitive placement of the hydrogen atoms since hydrogen has a reasonable neutron scattering cross section.[7] Unfortunately, the technique requires a large, high-quality crystal, and there are only a few operational instrument facilities in the world capable of collecting the data.

1.4.2 Solid-state NMR experiments. The observation of a Pake pattern doublet in solid-state NMR experiments arises when two spin-1/2 nuclei are close together and have a large dipolar coupling.[8] Deuteration of hydrogen atoms

in the ancillary ligands of the sample gives a simple spectrum. The observed coupling is inversely proportional to the cube of the internuclear distance (d_{HH}) (Equation and idealized observed spectrum shown in Figure 1-5).[9] The pattern can also be observed when select soft pulses are applied to saturate the ancillary ligand resonances. The d_{HH} estimate from these measurements is believed to be very accurate (on the order of ± 0.01 Angstrom) as a change in the coupling constant on the order of 10 kHz would result in significant changes to the estimated d_{HH}. Another advantage of this measurement is that molecular motion and other relaxation pathways are taken into account.

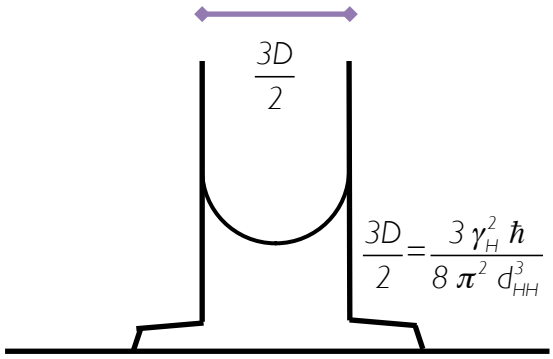

Figure 1-5. Pake pattern observed for dihydrogen ligand in solid-state NMR spectra. The observed dipolar coupling is inversely proportional to the internuclear distance. (γ_H = the gyromagnetic ratio for the proton, $\hbar$ is Planck's constant/2π).

1.4.3 Solution-state NMR experiments. Two completely independent solution-state NMR experiments can be utilized for the practical determination of d_{HH}. Solution-state NMR experiments are a desirable method for finding d_{HH} because no special instrumentation (beyond a standard NMR spectrometer) is required and the sample is not destroyed during data collection.

1.4.3a. T_1 relaxation time constant. The rate at which a nucleus relaxes back to alignment with the bulk magnetic field can provide insight into the environment around that nucleus. Nuclei relax by a variety of pathways. When two hydrogen nuclei are very close together, dipole-dipole relaxation becomes the dominant pathway. At these short distances, the relaxation rate is proportional to the sixth order of the distance between the nuclei, making this a very sensitive technique (discussed further below).

The T_1 relaxation time constant of a given resonance is measured by delivering a 180-degree pulse, allowing a relaxation delay (*tau*) and then delivering a 90-degree pulse to the sample. This "inversion recovery" experiment is outlined in Figure 1-6.[10] Varying the delay produces a series of spectra like the one shown in Figure 1-7. When the

recorded NMR spectrum has a null signal, tau_0 has been determined. This is related to the time required for the nucleus to relax fully from a 90-degree pulse as shown in Equation 1-1.

$$T_1\ (minimum) = \frac{\tau_0}{ln\ 2} \qquad \text{Equation 1-1.}$$

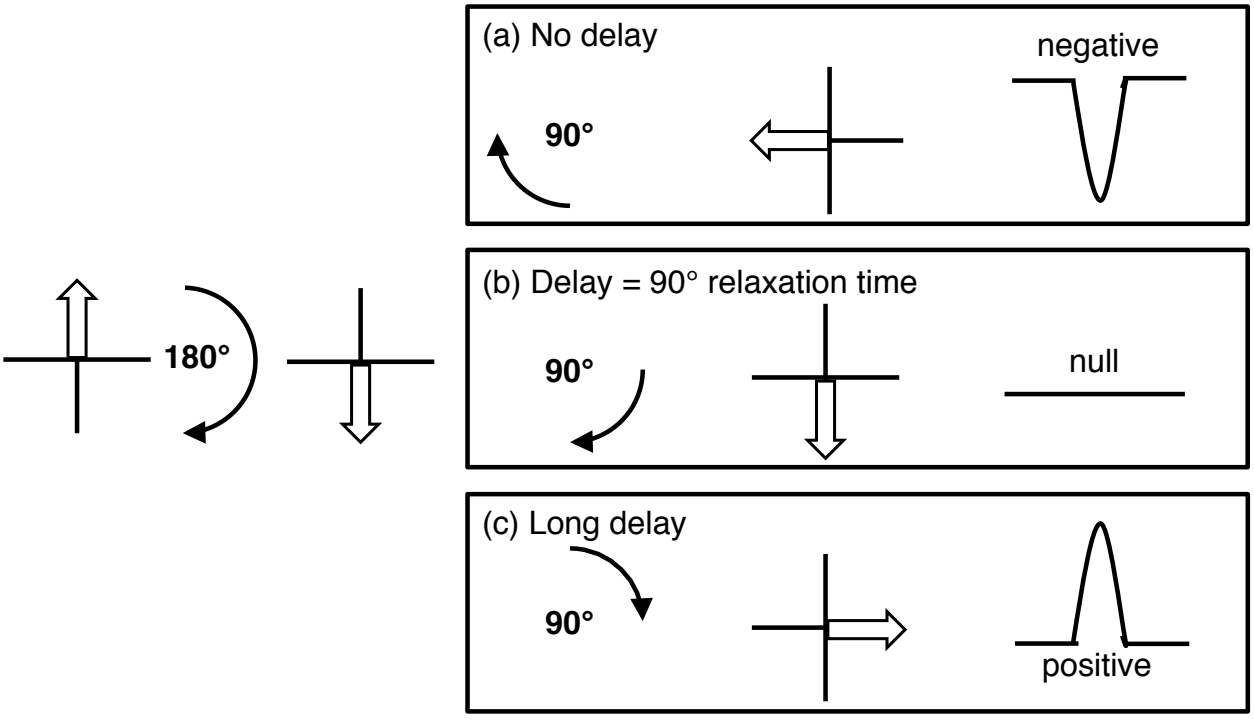

Figure 1-6. Schematic of an Inversion-Recovery NMR Experiment. The net magnetization of the bulk sample is initially aligned with the magnetic field. Following the 180° degree pulse, the net magnetization is inverted. A variable delay (tau) gives rise to results generalized by a-c. (a) If the delay is very short, almost no relaxation occurs prior to the 90° pulse. In this case, a negative signal is observed. (b) When the delay is equal to the time required for relaxation of the net magnetization back into the x-y plane, another 90° pulse will produce net magnetization in the –z direction, resulting in no signal detected in the x-y plane. (c) At infinitely long delays, a fully positive signal will be recorded. The net magnetization vector relaxes back into the +z dimension, followed by a traditional 90° pulse, resulting in a positive signal.

The relaxation of the nuclei in a dihydrogen ligand is characteristically fast. T_1 is generally observed to be on the order of 5-50 milliseconds for dihydrogen complexes. This is in contrast to the 0.2-0.5 second T_1 values observed for metal hydride resonances. T_1 values for protons attached to carbon atoms are often on the order of seconds to minutes.

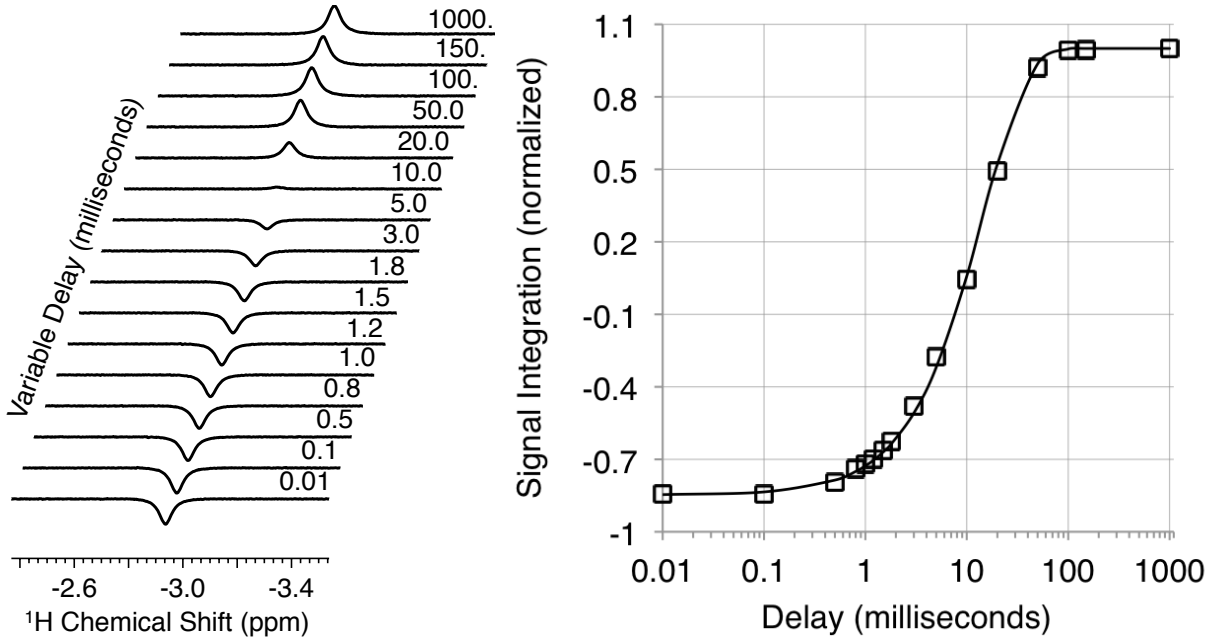

Figure 1-7. Data acquired from an Inversion-Recovery Experiment.[11] (a) Series of spectra with signal varying from fully negative to fully positive. (b) Plot of the integration of each signal against the delay time for that experiment. A fit of this data is used to accurately determine the T_1 relaxation time constant for a given resonance.

The rate of relaxation (T_1^{-1}) of a given resonance is dependent on how rapidly the potential energy acquired following perturbation from the bulk magnetic field can be dissipated throughout the system (spin-lattice relaxation). (This can be imagined as the rate that the needle on a compass would return to North after manually pulling it to point East and then releasing it.) In NMR experiments, the energy gap between the excited and ground states is on the order of the rotational energy of a small molecule tumbling in solution. As such, the relaxation rate can be maximized (leading to the minimum T_1 value) when the system is at a temperature providing the optimum energy transfer between the nuclei and rotational motion of the molecule.

The minimum T_1 value can then be related to d_{HH}. Equation 1-2 describes the relaxation of a proton resonance, where the dipole-dipole relaxation mechanism dominates.[12] Care must be taken in the use of this equation, as there can be other contributions to relaxation (e.g., from metal ions). Note that Equation 1-2 differs from the equation originally published by Halpern. An additional term $\{(\mu_0/4\pi)^2\}$ equivalent to 1.0 Gauss^{2}cm^3/erg must be included in order to correctly cancel units (but does not change the numerical value of the result).[13] Differentiation of Equation 1-2 with respect to τ_c gives Equation 1-3. The minimum of this polynomial function is found by setting the result equal to zero (also in Equation 1-3), and the minimum value of

the function describing molecular motion (τ_c) can be determined (Equation 1-4). Using that value in Equation 1-2 provides a relationship where the only variables are the Larmor frequency (ω), T_1 (now minimum, due to the differentiation to determine τ_c), and d_{HH}. Measurement of T_1(minimum) at any magnetic field strength can be used to determine d_{HH}. The simplified resulting relationship is given in Equation 1-5. (The derivation outlined here is described in Reference 12).

$$R_{HH} = \frac{1}{T_1} = \left(\frac{3}{160}\right)\frac{\mu_0^2 \gamma_H^4 \hbar^2}{\pi^2 d_{HH}^6}\left\{\frac{\tau_c}{1+\tau_c^2\omega^2} + \frac{4\tau_c}{1+4\tau_c^2\omega^2}\right\} \qquad \text{Equation 1-2.}$$

$$\frac{\partial R_{HH}}{\partial \tau_c} = \left(\frac{3}{160}\right)\frac{\mu_0^2 \gamma_H^4 \hbar^2}{\pi^2 d_{HH}^6}\left\{\frac{1-\tau_c^2\omega^2}{\left(1+\tau_c^2\omega^2\right)^2} + \frac{4\left(1-\tau_c^2\omega^2\right)}{\left(1+4\tau_c^2\omega^2\right)^2}\right\} = 0 = 32\tau_c^6\omega^6 + 20\tau_c^4\omega^4 + \tau_c^2\omega^2 - 5 \qquad \text{Equation 1-3.}$$

$$\tau_c\omega = 0.6158; \quad \textit{where } \omega = 2\pi\left(\gamma_H B_0\right) = 2\pi\left(\nu\right) \qquad \text{Equation 1-4.}$$

$$d_{HH} = 5.8173\sqrt[6]{\frac{T_1(minimum)}{\nu}} \qquad \text{Equation 1-5.}$$

Data is recorded at multiple temperatures and often on multiple spectrometers with varying frequencies to accurately determine T_1(min). T_1(min) occurs at a higher temperature in stronger magnetic fields (the higher Larmor frequency is matched by faster tumbling in solution), making the practical collection of data simpler. Figure 1- 8 shows a sample data set with T_1(min) determined at varying magnetic field strength.[14] The approximate T_1(min) values taken at each field strength (0.038, 0.052, and 0.065 seconds at 300, 400, and 500 MHz, respectively) are all in agreement when d_{HH} is solved using Equation 1-5 (approximately 1.3 Angstroms).

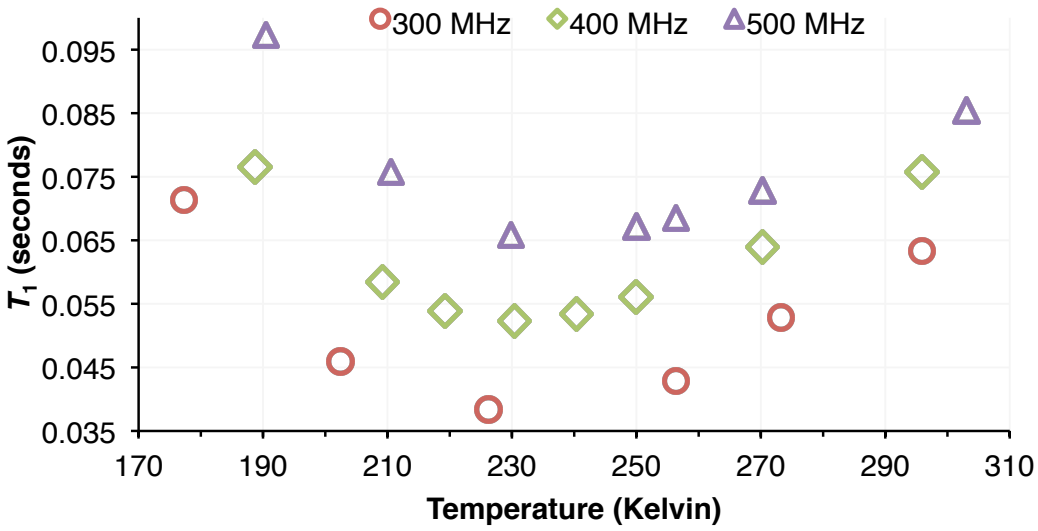

Figure 1- 8. Plot showing T_1 data acquired for the dihydrogen ligand of *trans*-$[Os(H_2)Cl(dppe)_2]^+$ (dppe = diphenylphosphinoethane) at several field strengths and temperatures. The data demonstrate that T_1 (minimum) occurs at higher temperatures in stronger magnetic fields. Data taken from Maltby, *et al. J. Am. Chem. Soc.***1996**, *118*, 5396-5407.

1.4.3b $^1J_{HD}$ coupling constant. The partially-deuterated form of dihydrogen gas (HD) appears as a 1:1:1 triplet with 43 Hz coupling in a ^{1}H NMR spectrum. When coordinated to a metal complex, a dihydrogen ligand (HD) maintains a strong, observable coupling constant. As the ligand binds more strongly to the metal center (*i.e.*, elongating the dihydrogen bond), the coupling constant diminishes in magnitude and undergoes sign inversion. That is to say, the coupling is strong when d_{HH} is short, and gets weaker as d_{HH} increases. The empirical relationship was originally proposed by Morris and co-workers (Equation 1-6).[15] Heinekey and coworkers improved the fit by including only the d_{HH} values determined by solid-state NMR experiments and neutron diffraction structures (Equation 1-7).[16] Another version of the equation applied some real-world parameters to the boundaries of the relationship,[17,18] and finally, Heinekey and co-workers[19] once again tweaked the fit of the data to produce Equation 1-9. Equation 1-9 (using b = 0.494 and $^2J_{HD}$ = -3.04 Hz) is plotted in Figure 1-9 with experimental data points to demonstrate the accuracy of predicting d_{HH} based on this empirical relationship.

$$d_{HH} = 1.42 - 0.0167(^1J_{HD})$$ Equation 1-6.

$$d_{HH} = 1.44 - 0.0168(^1J_{HD})$$ Equation 1-7.

$$^1J_{HD} = [43 - 2(^2J_{HD})]e^{\left\{\frac{0.74-d_{HH}}{b}\right\}} + (^2J_{HD})\left[e^{\left\{\frac{0.74-d_{HH}}{b}\right\}}\right]^2 + (^2J_{HD})$$ Equation 1-8.

Equation 1-9. Function best describing d_{HH} based on measured $^1J_{HD}$ coupling constants. Originally proposed by Hush,[17] Chaudret and co-workers published an equation where b = 0.404 and $^2J_{HD}$ = -2.8 Hz (based on calculations and literature precedent).[18] Heinekey and co-workers published a later report amending the equation to best fit the available data (b = 0.494 and $^2J_{HD}$ = -3.04 Hz).[19]

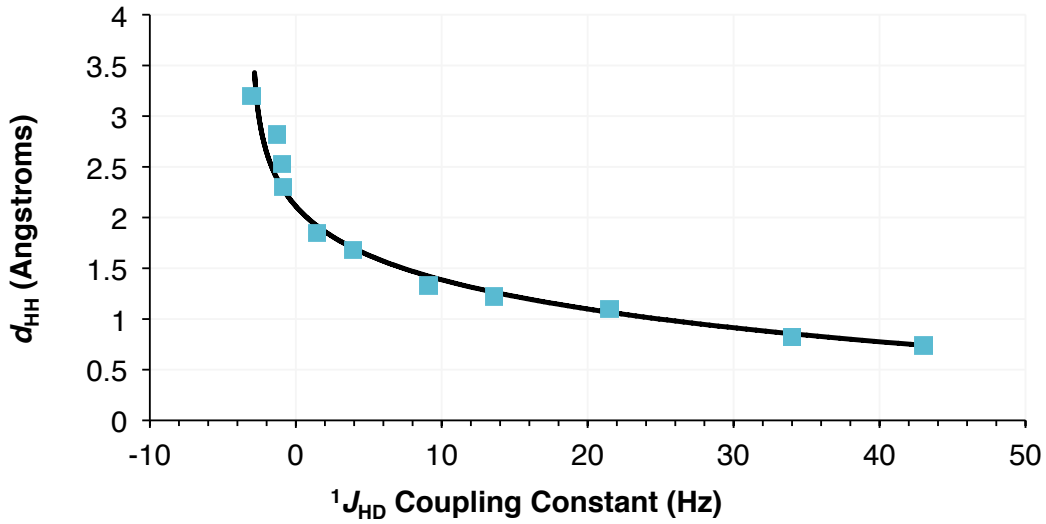

Figure 1-9. Plot of d_{HH} vs. $^1J_{HD}$ for a variety of complexes along the dihydrogen – dihydride continuum. Data were taken from Chaudret, *et al. J. Phys. Chem. A* **1999**, *103*, 4752-4754. The fit line plotted is Equation 1-9, employing the values for b and $^2J_{HD}$ prescribed by Heinekey *et al.*

1.4.4 Vibrational Spectroscopy. Infrared (IR) and Raman spectroscopy have limited utility in identification of dihydrogen complexes. IR spectroscopy relies on a change in the dipole of the molecule. As the dihydrogen ligand is non-polar and generally bound symmetrically, IR-signals are often weak and difficult to observe; however, if the ligand undergoes oxidative addition to form a dihydride, the M-H stretch is observable in the IR spectrum. Free H_2 has a strong Raman signal, but this is silenced upon coordination to a metal. While solution observation is difficult, both dihydrogen and dihydride complexes have been studied by vibration spectroscopy extensively in matrix samples.[20]

1.5 Organization of this thesis. This thesis seeks to develop the reader's understanding of dihydrogen complexes, their discovery, and their characterization in Chapter 1. Chapter 2 focuses on a reagent originally used in our lab to generate dihydrogen complexes. Along the way, it became clear that the silylium ion had interesting solution chemistry. Chapters 3-4 discuss advances in pincer-ligated nickel chemistry, including dihydrogen complexes, dinitrogen complexes, and a possible agostic complex. Chapter 5 highlights the first palladium dihydrogen complex and discusses similarities amongst the group 10 dihydrogen complexes.

References.

[1] U.S. Dept. of Energy Roadmap on Manufacturing R&D for the Hydrogen Economy, December 2005. Found at: http://www.hydrogen.energy.gov/manufacturing.html

[2] A. Wokaun, E. Wilhelm *Transition to Hydrogen: Pathways toward Clean Transportation*. Cambridge University Press, 2011.

[3] S. Hirschberg. *Hopes on Hydrogen: No Quick Fixes*. Energie-Spiegel, Paul Scherrer Institute. No. 12, November 2004.

[4] G. J. Kubas, R. R. Ryan, B. I. Swanson, P. J. Vergamini, H. J. Wasserman *J. Am. Chem. Soc.* **1984**, *106*, 451-452

[5] (a) M. J. S. Dewar *Bull. Soc. Chim. Fr.* **1951**, C71.

(b) M. J. S. Dewar *Bull. Soc. Chim. Fr.* **1951**, C79.

(c) For an historical review of the development of the Dewar Chatt Duncanson Model, see: D. M. P. Mingos *J. Organomet. Chem.* **2001**, *635*, 1-8.

(d) For the relationship to dihydrogen complexation see: G. J. Kubas *J. Organomet. Chem.* **2001**, *635*, 37-68.

[6] P. G. Jessop, R. H. Morris *Coord. Chem. Rev.* **1992**, *121*, 155-284.

[7] R. Bau, R. G. Teller, S. W. Kirtley, T. F. Koetzle *Acc. Chem. Res.* **1979**, *12*, 176-183.

[8] G. K. Pake *J. Chem. Phys.* **1948**, *16*, 327-336.

[9] (a) K. W. Zilm, R. A. Merrill, M. W. Kummer, G. J. Kubas *J. Am. Chem. Soc.* **1986**, *108*, 7837-7839.

(b) Discussed further in K. W. Zilm, J. M. Millar *Adv. Mag. Opt. Reson.* **1990**, *15*, 163-199.

[10] Inversion Recovery experiment first applied to distinguish dihydrogen complexes from polyhydrides by D. G. Hamilton, R. H. Crabtree *J. Am. Chem. Soc.* **1988**, *110*, 4126-4133.

[11] Data taken from AV700/sjconnel/SJC5_072713_1/Experiment 1: $[(^{tBu}POCOP)Ni(H_2)][B(C_6F_5)_4]$ in Fluorobenzene-H_5 at 283 K.

[12] P. J. Desrosiers, L. Cai, Z. Lin, R. Richards, J. Halpern *J. Am. Chem. Soc.* **1991**, *113*, 4173-4184.

[13] C. A. Bayse, R. L. Luck, E. J. Schelter *Inorg. Chem.* **2001**, *40*, 3463-3467.

[14] Data taken from: P. A. Maltby, M. Schlaf, M. Steinbeck, A. J. Lough, R. H. Morris, W. T. Klooster, T. F. Koetzle, R. C. Srivastava *J. Am. Chem. Soc.* **1996**, *118*, 5396-5407.

[15] P. A. Maltby, M. Schlaf, M. Steinbeck, A. J. Lough, R. H. Morris, W. T. Klooster, T. F. Koetzle, R. C. Srivastava *J. Am. Chem. Soc.* **1996**, *118*, 5396-5407.

[16] (a) D. M. Heinekey, T. A. Luther *Inorg. Chem.* **1996**, *35*, 4396-4399.

(b) T. A. Luther, D. M. Heinekey *Inorg. Chem.* **1998**, *37*, 127-132.

[17] N. S. Hush *J. Am. Chem. Soc.* **1997**, *119*, 1717.

[18] S. Gründemann, H. H. Limbach, G. Buntkowsky, S. Sabo-Etienne, B. Chaudret *J. Phys. Chem. A* **1999**, *103*, 4752-4754.

[19] R. Gelabert, M. Moreno, J. M. Lluch, A. Lledós, V. Pons, D. M. Heinekey *J. Am. Chem. Soc.* **2004**, *126*, 8813-8822.

[20] L. Andrews *Chem. Soc. Rev.* **2004**, *33*, 123-132.

Chapter 2: $[Et_3Si]^+$ as a Useful Reagent & Insights into the $[(Et_3Si)_2H]^+$ Species

2.1.1 General Introduction. Within the scientific literature, investigations of silylium ions ($[R_3Si]^+$) were first undertaken to investigate a heavier Group 14 analogue of the ubiquitous carbocation. In organic chemistry, heterolytic cleavage of a ^{sp3}C-X bond (where X^- is a good leaving group) is described as the first step of the common S_N1 reaction mechanism, resulting in formation of an $[R_3C]^+$ carbocation. This type of reaction mechanism, however, does not lead to formation of the corresponding planar $[R_3Si]^+$ silylium ions.[1]

In theory, the larger size, increased polarizability, and decreased electronegativity of silicon relative to carbon should stabilize the silylium ion.[2] Gas-phase mass-spectrometry methods showed that these ions exist,[3] but their isolation in condensed phases has proved remarkably difficult.

2.1.2 Determining the degree of coordination between cation and anion. The extent of coordination between a silylium ion and its counteranion can be determined using several methods:[4]

2.1.2a Freezing point depression. The extent to which the freezing point of a solvent deviates from its known value indicates the molality of solute particles present in a solution. The change in freezing point would be twice as large for un-paired ions relative to tightly-paired species.

2.1.2b Conductivity measurements. The conductivity of a solution is increased as a function of the number of ions present.

2.1.2c Solid-state structures. X-ray structures of crystalline silylium samples provide insight into the degree of coordination between cation and anion in the solid state, as well as any existing solvent coordination. Closest contacts within the range of the Van der Waals radii can indicate coordination. Additionally, silylium ions free of interaction with anion or solvent would be planar and the bond angles around silicon would sum to 360°. Both of these metrics can be used to determine if a silylium ion is truly "free".

2.1.2d Solution NMR Spectra. A down-field ^{29}Si chemical shift is related to the cationic character of the silicon nucleus. Silanes commonly have a chemical shift between 0 – 10 ppm, with increasingly cationic silicon nuclei shifted further downfield: Et_3SiCl = 36 ppm;[5] Me_3SiClO_4 = 47 ppm.[6] Computational predictions estimate that a truly three-coordinate silicon cation would have a chemical shift greater than 200 ppm.[7] This has been achieved for bulky triarylsilylium species such as trimesitylsilylium, which has a reported chemical shift of 226 ppm (^{29}Si versus TMS),[8] corresponding nicely to the computationally predicted 226-230 ppm.[9] Additionally, heteronuclear NMR spectra of the anion can be monitored for changes indicating coordination to the cation.[10]

The discussion within this chapter will focus primarily on triethylsilylium ions, which are relevant to this thesis because they are helpful reagents for the synthesis of dihydrogen complexes (discussed below). Extensive literature discusses work with $[Me_3Si]^+$,[11] protonated siloxanes,[12] sterically bulkier cations,[13] tethered cations,[14] bissilylated halonium ions,[15] and silyl-substituted rings where the cationic charge is displaced over the ring.[16]

2.2 Background on Triethylsilylium.

Lambert and co-workers at Northwestern University reported the first isolated species utilizing a hydride-transfer reaction to formally generate the silylium ion (Scheme 2-1).[17] This type of reaction was initially described for a halogen-hydrogen exchange reaction by Bartlett, Condon, & Schneider,[18] and was later applied to silicon chemistry by Corey & West.[19] Corey first investigated the utility of hydride-transfer from a silane to a carbocation to generate silylium ions in solution while on sabbatical in Mislow's Princeton laboratory in 1974-1975.[20]

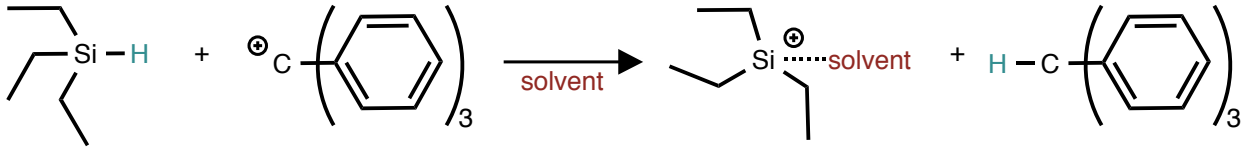

Scheme 2-1. As described by Lambert & coworkers, a hydride-transfer reaction resulting in formation of a formal silylium cation.

Lambert and coworkers reported the crystal structure of the species generated from the reaction between $[Ph_3C][B(C_6F_5)_4]$ and Et_3SiH in Et_3SiH as sovlent and recrystallized from toluene/hexanes. The resulting species, $[Et_3Si(C_7H_8)][B(C_6F_5)_4]$, triethylsilylium(toluene) tetrakis(pentafluorophenyl)borate (**2-1a**) was reported to be the first non-coordinating silylium cation (Figure 2-1). Controversy ensued[21] as to whether this was truly a non-coordinating silylium ion.

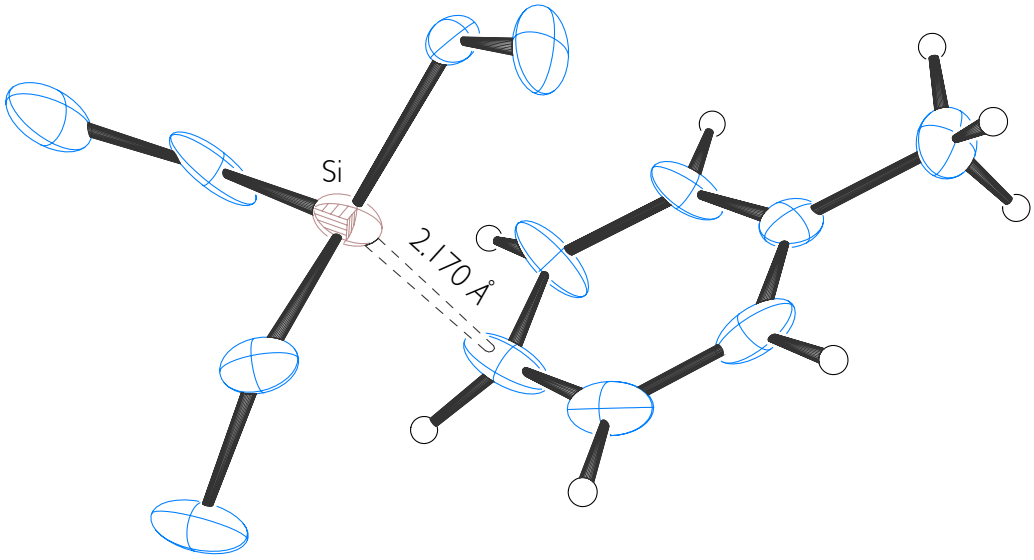

Figure 2-1. ORTEP[22] of $[Et_3Si(toluene)][B(C_6F_5)_4]$ (**2-1a**). All hydrogen atoms and the counteranion are omitted for clarity. The unit cell contains two cations (with bound toluene molecules), two non-coordinated anions, and three non-coordinated toluene molecules (with some degree of disorder). The structure originally reported by Lambert & co-workers was confirmed in our laboratory. File name: Heinekey/Samantha/sjc02.

The X-ray structure showed that the shortest distance between the silicon atom and the toluene ring (2.17 Angstroms) was short enough to suggest some degree of coordination. The coordination appeared to be intermediate to purely **σ-** or **π-** coordination. Sigma coordination of the silylium ion to the toluene ring would suggest that the coordinating carbon atom would be nearing sp^3- and have 4-coordinate geometry, which would require distortion of the toluene molecule. Instead, the solvent molecule remained planar, and no significant changes to the bond lengths or angles were noted. Pi coordination would be indicated by the silylium ion binding orthogonal to the plane of the ring. This was not observed (Figure 2-2). Some coordination was established by the lack of planarity around the silicon atom.

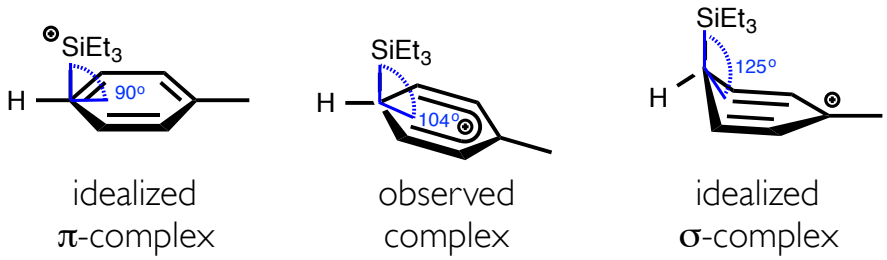

Figure 2-2. Depiction of arene-coordinated silylium ions, showing **π**-coordination, **σ**-coordination, and the geometry observed in the crystal structure of $[Et_3Si(C_7H_8)][B(C_6F_5)_4]$ (**2-1a**).

In order to minimize the interaction between the silylium ion and the solvent, Reed & others utilized inert carborane anions.[23] Extensive work into silylium chemistry produced crystal structures of several cations ($[C_6H_7]^+$,[24] $[Me_3Si]^+$,[25] and $[^iPr_3Si]^+$ [26]) with carborane anions. The synthetic roadblocks to achieving truly non-coordinated alkylsilylium cations have been discussed.[26]

2.3 Synthetic utility for the generation of $L_nM(H_2)$ complexes. Silylium ions are versatile reagents with multiple applications in the synthesis of transition metal dihydrogen complexes. In this research, triethylsilylium reagents have been used extensively to generate novel compounds via two different pathways. Both pathways rely on the strength of the Si-Cl bond (BDE = 109 kcal/mol) (Scheme 2-2).[27]

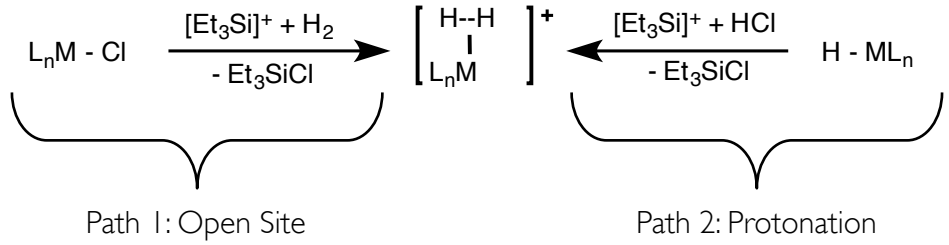

Scheme 2-2. Two routes to dihydrogen complexes employing the silylium reagent.

2.3a Chloride Abstraction to generate an open site at the metal. Triethylsilylium species can be used to generate dihydrogen complexes by utilizing the driving force from the formation of a strong Si-Cl bond. An open site is then available at the transition metal to bind a weakly-coordinating ligand such as dihydrogen.

2.3b Protonation of a metal hydride. If the ligand is free of any basic sites, protonation of a metal hydride bond can lead to a dihydrogen complex. The silylium reagent is useful for this purpose as it can be used to generate a strong acid in solution. Reaction of triethylsilylium species with HCl gas results in formation of chlorotriethylsilane and protonated solvent. This can result in formation of the desired H_2 complex.

2.4 Original characterization and scrutiny of proposed structure. Lambert describes the original preparation of the silylium species in the *Organometallics* paper[28] that was published as a follow-up to the *Science* publication containing the structure of **2-1**.[17] A neat reaction of colorless liquid Et_3SiH with solid yellow

$[Ph_3C][B(C_6F_5)_4]$ results in the transformation of the yellow solid into a white solid over a period of days. While insoluble in Et_3SiH, the white solid is soluble in arene solvents.

Over 15 years later, Reed & Nava proposed that the cation generated was not $[Et_3Si]^+$, but instead that the solvent used for the reaction (Et_3SiH) was, in fact, bound to the cation.[29] The basis for this assignment came from IR spectroscopic data where a broad band associated with the Si-H-Si stretch was observed at ~1900 cm^{-1}. (This stretch had been observed and assigned previously for the $[(Me_3Si)_2H]^+$ cation with a carborane anion).[30] This band did not decrease in intensity upon heating the sample *in vacuo*. Reed & Nava noted that dissolution of $[(Et_3Si)_2H]^+$ in coordinating arenes resulted in the release of Et_3SiH, and that the silane could be observed bubbling out of the solution.[29]

Our laboratory speculated about the coordination of an equivalent of Et_3SiH based on the results of some rhenium chemistry performed in the laboratory. Pons & Heinekey reported the reaction of $Re(CO)_5Cl$ with silylium ions in the presence of dihydrogen. If the white solid generated from the neat reaction of Et_3SiH with $[Ph_3C][B(C_6F_5)_4]$ was used, $[Re(CO)_5(Et_3SiH)]^+$ was the observed product. However, if the silylium ion was generated with only one equivalent of Et_3SiH in benzene, the dihydrogen complex ($[(Re(CO)_5(H_2)]^+$) was the observed product of the reaction (Scheme 2-3).[31]

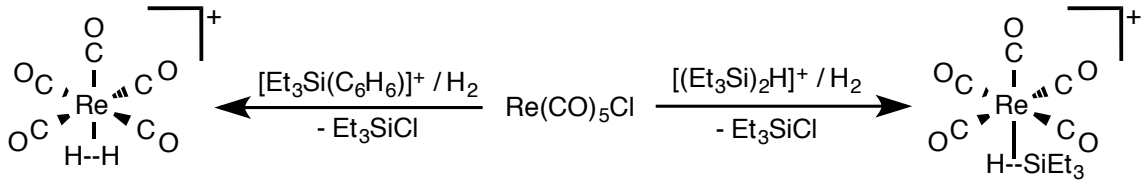

Scheme 2-3. Rhenium dihydrogen and triethylsilane sigma-complexes generated with the use of silylium reagents.

2.5 Crystal Structure of $[(Et_3Si)_2H][B(C_6F_5)_4]$ (2-2). The white solid generated from the reaction between $[Ph_3C][B(C_6F_5)_4]$ and Et_3SiH was isolated, washed with pentane, and dissolved in chlorobenzene. Layering the solutions with excess triethylsilane or alkane solvent precipitated X-ray quality crystals of $[(Et_3Si)_2H][B(C_6F_5)_4]$. The structure is shown below in Figure 2-3. There are no pentane or arene solvent molecules in the unit cell, and the closest contact between the silylium ion and the counteranion exceeds 3.5 Angstroms.

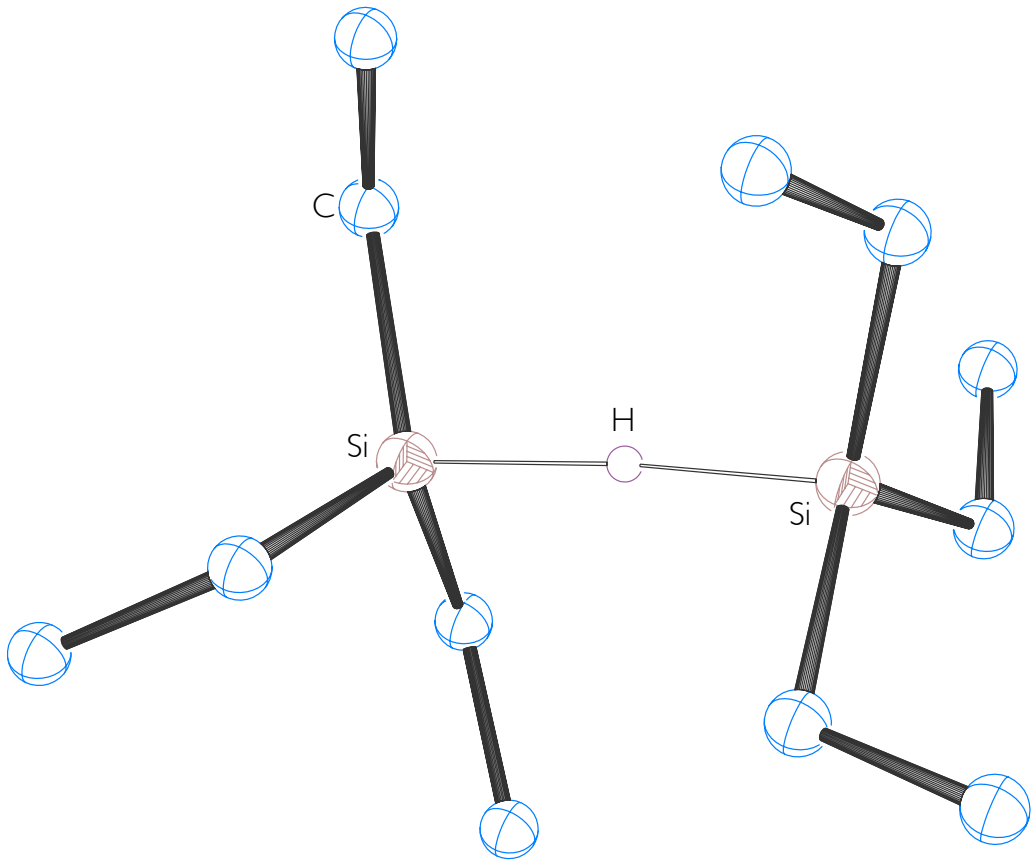

Figure 2-3. ORTEP[22] of $[(Et_3Si)_2H][B(C_6F_5)_4]$. Ellipsoids are drawn at the 50% probability level. Hydrogen atoms (except for bridging hydrogen) and the anion have been omitted for clarity. Relevant distances and angles: Si-Si = 3.217(9) Å; Σ C-Si1-C = 347.4(4)°; Σ C-Si2-C = 349.2(4)°; R_{int} = 0.0573. File names: Heinekey/Samantha/sjc04 (twinned) and Heinekey/Samantha/sjc06 (some decomposition apparent).

The Si-Si distance is greatly lengthened from that observed for disilanes. Generally, disilanes have a distance around 2.3 Å. In the solid state, $[(Et_3Si)_2H][B(C_6F_5)_4]$ exhibits an Si-Si distance over 3.2 Å, consistent with the distances reported in similar molecules (shown in Table 2-1)[14]. Because the hydrogen atom position is not fully refined in these structures (sjc04 and sjc06), the bond angle is depicted as linear in Figure 2-3.

Table 2-1. Bridging silylium species and selected metrics. # Value calculated from B3LYP/6-31G* level calculated structures.

	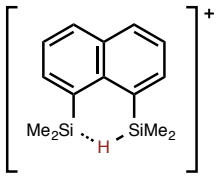	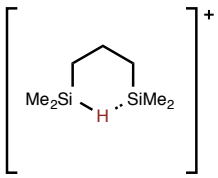	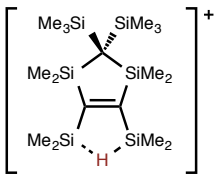	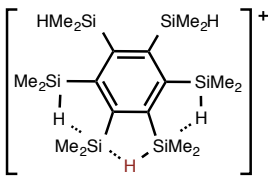
	a	**b**	**c**	**d**
Si-Si (Å)	2.98	3.10#	not reported	3.06#
$^{1}J_{SiH}$ (Hz)	45.7	39	26.0	46.3
$\delta_{Si\text{-}H\text{-}Si}$ (ppm)	3.34	1.47	not reported	4.26

2.6 Understanding the solution chemistry. Dissolution of $[(Et_3Si)_2H][B(C_6F_5)_4]$ (**2-2**) in nominally unreactive solvents resulted in a ^{1}H solution NMR spectrum containing a small broad signal and signals for an ethyl moiety. It was anticipated that the bridging hydride would appear as a multiplet with silicon satellites (similar to that observed in complexes **a**-**b**,**d** above). As the silicon satellites were not observed, experiments were undertaken to understand the nature of the cation in solution.

2.6.1 True chemical shift of the bridging hydride. It was anticipated that $[(Et_3Si)_2H]^+$ reached an equilibrium in chlorobenzene and fluorobenzene solution where some of the triethylsilane was displaced by solvent to give free triethylsilane and the solvent-bound silylium species (Scheme 2-4).

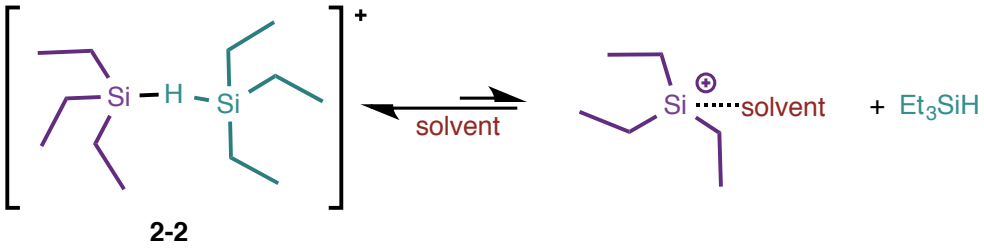

2-2

Scheme 2-4. Dissociation of complex **2-2** in arene solvents results in some displacement of Et_3SiH to form the solvent-coordinated silylium ion.

In order to investigate the equilibrium established upon dissolution of **2-2** in chlorobenzene, the true chemical shifts of the species needed to be identified. The bridging hydride is in equilibrium with $Et_3Si\mathit{H}$ in solution. The true chemical shift of $Et_3Si\mathit{H}$ is easily observed to be a septet with ^{29}Si satellites at 3.76 ppm (Scheme 2-4).

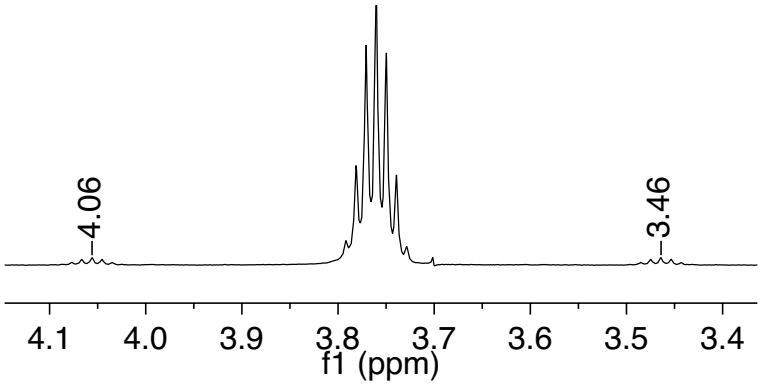

Figure 2-4. ^{1}H NMR spectrum of $Et_3Si\mathit{H}$ in chlorobenzene showing observed septet ($^{3}J_{HH}$ = 3.4 Hz) and ^{29}Si satellites ($^{1}J_{SiH}$ = 177 Hz).

2.6.2 Ethyl region of the ^{1}H and ^{13}C{1H} NMR spectra. To investigate this equilibrium, the boundary NMR spectra for each of the species in solution had to be identified. The ethyl moieties have some variation between the species, but all signals are between 0.5 and 1.0 ppm in the ^{1}H NMR spectrum. This resulted in very complicated and convoluted spectra. In addition, the magnitude of the coupling between the predicted $C\mathit{H}_3$ quartet and $C\mathit{H}_2$ triplet was on the same order as the chemical shift difference. This resulted in the observed spectra displaying second-order perturbations. Figure 2-5 shows the effect of increasing coincidence of the two signals for a simple ethyl group with no exchange reactions occurring as modeled by *gNMR*.[32]

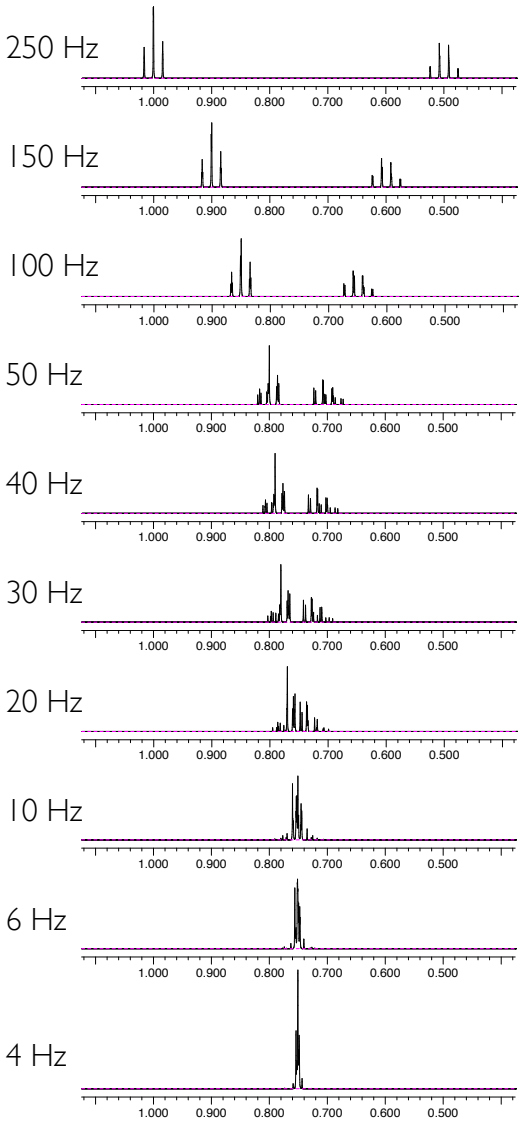

Figure 2-5. Predicted ^{1}H NMR spectra demonstrating the effect of nearing coincident chemical shifts on the appearance of an ethyl moiety: 500 MHz, 0.25 Hz Line Width.

2.6.3 Determination of K_{eq}. Cooling a solution of 2-2 in chlorobenzene to the freezing point of the solvent did not decoalesce of the observed bridging signal, so the chemical shift had to be estimated. If the dissociation described in Scheme 2-4 was not occurring, the observed signal for an *in situ* reaction between trityl cation and less than two equivalents of Et_3SiH would have one observed chemical shift for the bridging hydride. The observation, however, is that the chemical shift moves as the amount of Et_3SiH added increases. This continues with increasing amounts of Et_3SiH added to isolated **2-2** as well (Figure 2-6).

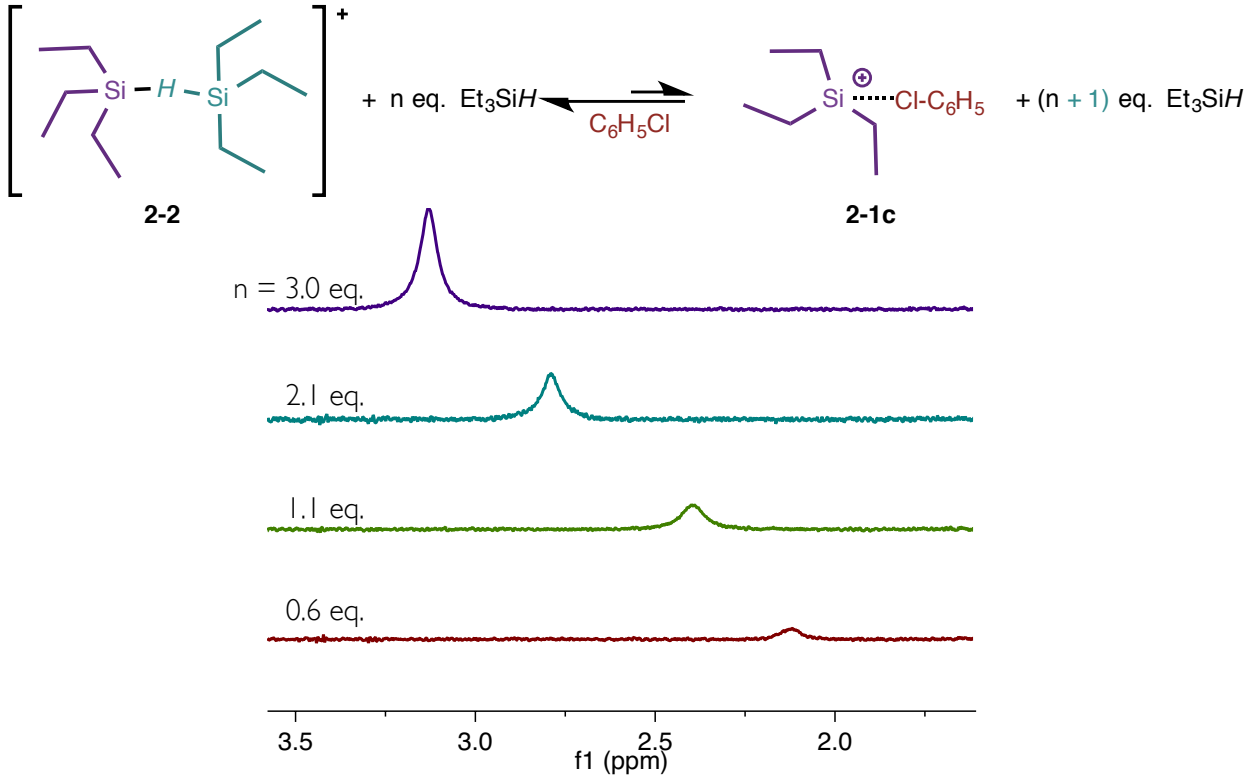

Figure 2-6. ^{1}H NMR spectra showing the change in chemical shift of the weighted average signal for the italicized protons in the reaction scheme shown with increasing amounts of Et_3SiH. Spectra are from Experiments 5, 8, 14, & 16 in SJC5_041613_1.

Kaleidograph™ was used to fit the data resulting from both *in situ* experiments from trityl + Et_3SiH and isolated **2-2**, and it was determined that the true chemical shift for $[(Et_3Si)_2\mathit{H}][B(C_6F_5)_4]$ in chlorobenzene is 1.35 ± 0.12 ppm (Figure 2-7). Using this value, it was concluded that at room temperature, **2-2** undergoes approximately 30% dissociation in chlorobenzene solution. There is then rapid exchange between bound and free Et_3SiH. Simulations[32] using *gNMR* suggest that the exchange must be faster than 200 sec^{-1} for the observed signal to lose all coupling to the bridging proton. Additionally, faster exchange will result in the complete coalescence of the signal for free Et_3SiH and $[(Et_3Si)_2H]^+$.

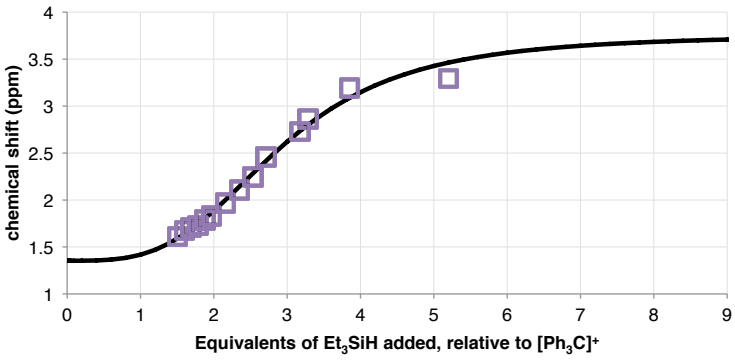

Figure 2-7. Compiled data for the observed ^{1}H chemical shift of $[(Et_3Si)_2\mathit{H}][B(C_6F_5)_4]$ in chlorobenzene from reaction between $[Ph_3C][B(C_6F_5)_4]$ and the indicated number of equivalents of Et_3SiH. The solid line shows the fit from the Kaleidograph™ software used to determine the true chemical shift of the bridging H, independent of the exchange reaction with free Et_3SiH.

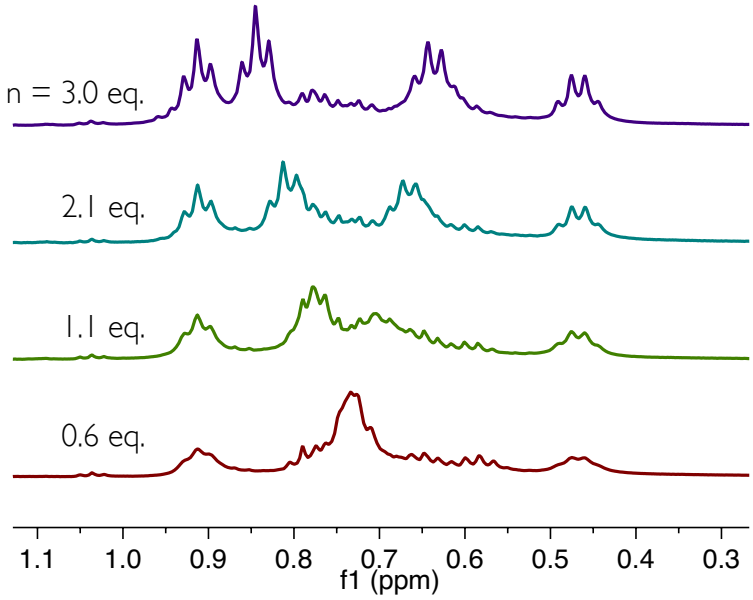

Figure 2-8. Ethyl region of ^{1}H NMR spectra from reaction mixtures containing **2-1** with the number of additional equivalents of Et_3SiH indicated. Spectra are from Experiments 5, 8, 14, & 16 in SJC5_041613_1.

As shown in Figure 2-8, the region between 0.5 and 1.0 ppm of these ^{1}H NMR spectra are quite complicated. In addition to the second-order effects described in Figure 2-5, the rapid exchange resulting in the coalesced bridging hydride signal will also produce complex spectra. To get a better handle on this, the $^{13}C\{^{1}H\}$ NMR spectra were obtained (Figure 2-9).

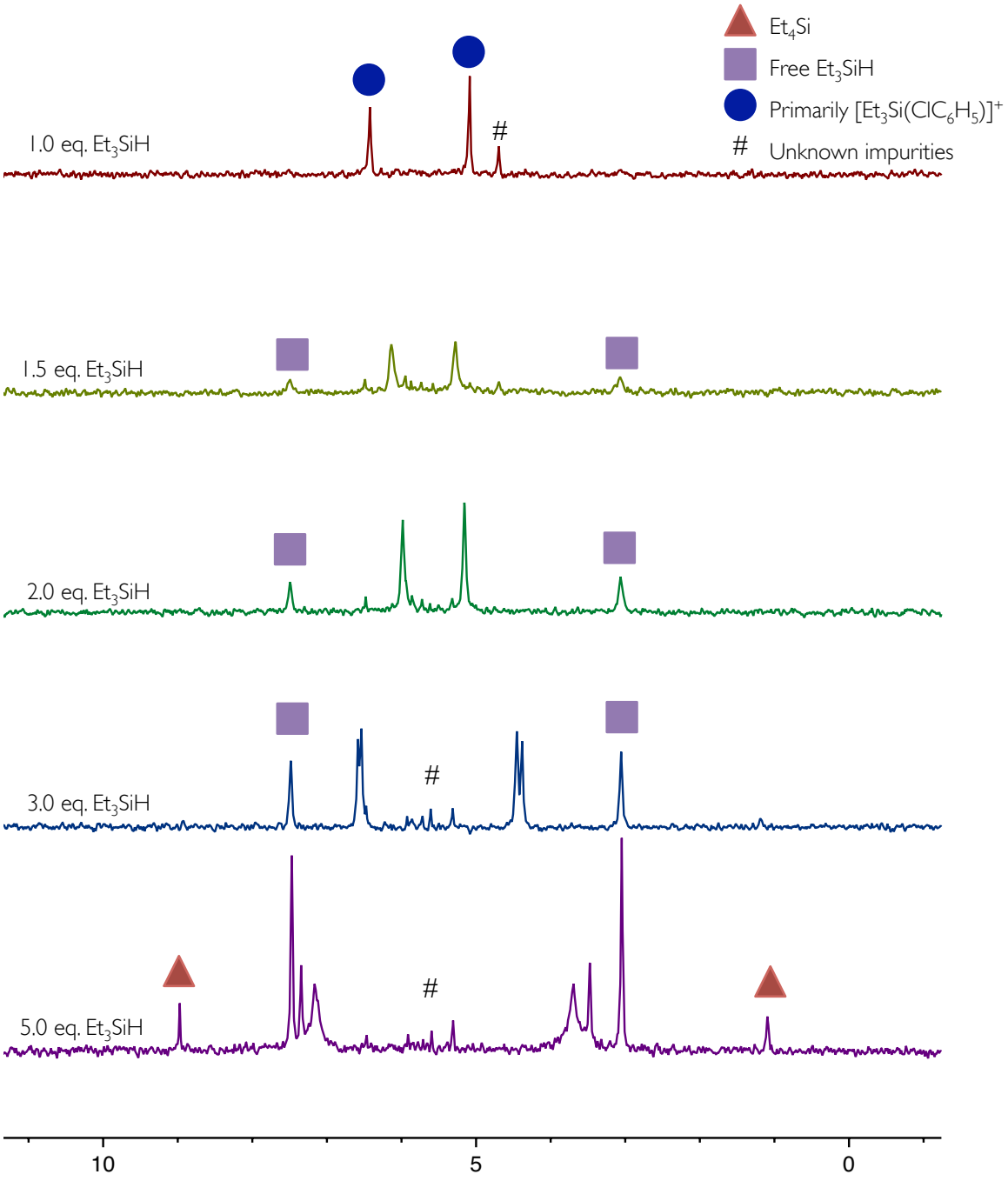

Figure 2-9. $^{13}C\{^{1}H\}$ NMR spectra recorded at 176 MHz in chlorobenzene-H_5. The top spectrum shows the ethyl region of a reaction between $[Ph_3C][B(C_6F_5)_4]$ and 1.0 equivalents of Et_3SiH. This resulted in formation of Ph_3CH and $[Et_3Si(ClC_6H_5)][B(C_6F_5)_4]$ (**2-1c**) (shown). Additional equivalents of Et_3SiH were added (indicated above) and the resulting spectra were recorded. The $^{13}C\{^{1}H\}$ spectra are simpler than those observed by ^{1}H NMR. Spectra from experiments 4, 6, 8, 10, and 12 in SJC5_082213_1.

Species **2-1c** shown in Figure 2-6 could be independently synthesized. Addition of 1.0 eq. of Et_3SiH to $[Ph_3C][B(C_6F_5)_4]$ in chlorobenzene resulted in complete loss of color from the reaction mixture. New signals associated with **2-1c** were identified by ^{1}H, $^{13}C\{^{1}H\}$, and ^{29}Si-^{1}H HMQC NMR spectroscopy (Figure 2-10). This reaction also proceeds in benzene and toluene (described by Lambert).

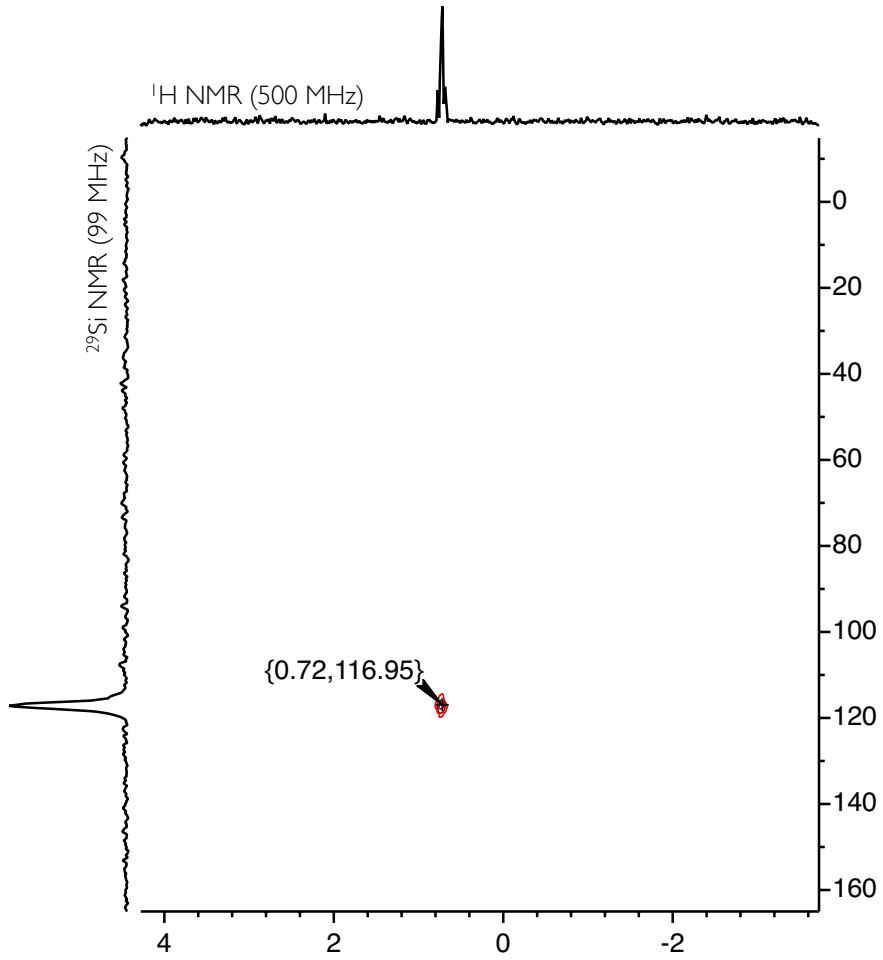

Figure 2-10. ^{29}Si-^{1}H HMQC 2D NMR Spectrum. Shows correlation between peak at 0.72 ppm (ethyl signals) and a ^{29}Si signal at 117 ppm. The NMR tube contained a reaction mixture of $[Ph_3C][B(C_6F_5)_4]$ and 1.0 equivalents Et_3SiH in chlorobenzene-H_5, affording $[Et_3Si(ClC_6H_5)][B(C_6F5)4]$ (**2-1c**) as the primary product. Data from experiment 3 in SJC5_011813_3.

As mentioned previously, the downfield-shifted ^{29}Si NMR signal is indicative of the degree of the cationic character of the silicon species. The observed chemical shift of **2-1c** is 117 ppm, which is further shifted than other arene-complexed cations, such as **2-1a** and **2-1b** and correlates nicely with a compound reported by Reed, where $[^{i}Pr_3Si]^{+}$ is complexed with a hexachlorocarborane anion (115 ppm).[33]

2.7 Thermodynamics of solvent coordination.

The bond dissociation energies of triphenylmethane and triethylsilane provide some insight into the strength of the interaction between the silylium cation and the coordinated solvent molecule. The hydride abstraction reaction shown in Scheme 2-1 is endothermic by approximately 25 kcal/mol,[34] indicating that the solvation of the silylium ion must provide at least that in order for the reaction to proceed. In fluorobenzene, combination of 1 eq. Et_3SiH with 1 eq. $[Ph_3C][B(C_6F_5)_4]$ does not react to completion. This indicates that fluorobenzene coordination energy is not sufficient to drive the thermodynamics of reaction.

The NMR resonance for the bridging H atom in a solution of **2-2** with several extra equivalents of Et_3SiH in chlorobenzene can be monitored at varying temperatures. As the solution is cooled from room temperature to 240 K, the signal can be observed to be moving toward the true chemical shift of **2-2**, indicating that K_{eq} is shifting toward association of the free Et_3SiH to the silicon cation. Dissociation of Et_3SiH from **2-2** to form the solvent complex **2-1c** is an endothermic process (Figure 2-11). This is intuitive – Et_3SiH is a better ligand for $[Et_3Si]^+$ than chlorobenzene, as **2-2** is the primary observed product in a reaction mixture, even in nearly 10.0 M chlorobenzene.

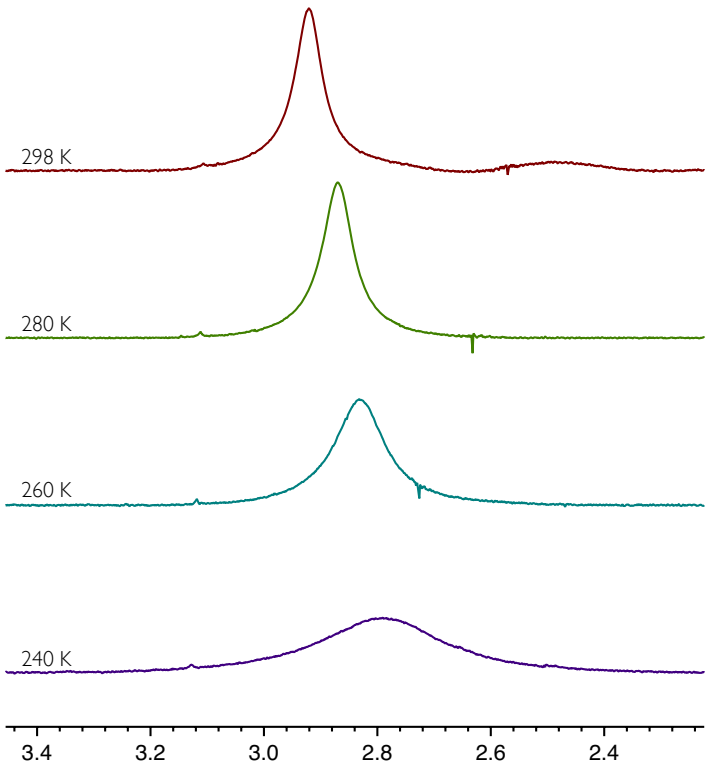

Figure 2-11. Signal for $[(Et_3Si)_2H][B(C_6F_5)_4]$ averaging with free Et_3SiH in chlorobenzene at the temperature indicated. The signal shifts upfield as the temperature is lowered, indicating that the dissociation of Et_3SiH from **2-2** to form **2-1c** decreases. The dissociation reaction is an endothermic process. The broadening of the signal is likely due to the decrease in the rate of exchange as the temperature drops. Data from experiments 1-4 in SJC4_080412_1.

2.8 Catalytic formation of tetraethylsilane. Based on the crystal structure reported by Lambert (Figure 2-1), dissolution of **2-2** in toluene results in the release of triethylsilane, and the formation of the solvent complex, **2-1a**. This reaction is accompanied by the evolution of a gas. As was mentioned previously, Reed & Nava[29] proposed that this gas was triethylsilane. As the boiling point of Et_3SiH is 108 *°C*, it will not vigorously bubble out of a room temperature solution. In this work, the gas has been identified as hydrogen by NMR spectroscopy. The other product was conclusively identified as tetraethylsilane. The mechanism of this reaction is not clear. Dissolution of **2-2** in benzene-d_6 and toluene-d_8 both produce HD gas as the observed product. Similarly, $[(Et_3Si)_2D][B(C_6F_5)_4]$ dissolved in protio-solvent also evolves HD gas. Our initial proposed mechanism involved deprotonation of **2-1** to produce a super-acid in solution capable of protonating Et_3SiH, effecting release of hydrogen gas, and catalytically reforming the $[Et_3Si]^+$ species (Figure 2-12). This is consistent with the observation of additional gas evolution when additional equivalents of Et_3SiH are added.

The neutral product generated by this proposed catalytic cycle is the Et_3Si-substituted arene. We have confirmed that Et_3Si-substituted arenes are *not* observed products of the reaction by GC/MS and NMR spectroscopy. In fact, a reaction with 8 equivalents of Et_3SiH resulted in a large amount of Et_4Si (as confirmed by GC-MS and NMR spectroscopy). We now attribute this reactivity to a Lewis acid-catalyzed redistribution reaction.[35]

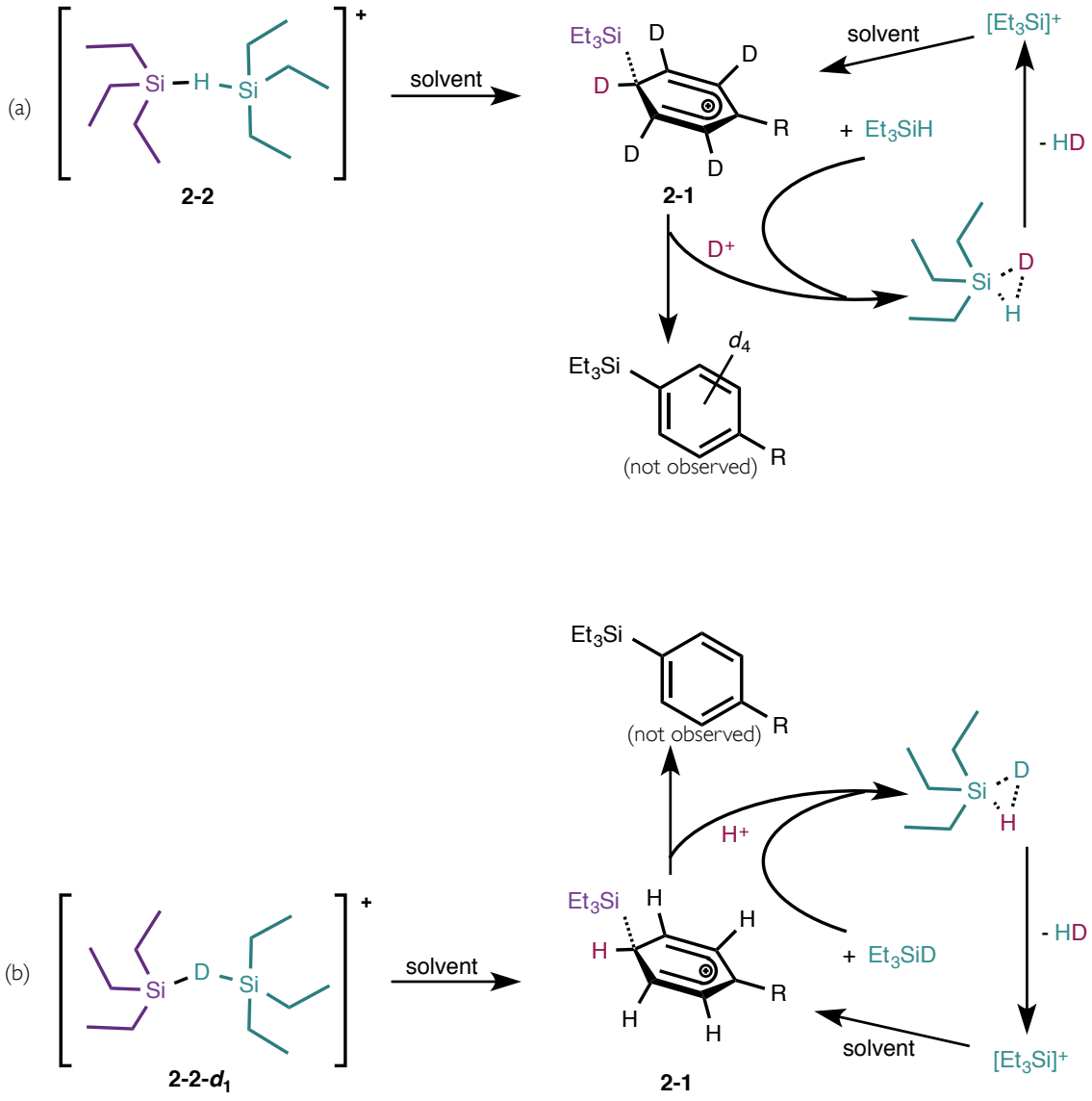

Figure 2-12. Initial proposed catalytic cycle resulting in the consumption of Et_3SiH and production of hydrogen and a neutral triethylsilicon-containing product. The two mirrored pathways ((a) and (b)) demonstrate the production of HD in toluene or benzene solution found during isotopically-labelled experiments (where R = D, H, or CH_3). This cycle is not observed, however, as the triethylsilylarene is not an observed product of the reaction. Authentic samples of triethylphenylsilane and triethyl-*p*-tolylsilane were synthesized and did not match the NMR spectra or GC-MS data for the neutral product of the catalysis.

2.9 Decomposition in the solid state. These reaction mixtures have extreme water-sensitivity. In solution, silylium species readily react with trace water to form silanols and ultimately siloxanes. It should be noted that in the solid state, the cations have been shown to be unstable to long-term storage. Even the nominally non-reactive counteranion, $[B(C_6F_5)_4]^-$, is susceptible to activation by the highly Lewis-acidic cation. A solid sample of **2-2** stored for three weeks under argon darkened in color, and colorless crystals sublimed to the top of the vial. The sublimate was identified by X-ray crystallography to be $(C_6F_5)BF_2$ (Figure 2-13).

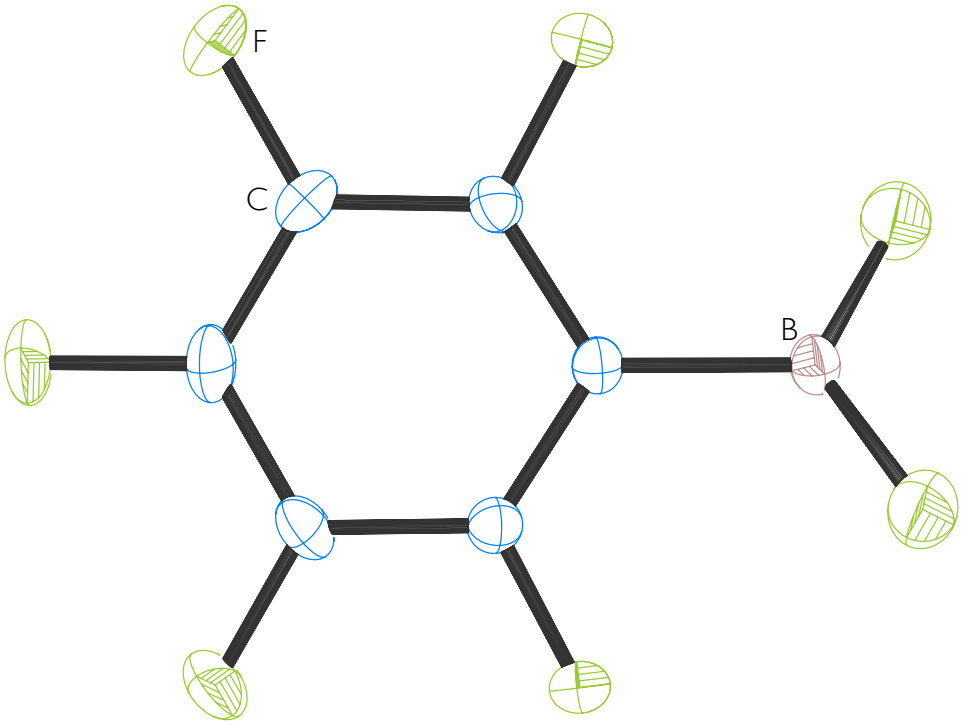

Figure 2-13. ORTEP[22] of $(C_6F_5)BF_2$. Ellipsoids are drawn at the 50% level. The geometry is planar around boron, with the phenyl ring tipped slightly out of the plane. R_{int}=0.0234. File name = Heinekey/Samantha/sjc10.

2.10 Relevant NMR notes. ^{29}Si nuclei are difficult to probe using direct detect experiments due to their low sensitivity, low natural abundance, and the low concentrations in the reaction mixtures discussed here. Commonly, ^{29}Si nuclei are studied using INEPT pulse programs. INEPT (Insensitive Nuclei Enhancement by Polarization Transfer). These experiments rely on the scalar coupling between a more sensitive nuclide (generally ^{1}H) and ^{29}Si. We avoided use of the INEPT experiments as the appropriate scalar coupling was unknown for the bridging proton of **2-2**, and the other species do not have protons on the ^{29}Si nucleus of interest.

Due to the coincidence of ethyl signals between 0.5 and 1.0 ppm in the ^{1}H NMR spectra for these species, two-dimensional correlation experiments were employed. The pulse program utilized is a Heteronuclear Multiple Quantum Correlation (HMQC) experiment. This experiment detects ^{1}H nuclei that are coupled (with a particular scalar coupling constant) to a heteronuclide (in this case, ^{29}Si), and spreads the signals out in the second dimension according to the chemical shift of the heteronucleus. The coupling constant selected was that between the protons of the ethyl groups and the ^{29}Si nucleus. The sensitivity of the HMQC experiment is increased relative to older HETCOR (heteronuclear correlation) experiments where proton magnetization was transferred to the lower gamma nuclide for detection.

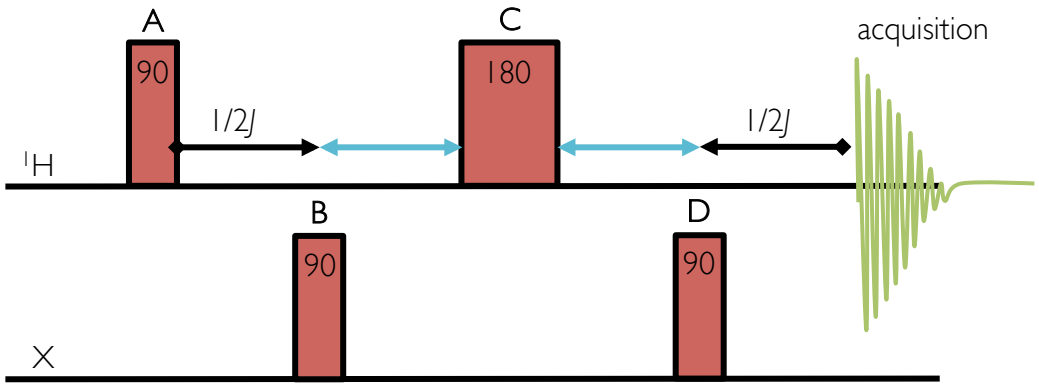

Figure 2-14. Simplified depiction of an HMQC pulse program. Pulse A delivers magnetization to the sample. The delay 1/2*J* allows evolution of that magnetization to the heteronucleus according to the scalar-coupling constant. Pulses B & D allow separation of the signals in the X-dimension according to chemical shift. Pulse C decouples the ^{1}H nuclei from the X-channel, and refocuses the non-correlated ^{1}H nuclei *via* a spin-echo to allow elimination of those signals by phase cycling the detector.

A simplified version of the pulse program is shown in Figure 2-14, and involves just four pulses. The top line contains the pulses delivered at the ^{1}H frequency. For nuclei not interacting with the heteronucleus, pulses A and C provide a basic spin-echo experiment, where the magnetization from a 90-degree pulse is allowed to evolve for a time, is then pulsed 180 degrees, and then allowed to evolve for the same time. This can be visualized by imagining a horse race where the horses start in opposite directions at the starting line, run either direction until a second time (the 180

degree pulse) when they change direction. If the time between the start and the 180 degree pulse, and the 180 degree pulse and the end of the race, all of the horses will return the starting line at the same time (Figure 2-15).[36] The spin-echo experiment refocuses the magnetization to a detectable signal. To prevent these non-correlated protons from appearing in the HMQC experiment, the detector is phase cycled; meaning, on the first scan, the detector collects fully positive signal, and on the second scan, fully negative signal. The combination of these experiments results in a null signal for the non-correlated protons.

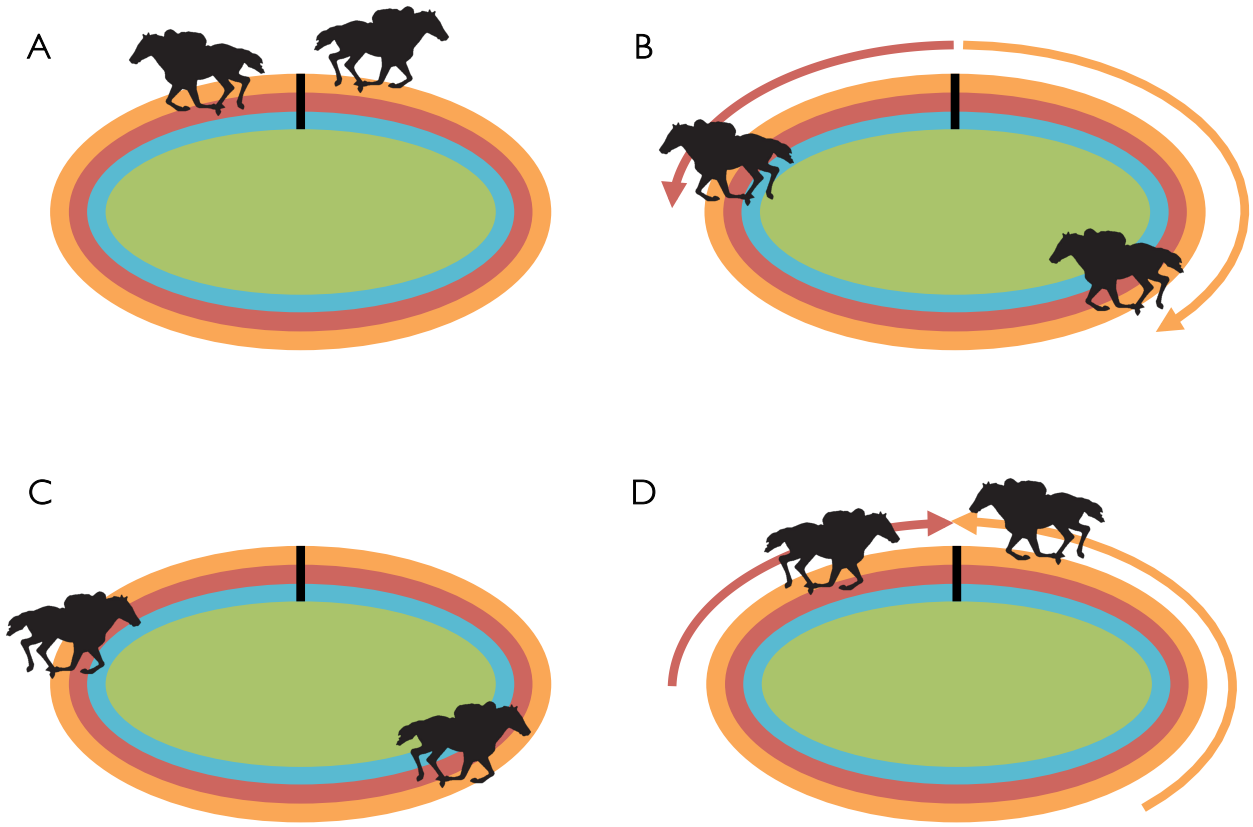

Figure 2-15. Spin-echo pulse program visualized as a horse race. A) Race begins. The horses begin in opposite directions. B) After some time (1/2*J* delay), the horses have moved away from the starting line at different (but steady) speeds. C) A 180-degree pulse instantaneously reverses the direction of the horses. D) The horses continue at the same steady speed, and will reach the starting/finish line at the same time (refocusing the magnetization of the experiment).

The second line of the simplified HMQC pulse program shown in Figure 2-14 depicts the pulses delivered at the frequency of the heteronucleus. After the first 90-degree pulse (pulse A) is delivered in the ^{1}H dimension, a delay time corresponding to 1/2*J* precedes a 90-degree pulse in the X dimension (pulse B). This delay allows the evolution of the magnetization, and then pulse B transfers coherence to the X nuclei. This is refocused and returned to the ^{1}H

dimension with the second X-dimension pulse (Pulse D). Signal is then acquired in the ^{1}H dimension. For the ^{1}H nuclei attached to a heteronuclide, pulse C acts as a decoupling pulse. An example of a resulting 2D NMR spectrum from a ^{29}Si-^{1}H HMQC experiment of a mixture of tetramethylsilane, tetraethylsilane, and chlorotriethylsilane is shown in Figure 2-16.

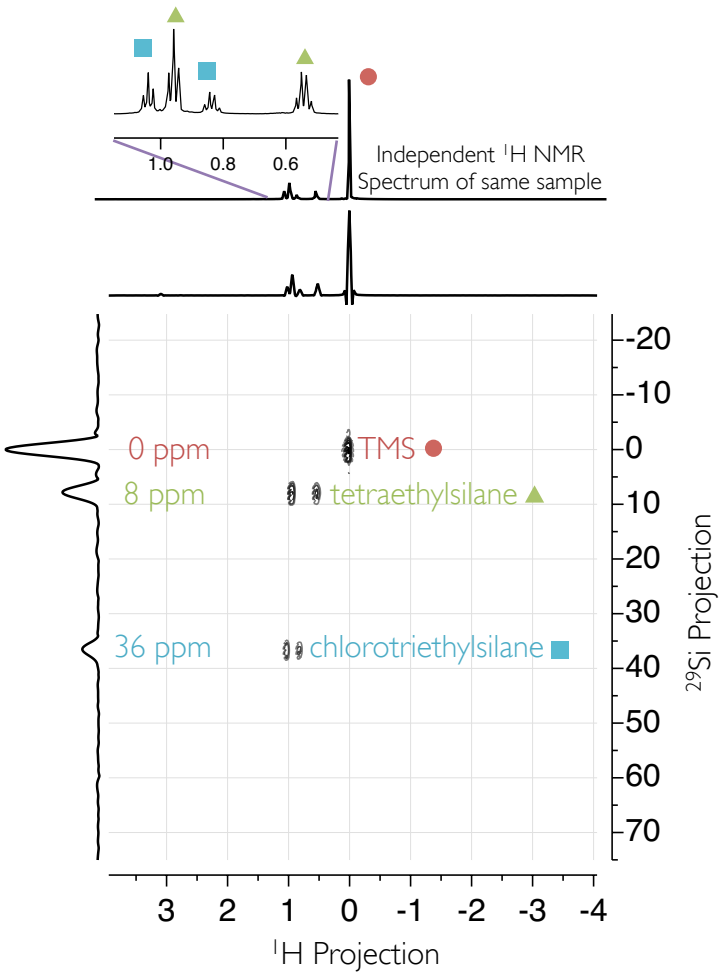

Figure 2-16. Sample of a ^{29}Si HMQC 2D NMR spectrum showing tetramethylsilane, tetraethylsilane, and chlorotriethylsilane.

2.11 Experimental Details.

General Considerations. The silylium species are remarkably water sensitive and it is imperative to thoroughly dry all glassware, reagents, and solvents. All experiments were carried out in an argon atmosphere using standard Schlenk techniques and a glove box. Solvents were dried over CaH_2 and then stored over 4.0-Å activated molecular sieves (halogenated solvents and Et_3SiH) or sodium metal (benzene/toluene/alkane solvents).[37] All solvents were added to reaction mixtures by vacuum transfer immediately prior to use.

Silylation of glassware. All glassware was silylated following a procedure outlined by Rheingold, *et al.* [38] The passivation of the surface removed any water or hydroxyl groups by methylation. Teflon screw-top NMR tubes were charged with approximately 100 μL N,O-bis(trimethylsilyl)acetamide (purchased from Sigma-Aldrich) under argon or nitrogen purge. The liquid was degassed with three freeze-pump-thaw cycles, and then heated to reflux with a heat gun (8-10 minutes). No obvious changes to the visual characteristics of the glass or liquid were noted at this step. The NMR tubes were then rinsed three times with 2 mL portions of acetone. Ultimately, the acetone ran cleanly from the surface of the glass indicating that silylation was effective. The NMR tube was then evacuated on a Schlenk line for at least one hour prior to use. A similar procedure (with slightly more N,O-bis(trimethylsilyl)acetamide) was used for larger Teflon-stoppered flasks. Generally, flasks with ground-glass joints were avoided due to the extreme air-sensitivity of the reaction mixtures.

$[Ph_3C][B(C_6F_5)_4]$, Trityl $B(Ar)_4F_{20}$.

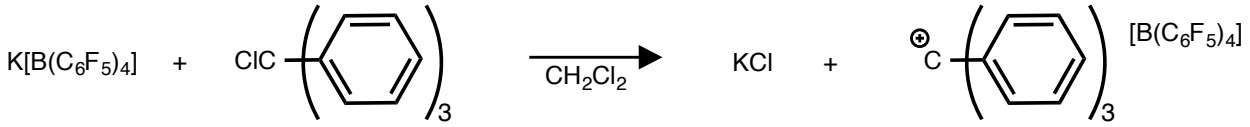

The following procedure was modified from several literature preparations.[29,39] $K[B(C_6F_5)_4]$ was purchased from Boulder Scientific. Ph_3CCl was purchased from Aldrich. A round-bottom flask was charged with $K[B(C_6F_5)_4]$ (0.720 g, 1 mmole) and Ph_3CCl (0.280g, 1 mmole) in an argon glove box. The solids were dissolved in dichloromethane (~100 mL), and the reaction mixture was allowed to stir under an argon atmosphere. The solution became yellow-orange immediately.

After stirring for 1 h, the solution was then filtered through Celite to remove KCl. The solvent volume was reduced to ~10 mL on a rotary evaporator to give a dark red oil. Addition of pentane resulted in yellow precipitate and a red oil. With sonication, the oil dispersed to give only yellow precipitate. The solid was isolated by filtration and dried *in vacuo*.

Alternatively, the crude filtrate could be layered with pentane, and over the course of days to hours, crystalline product formed. Isolated yield: 0.703 grams, 76%.

^{1}H NMR	($CDCl_3$, 500 MHz, 298 K): 7.62 (d of d, 6H), 7.85 (t, 6H), 8.24 (t of t, 3H)
	(C_6H_5F, 500 MHz, 298 K): 7.10 (d, 6 H), 7.34 (t, 6H), 7.71 (t, 3H)
$^{13}C\{^{1}H\}$ NMR	($CDCl_3$, 125 MHz, 298 K): 130.8, 142,6, 143.8 (cation only)
^{11}B NMR	($CDCl_3$, 160 MHz, 298 K): -16 (s)

$[Et_3Si(C_7H_8)][B(C_6F_5)_4]$ (2-1a).

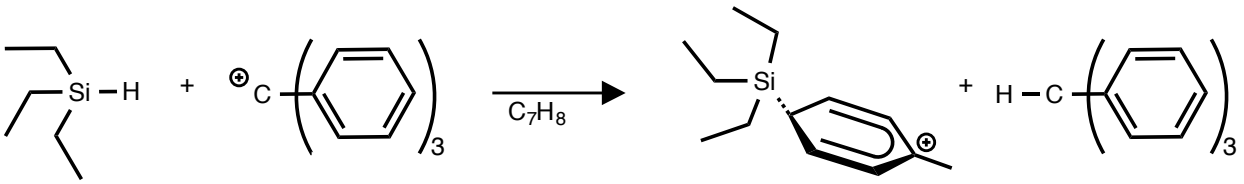

2-1a

In a passivated NMR tube fitted with a Teflon screw-top cap, $[Ph_3C][B(C_6F_5)_4]$ (0.020 g, 0.022 mmol) was exposed to a dynamic vacuum for approximately 30 minutes. Toluene (0.5 mL) was added by vacuum transfer. The $[Ph_3C][B(C_6F_5)_4]$ did not completely dissolve in the toluene, but formed an orange solution above a dark orange oil.

Et_3SiH (2.5 mg, 0.0035 mL, 0.04 mmol) was added with a microliter syringe and steady argon counterflow. The biphasic solution became colorless upon mixing. The NMR spectra indicated the presence of triphenylmethane and a triethylsilicon-containing cationic product. Layering the solution with pentane or heptane precipitated X-ray quality crystals (yield of crystalline product ~35%). Powdered product could be obtained in higher yield (~ 55%) following addition of alkane solvent and mixing.

^{1}H NMR	(C_7D_8, 500 MHz, 298 K): Complex multiplet 0.5-1.0 ppm
^{11}B NMR	(C_7D_8, 160 MHz, 298 K): -16 (s)
^{29}Si NMR	(C_7D_8, 99 MHz, 298 K, 2D HMQC Experiment): 85 ppm

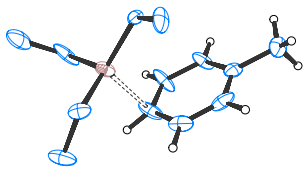

Crystal structure first determined by Lambert & coworkers. Crystal grown and analyzed in this work shown in Figure 2-1. File Name: Heinekey/Samantha/sjc02

$[Et_3Si(C_6H_6)][B(C_6F_5)_4]$ (2-1b).

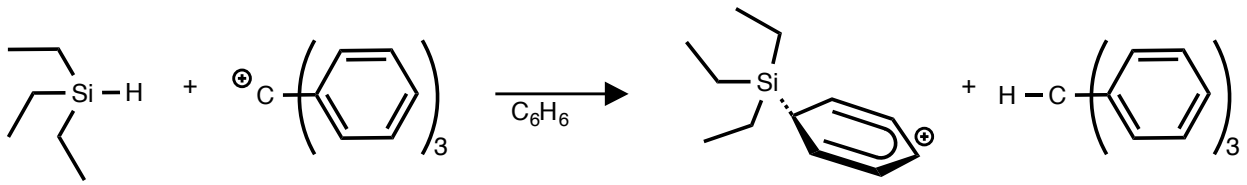

2-1b

In a passivated glass flask fitted with a Teflon screw-top cap and charged with a Teflon-coated magnetic stir bar, $[Ph_3C][B(C_6F_5)4]$ (0.085 g, 0.092 mmol) was exposed to a dynamic vacuum for approximately 30 minutes. Benzene solvent (5 mL) was added by vacuum transfer. The $[Ph_3C][B(C_6F_5)_4]$ did not completely dissolve, but formed an orange solution above a dark orange oil.

Quantitative addition of Et_3SiH (0.015 mL, 0.094 mmol (ca. 1.02 equivalent)) was accomplished by vacuum transfer of a small amount of Et_3SiH into a pre-weighed vessel, determination the exact mass present, and then using the corresponding amount of $[Ph_3C][B(C_6F_5)_4]$ to start the reaction. The solution became colorless almost immediately, and the oil remained deeply colored. Addition of pentane (5-10 mL) by vacuum transfer precipitated a white solid from the oil with stirring. The solid was allowed to settle, and the supernatant was removed by cannula. The solid was washed with pentane (via vacuum or cannula transfer) 2-3 times to remove all triphenylmethane. Isolated yield was generally ca. 85%. The product formed an oily layer in a benzene solution (10 mg in 0.5 mL), so fluorobenzene was used for NMR spectroscopic characterization. More dilute solutions in benzene had insufficient ^{29}Si concentration for observation.

^{1}H NMR	(C_6H_5F, 500 MHz, 298 K): 0.4-1.0 ppm (complex multiplet)
^{11}B NMR	(C_6H_5F, 160 MHz, 298 K): -16 (s)
^{29}Si NMR	(C_6H_5F, 99 MHz, 298 K, 2D HMQC Experiment): 99 ppm

$[Et_3Si(C_6H_5Cl)][B(C_6F_5)_4]$ (2-1c).

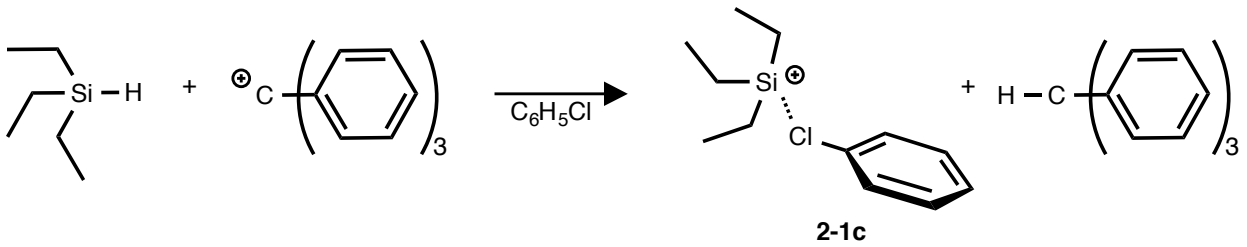

2-1c

In a passivated NMR tube fitted with a Teflon screw-top cap, $[Ph_3C][B(C_6F_5)_4]$ (0.020 g, 0.022 mmol) was exposed to a dynamic vacuum for approximately 30 minutes. Chlorobenzene (0.5 mL) was added by vacuum transfer. The $[Ph_3C][B(C_6F_5)_4]$ was very soluble in chlorobenzene, and no oily phase was observed.

Et_3SiH (2.5 mg, 0.0035 mL, 0.04 mmol) was added with a microliter syringe and steady argon counterflow. (Alternatively, a 1.0 M stock solution of Et_3SiH in C_6H_5Cl can be added. These volumes are substantially larger, and result in a more precise addition). The solution was colorless following inversion. The NMR spectra indicated the presence of triphenylmethane and a triethylsilicon-containing cationic product. No pure solid products were isolated, as an oily solid generally formed upon removal of solvent *in vacuo*.

^{1}H NMR	(C_6H_5Cl, 500 MHz, 298 K): Complex multiplet 0.5-1.0 ppm
$^{13}C\{^{1}H\}$ NMR	(C_6H_5Cl, 125 MHz, 298 K): 6.6 (s), 5.2 (s)
^{11}B NMR	(C_6H_5Cl, 160 MHz, 298 K): -16 (s)
^{29}Si NMR	(C_6H_5Cl, 99 MHz, 298 K, 2D Experiment): 117 ppm

The ChemDraw structure of **2-1c** is drawn with the chlorine atom coordinating to the silylium species based on crystal structures showing $[Et_3Si]^+$ coordinated to halogenated carborane anions in work by Reed & co-workers.[30,40]

$[(Et_3Si)_2H][B(C_6F_5)_4]$ (2-2).

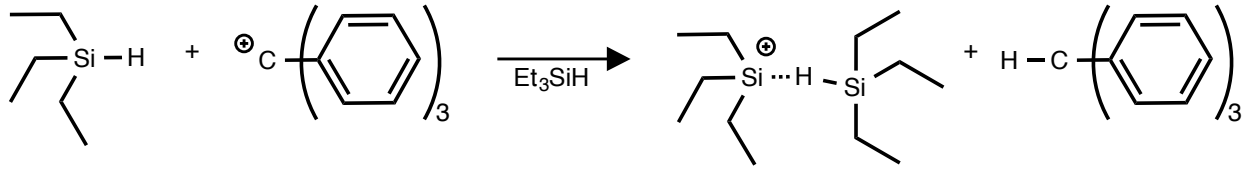

2-2

In a passivated flask fitted with a Teflon screw-top cap and charged with a glass magnetic stir bar, $[Ph_3C][B(C_6F_5)_4]$ (0.085 g, 0.092 mmol) was exposed to a dynamic vacuum for approximately 30 minutes.

Et_3SiH (3 mL, 19 mmol) was added to the reaction vessel by vacuum transfer. The $[Ph_3C][B(C_6F_5)_4]$ did not dissolve in the neat Et_3SiH. The yellow solid paled to off-white, and then white, over the course of 24-72 hours of stirring. The supernatant was removed by cannula transfer, and the solid was washed with pentane (via vacuum and cannula transfers) 2-3 times to remove triphenylmethane. Generally, isolated yield were nearly quantitative (95-98%).

The solid was readily soluble in chlorobenzene and fluorobenzene. The product was recrystallized by dissolution of the crude product in minimal chlorobenzene. The solution was then layered with pentane or triethylsilane to precipitate crystals. Recrystallized yield was generally much lower (35-45%). These crystals were characterized by X-ray crystallography. The solid was dissolved in fluorobenzene and chlorobenzene for NMR characterization.

^{1}H NMR	(C_6H_5F, 500 MHz, 298 K): multiplet 0.5-1.0 ppm, 2.06 ppm (br s)
^{11}B NMR	(C_6H_5F, 160 MHz, 298 K): -16 (s)
^{29}Si NMR	(C_6H_5F, 99 MHz, 298 K, 2D Experiment): 57 ppm

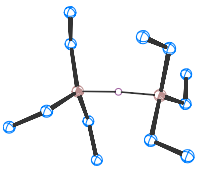

Crystal Structure shown in Figure 2-3.

File Names: Heinekey/Samantha/sjc04 (twinned) and /sjc06 (small impurity)

$[(Et_3Si)_2D][B(C_6F_5)_4]$ (2-2-d_1).

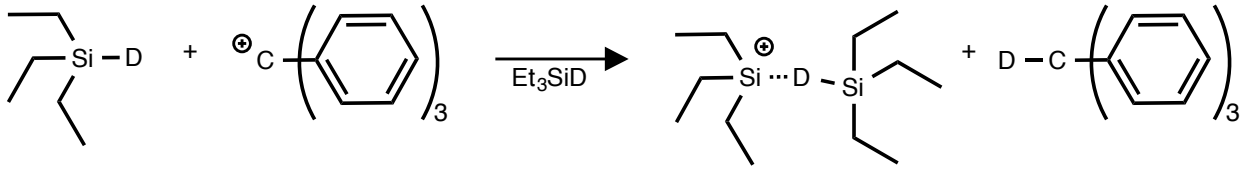

2-2-d_1

In a passivated flask fitted with a Teflon screw-top cap and charged with a glass magnetic stir bar, $[Ph_3C][B(C_6F_5)_4]$ (0.085 g, 0.092 mmol) was exposed to a dynamic vacuum for approximately 30 minutes.

Et_3SiD had been previously synthesized by the neat reaction between Et_3SiCl and $LiAlD_4$ after 24 h reflux. Several literature preparations[41] of Et_3SiD called for reaction in THF or with TMEDA to break up the polymeric $LiAlD_4$, but it was difficult to completely separate byproducts of these reactions from the Et_3SiD product.

Et_3SiD (3 mL, 19 mmol) was added to the reaction vessel by vacuum transfer. The reaction proceeded as described for the *protio*-compound.

Catalytic reactions.

The catalysis described was investigated by dissolving **2-2** (0.010 g, 0.011 mmol) in benzene (0.5 mL). The biphasic reaction mixture evolved gas. When **2-2** was dissolved in C_6D_6, HD gas was observed. Similarly, when **2-2-*d*$_1$** was dissolved in C_6H_6, HD gas was still the observed product by NMR. Addition of additional equivalents of Et_3SiH (observed up to 8 equivalents) produced more hydrogen gas. The same reactivity is observed in toluene.

A second product is observed by ^1H NMR and appeared to be a neutral silyl-containing product. Authentic samples of Et_3SiPh and Et_3SiTol were prepared for comparison (as suspected from the proposed mechanism shown in Figure 2-12), but did not match the species produced in the reaction.

GC-MS experiments suggested that the neutral silicon product generated in the reaction was Et_4Si. This was confirmed by ^1H and ^{29}Si-^1H HMQC NMR experiments with addition of an authentic sample of Et_4Si. To balance the stoichiometry, another silyl-containing product must be formed. While it is not apparent in the ^1H or ^{29}Si-^1H HMQC NMR spectra, a heavier product is observed, but not identified, by GC-MS.

References.

[1] T. Müller *Cations of Group 14 Organometallics* in *Advances in Organometallic Chemistry*, Vol. 53, Elsevier Inc., **2005**, 155-215.

[2] P. D. Lickiss in *The Chemistry of Organic Silicon Compounds*, Volume 2, Part 1; Z. Rappoport, Y. Appeloig, Eds.; John Wiley & Sons, **1998**, 557-594.

[3] For an overview, see (a) H. Schwartz in *The Chemistry of Organic Silicon Compounds*, Volume 1, Part 1; S. Patai, Z. Rappoport, Eds.; John Wiley & Sons, **1989**, 445-510. Additional discussion in (b) W. P. Weber, R. A. Felix, A. K. Willard *Tetrahedron Lett.* **1970**, *11*, 907-910 and references therein.

[4] (a) J. B. Lambert, W. J. Schultz, Jr., J. A. McConnell, W. Schilf *J. Am. Chem. Soc.* **1988**, *110*, 2201-2210.

[5] R. K. Harris, B. E. Mann, *NMR and the Periodic Table*, Academic Press, **1978**, Chapter 10.

[6] G. A. Olah, L. Heiliger, X-Y. Li, G. K. Surya Prakash *J. Am. Chem. Soc.* **1990**, *112*, 5991-5995.

[7] (a) C.-H. Ottosson, K. J. Szabó, D. Cremer *Organometallics* **1997**, *16*, 2377.

(b) U. Pidun, M. Stahl, G. Frenking *Chem. Eur. J.* **1996**, *2*, 869.

(c) G. A. Olah, G. Rasul, G. K. Surya Prakash *J. Organomet. Chem.* **1996**, *521*, 271.

(d) C.-H. Ottosson, D. Cremer, *Organometallics* **1996**, *15*, 5495.

(e) L. Olsson, C.-H. Ottosson, D. Cremer *J. Am. Chem. Soc.* **1995**, *117*, 7460.

[8] K.-C. Kim, C. A. Reed, D. W. Elliott, L. J. Mueller, F. Tham, L. Lin, J. B. Lambert *Science* **2002**, *297*, 825-827.

[9] (a) E. Kraka, C. P. Sosa, J. Gräfenstein, D. Cremer *Phys. Chem Lett.* **1997**, *279*, 9-16.

(b) T. Müller, Y. Zhao, J. B. Lambert *Organometallics* **1998**, *17*, 278-280.

[10] J. B. Lambert, W. Schilf *J. Am. Chem. Soc.* **1988**, *110*, 6364-6367.

[11] (a) A. Schulz, J. Thomas, A. Villinger *Chem. Commun.* **2010**, *46*, 3696-3698.

[12] (a) G. A. Olah, D. H. O'Brien, C. Y. Lui *J. Am. Chem. Soc.* **1969**, *91*, 701-706.

(b) G. K. S. Prakash, C. Bae, G. Rasul, G. A. Olah *J. Org. Chem.* **2002**, *67*, 1297-1301.

(c) G. A. Olah, X-Y. Li, Q. Wang, G. Rasul, G. K. S. Prakash *J. Am. Chem. Soc.* **1995**, *117*, 8962-8966.

[13] J. B. Lambert, Y. Zhao *Angew. Chem. Int. Ed.* **1997**, *36*, 400-401.

[14] (a) A. Y. Khalimon, Z. H. Lin, R. Simionescu, S. F. Vyboishchikov, G. I. Nikonov *Angew. Chem.* **2007**, *119*, 4614-4617.

(b) R. Panisch, M. Bolte, T. Müller *J. Am. Chem. Soc.* **2006**, *128*, 9679-9682.

(c) T. Müller *Angew. Chem. Int. Ed.* **2001**, *40*, 3033-3036.

(d) A. Sekiguchi, A. Muratami, N. Fukaya, Y. Kabe *Chem. Lett.* **2004**, *33*, 530-531.

[15] M. Lehmann, A. Schulz, A. Villinger *Angew. Chem. Int. Ed.* **2009**, *48*, 7444-7447.

[16] M. F. Ibad, P. langer, A. Schulz, A. Villinger *J. Am. Chem. Soc.* **2011**, *133*, 21016-21027.

[17] J. B. Lambert, S. M. Zhang, C. L. Stern, J. C. Huffman *Science* **1993**, *260*, 1917-1918.

[18] P. D. Bartlett, F. E. Condon, A. Schneider *J. Am. Chem. Soc.* **1944**, *66*, 1531-1539.

[19] J. Y. Corey, R. West *J. Am. Chem. Soc.* **1963**, *85*, 2430-2433.

[20] (a) J. Y. Corey *J. Am. Chem. Soc.* **1975**, *97*, 3237-3238.

(b) J. Y. Corey, D. Gast, K. Mislow *J. Organomet. Chem.* **1975**, *101*, C7-C8.

[21] (a) L. Pauling *Science* **1994**, *263*, 983.

(b) G. A. Olah, G. Rasul, X-y. Li, H. A. Buchholz, G. Sandford, G. K. S. Prakash *Science* **1994**, *263*, 983-984.

(c) J. B. Lambert, S. Zhang *Science* **1994**, *263*, 984-985.

(d) C. A. Reed, Z. Xie *Science* **1994**, *263*, 985-986.

[22] ORTEP for Windows 2013. L. J. Farrugia *J. Appl. Cryst.* **2012**, *45*, 849-854.

[23] (a) C. A. Reed *Acc Chem. Res.* **2010**, *43*, 121-128.

(b) M. Kessler, C. Knapp, V. Sagawe, H. Scherer, R. Uzun *Inorg. Chem.* **2010**, *49*, 5223-5230.

[24] C. A. Reed, K.-C. Kim, E. S. Stoyanov, D. Stasko, F. S. Tham, L. J. Mueller, P. D. W. Boyd *J. Am. Chem. Soc.* **2003**, *125*, 1796-1804.

[25] T. Kuppers, E. Bernhardt, R. Eujen, H. Willner, C. W. Lehmann *Angew. Chem. Int. Ed.* **2007**, *46*, 6346-6349.

[26] C. A. Reed *Acc. Chem. Res.* **1998**, *31*, 325-332.

[27] D. J. Grant, D. A. Dixon *J. Phys. Chem. A* **2009,** *113*, 3656-3661.

[28] J. B. Lambert, S. Zhang, S. M. Ciro *Organometallics* **1994**, *13*, 2430-2443.

[29] C. A. Reed, M. Nava *Organometallics* **2011**, *30*, 4798-4800.

[30] S. P. Hoffman, T. Kato, F. S. Tham, C. A. Reed *Chem. Commun.* **2006**, 767-769.

[31] S. L. Matthews, V. Pons, D. M. Heinekey *J. Am. Chem. Soc.* **2005**, *127*, 850-851.

[32] Simulations were done using *gNMR* software developed by P. H. M. Budzelaar, Version 5.1.

[33] Z. Xie, J. Manning, R. W. Reed, R. Mathur, P. D. W. Boyd, A. Benesi, C. A. Reed *J. Am. Chem. Soc.* **1996**, *118*, 2922-2928.

[34] (a) BDE of Et_3Si-H = 95 kcal/mol: C. Chatgilialoglu *Chem. Rev.* **1995**, *95*, 1229-1251 (pg. 1231).

(b) BDE of Ph_3C-H = 83 kcal/mol: E. T. Denisov, Zh. Fiz. Khim. **1993**, *67*, 2416 cited in E. T. Denisov, T. Denisova *Handbook of Antioxidants: Bond Dissociation Energies, Rate Constants, Activation Energies, and Enthalpies of Reactions, Second Edition* **1999**, CRC Press, pg. 23.

[35] T. J. Barton, P. Boudjouk, Chapter 1, "Organosilicon Chemistry: A Brief Overview" in *Silicon-Based Polymer Science*; J. Zeigler, *et al*. Advances in Chemistry, American Chemical Society, **1989**, pp. 3-46. Redistribution reactions are discussed beginning on page 16.

[36] Adapted from R. Mulken, Chapter 5, "Fast Imaging Principles", in *Magnetic Resonance Imaging of the Brain and Spine*, Volume 1, 4th Ed. Ed. S. W. Atlas, Wolters-Kluwers Health; Lippincott, Williams & Wilkins; **2008**, pp. 99-101. Initially described by E. L. Hahn, *Physics Today* **1953**, *6*, 4-9.

[37] For an overview of various solvents and drying agents, see: D. B. G. Williams, M. Lawton *J. Org. Chem.* **2010**, *75*, 8351-8354.

[38] R. P. Hughes, P. R. Rose, A. L. Rheingold *Organometallics* **1993**, *12*, 3109-3117.

[39] (a) V. Scott, R. Celenligil-Cetin, O. Ozerov *J. Am. Chem. Soc.* **2005**, *127*, 2852-2853. Supporting Information, Method 2, page 2.

(b) P. Romanato, S. Duttwyler, A. Linden, J. S. Siegel *J. Am. Chem. Soc.* **2010**, *132*, 7828-7829.

[40] A. Avelar, F. S. Tham, C. A. Reed *Angew. Chem. Int. Ed.* **2009**, *48*, 3491-3493.

[41] (a) M. P. Doyle, C. C. McOsker, C. T. West *J. Org. Chem.* **1976**, *41*, 1393-1396.

(b) W. Caseri, P. S. Pregosin *J. Organomet. Chem.* **1988**, *356*, 259-269.

(c) P. P. Gaspar, A. M. Beatty, T. Chen, T. Haile, D. Lei, W. R. Winchester, J. Braddock-Wilking, N. P. Rath, W. T. Klooster *Organometallics* **1999**, *18*, 3921-3932.

Chapter 3: Dihydrogen Complexes of Nickel

3.1 General Introduction. At the outset of this project, there was only one example of a nickel dihydrogen complex in the literature. As the reaction between hydrogen and first-row transition metals is fundamentally relevant to energy storage and use, we were interested in pursuing these molecules. We set out to identify a thermally stable nickel dihydrogen complex to aid our understanding of the interaction between hydrogen and first-row elements.

3.2 Nickel Hydrogenase Background. Hydrogenase enzymes are found in a wide range of anaerobic microbes. These enzymes facilitate the reaction between protons and electrons to produce hydrogen gas, as well as the reverse reaction:

$$2\ H^+ + 2\ e^- \quad \leftrightarrow \quad H_2$$

Understanding the reaction mechanism and efficiently replicating the chemistry would allow the global community and chemical enterprise to move away from using fossil fuels as our primary source of hydrogen.[1] The [FeFe] enzyme consists of two iron centers bridged by a dithiolate ligand (Figure 3-1).[2] The active site of the native species has been crystallographically identified,[3] and several structural and functional models have been reported.[4] No dihydrogen complexes with a similar structural motif have been observed, however.

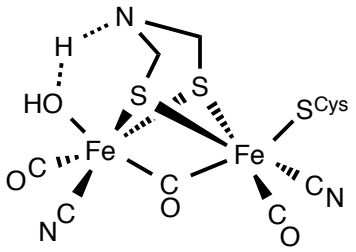

Figure 3-1. Active site of FeFe hydrogenase enzymes as determined by Peters (1.8 Angstrom resolution, *Clostridium pasteurianum*) & Fontecilla-Camps (1.6 Angstrom resolution, *Desulfovibrio desulfuricans*). It is anticipated that the ligated water molecule is displaced by H_2 to enter the catalytic cycle.

A second hydrogenase enzyme has been determined to have a dinuclear core containing a nickel atom and an iron atom, abbreviated [NiFe]. A high-resolution crystal structure was determined for the enzyme from *Desulfovibrio gigas*.[5] This structure confirmed the presence of an iron atom and thiolate ligands in the active site. Several proposed mechanisms have been asserted for the operation of [NiFe] hydrogenase enzymes. Proton reduction and hydrogen

oxidation both occur depending on the H_2 concentration, pH and redox state of the cell. The structures of some forms of the enzyme have been determined using FT-IR spectroscopy, EPR spectroscopy, electrochemical measurements, pH studies, crystallographic studies, and DFT calculations.[6] Figure 3-2 shows one pathway for the subsequent protonation and reduction of the active site of the enzyme proposed by Ogata & coworkers.[7] The formation and association of the hydrogen molecule is proposed to occur at the nickel center; nickel dihydrogen complexes are scarce in the scientific literature, however.

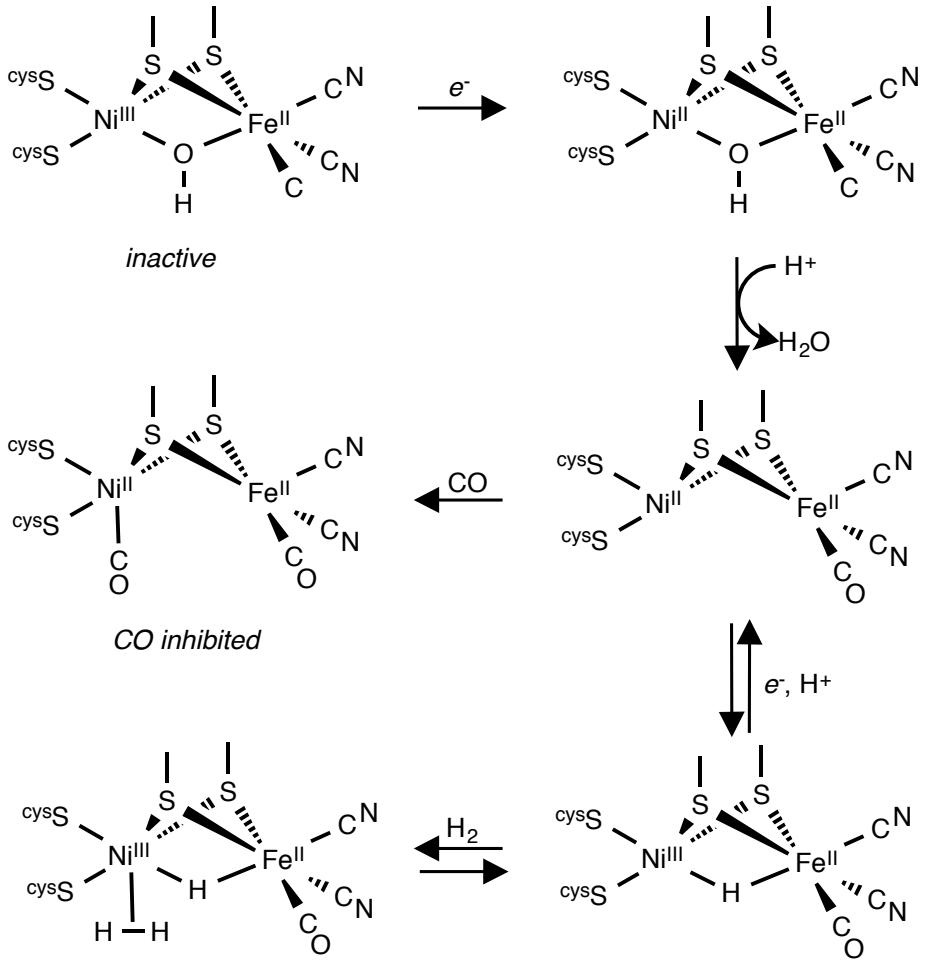

Figure 3-2. A proposed mechanism for the interaction between protons, electrons, and hydrogen gas at the [NiFe] hydrogenase active site. Adapted from work by Ogata, Lubitz, and Higuchi.[7]

The development of functional models of hydrogenase enzymes has been undertaken. A group at the Pacific Northwest National Lab working under DuBois and Bullock has engineered a system capable of performing the reversible reaction between protons and electrons.[8] The general scaffold is shown in Figure 3-3. Electrochemical

reduction of the species readily evolves hydrogen gas at fairly low overpotentials. Alternatively, hydrogen gas can be transformed into metal hydrides and protons. The group has manipulated the first and second coordination spheres of the metal to control proton and electron delivery, achieving competent TONs and TOFs. It should be noted, however, that no nickel dihydrogen complexes have been observed in their careful mechanistic work. Instead, a Ni^{IV} dihydride intermediate was believed to form at the active site.[9] Recent work from the group on similar Mn[10] and Co[11] species demonstrated the role of the pendant amine in the formation of the dihydrogen molecule.

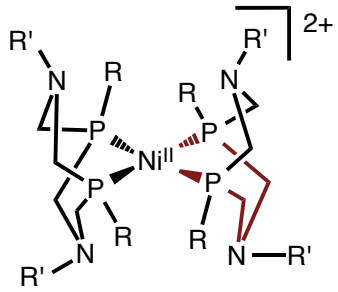

Figure 3-3. Schematic diagram of the generalized scaffold developed at the Pacific Northwest National Lab. The system is capable of catalyzing both the proton reduction and hydrogen oxidation reactions. The four 6-membered rings (one of which is highlighted in maroon) can take on boat or chair configurations to aid the proton relay to the active site.

3.3 Existing Nickel Dihydrogen Complexes.

3.3.1 First example of dihydrogen complex of nickel reported by Caulton. At the onset of this project, only one nickel dihydrogen complex was reported in the literature. Caulton's group at Indiana University published a report on a nickel pincer complex, (PNP)NiCl where PNP = $[\kappa^3\text{-}(tBu_2PCH_2SiMe_2)_2N]^{1-}$. Chloride-abstraction from the starting material afforded an open site at nickel capable of binding dihydrogen at low temperature (Scheme 3-1). However, as the temperature increased, the bound dihydrogen ligand was cleaved heterolytically to give a nickel hydride with an ammonium site in the ligand, $[(PNP\text{-}H)NiH][B(3,5\text{-}(CF_3)_2C_6H_3)_4]$ (Scheme 3-2).[12] Interestingly, with no ligand present to fill the open site, the 3-coordinate nickel complex distorts: this intermediate (Scheme 3-1) was isolated and characterized by X-ray diffraction experiments, NMR spectrometry, and DFT calculations.[13]

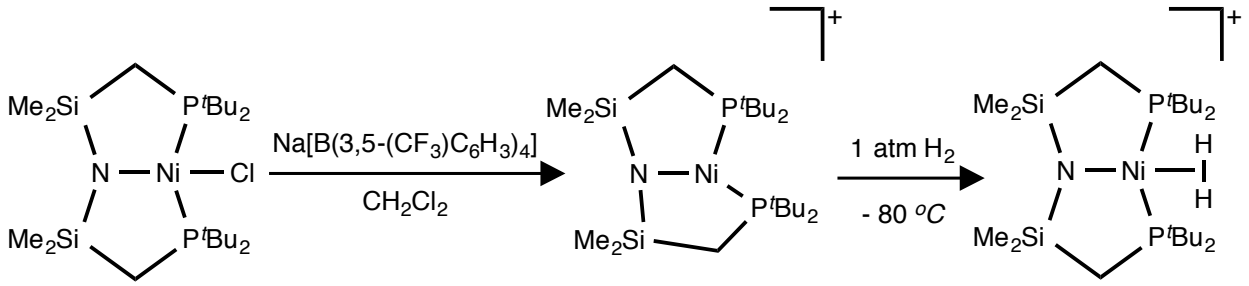

Scheme 3-1. Reaction of (PNP)NiCl with $Na[B(3,5\text{-}(CF_3)C_6H_3)_4]$ in dichloromethane affords a 3-coordinate nickel complex. Addition of H_2 gives the first nickel dihydrogen complex reported in the literature (Caulton, *et al.*). The resulting complex is thermally unstable and reacts further upon warming of the solution above -60 *°C*.

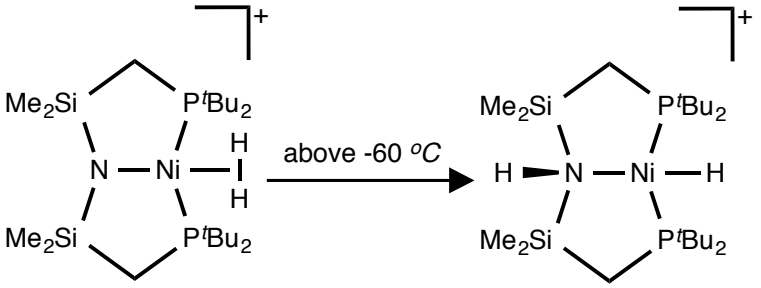

Scheme 3-2. As the temperature increases, Caulton & coworkers report heterolytic cleavage of the dihydrogen ligand to give a nickel hydride with a protonated ligand.[12]

3.3.2 Examples from Peters and coworkers. A few nickel dihydrogen complexes synthesized by Peters and coworkers have been reported over the course of this project. Scheme 3-3 shows a tetradentate ligand bound to a methyl complex of nickel. Protonation of the methyl ligand leads to loss of methane and the newly generated open site readily binds a dinitrogen ligand. Addition of hydrogen cleanly displaces the ligated nitrogen molecule, and the dihydrogen complex is observed.[14] This cationic molecule is thermally stable in solution, but no crystalline material was isolated. More recently, an intermediate has been identified in a frustrated Lewis pair (FLP)-analogous reaction between a Ni-borane complex and H_2.[15] The identified species, (shown in Figure 3-4) is a rare d^{10} dihydrogen complex.

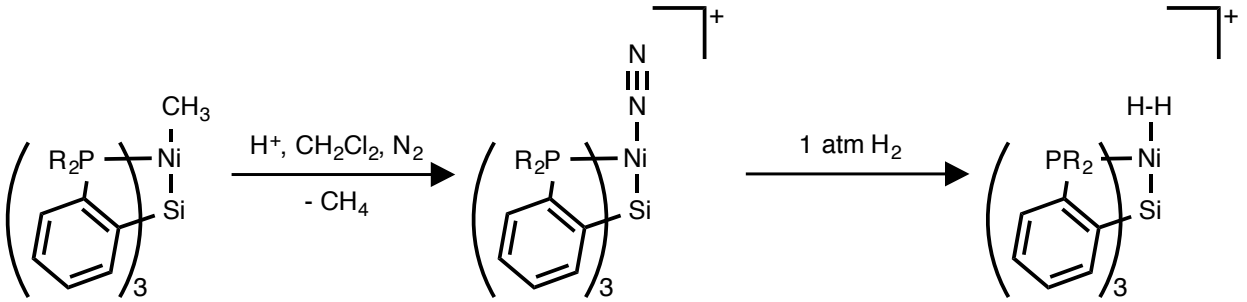

Scheme 3-3. Tsay and Peters reported these species, where protonation of a methyl ligand results in loss of methane in a nitrogen atmosphere. Addition of 1 atm H_2 gas affords the dihydrogen complex. R = ^{i}Pr, Cy.[14]

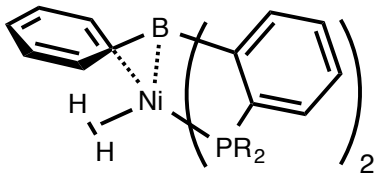

Figure 3-4. Recent dihydrogen-ligated nickel complex reported by Peters, *et al*. This complex is unique as it is a d^{10}-metal (Ni^0) dihydrogen complex. R = ^{i}Pr.[15]

3.4 [(^{tBu}PCP)Ni(H_2)][$B(C_6F_5)_4$] (Complex 3-2). Concurrent to our work, Hazari & co-workers were working with pincer-ligated nickel compounds to electrocatalytically produce hydrogen.[16] Their proposed catalytic cycle is shown in Scheme 3-4. Acetonitrile solvent immediately displaces the generated dihydrogen molecule. This complex then undergoes reduction and protonation to repeat the catalytic cycle. Our work confirms the plausibility of the dihydrogen complex.

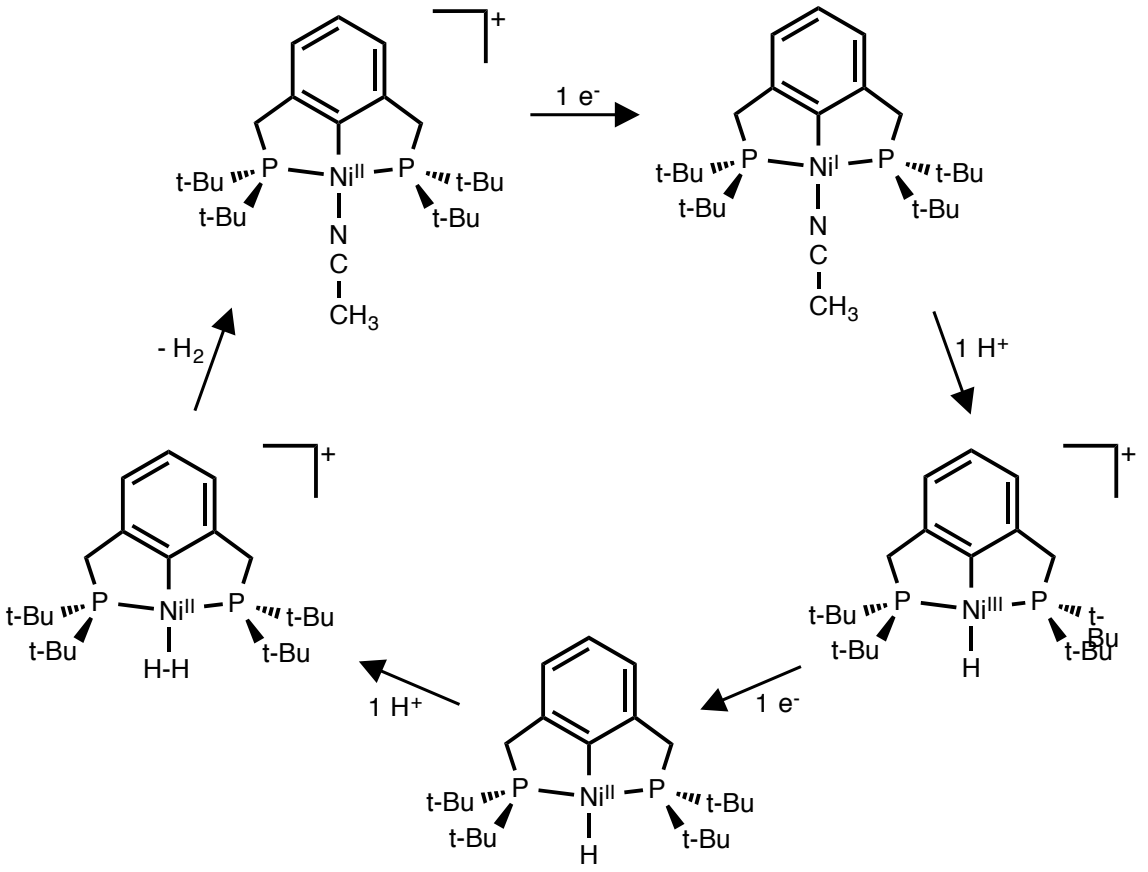

Scheme 3-4. Proposed catalytic cycle for the electrocatalytic production of hydrogen from acidic solution reported by Luca, *et al.*[16] The dihydrogen complex intermediate was not observed, likely due to the presence of the coordinating acetonitrile solvent.

3.4.1 Synthetic Strategy. Our aim was to generate a thermally stable and isolable nickel dihydrogen species. This was accomplished with the use of well-characterized pincer complex starting materials and the reagent discussed in Chapter 2.

3.4.1a Synthetic Utility of Pincer Ligands. Moulton & Shaw first developed pincer ligands in 1976.[17] Named "pincer" ligands due to their crab-like grasp on a metal, these ligands have been utilized extensively in catalysis research.[18] The ^{tBu}PCP ligand employed here, (^{tBu}PCP = κ^3-1,3-bis[(di-tert-butylphosphino)methyl]phenyl), is a ligand reported in the first communication from Moulton & Shaw. These ligands afford complexes that are more stable than their analogous mono-dentate ligated counterparts as the overall lability of the ligand is decreased, leading to reduced decomposition of the ligated complexes (Figure 3-5). It is synthetically straightforward to vary substituents on the

phosphines and the backbone of the phenyl ring (Figure 3-5), making these ligands ideal candidates for studying the effect of steric and electronic changes in the ligand on the coordination chemistry of nickel dihydrogen complexes.

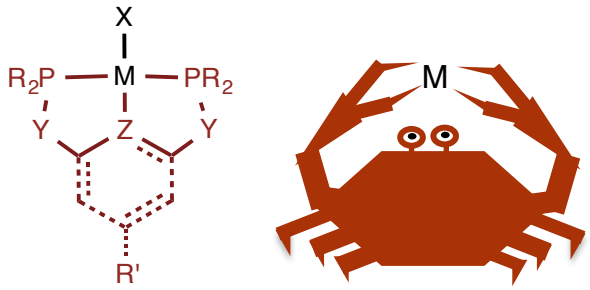

Figure 3-5. Generalized pincer ligand motif. The ligand framework has been called "pincer" in reference to the crab-like shape around the metal. The ligands are less labile than analogous mono-dentate ligands, and, therefore, the complexes are less prone to decomposition. Variations in the ligand at positions Y, Z, R, and R' are synthetically accessible.

3.4.1b Routes to Dihydrogen Complexes using Silylium Species. Using the silylium reagent described in Chapter 2, there are two synthetic routes to dihydrogen complexes. The silylium species can be used to generate a super acid in solution, capable of protonating a metal-hydride complex. Conversely, the reagent can be used to abstract a chloride ligand, resulting in an open site at the metal (Scheme 2-2).

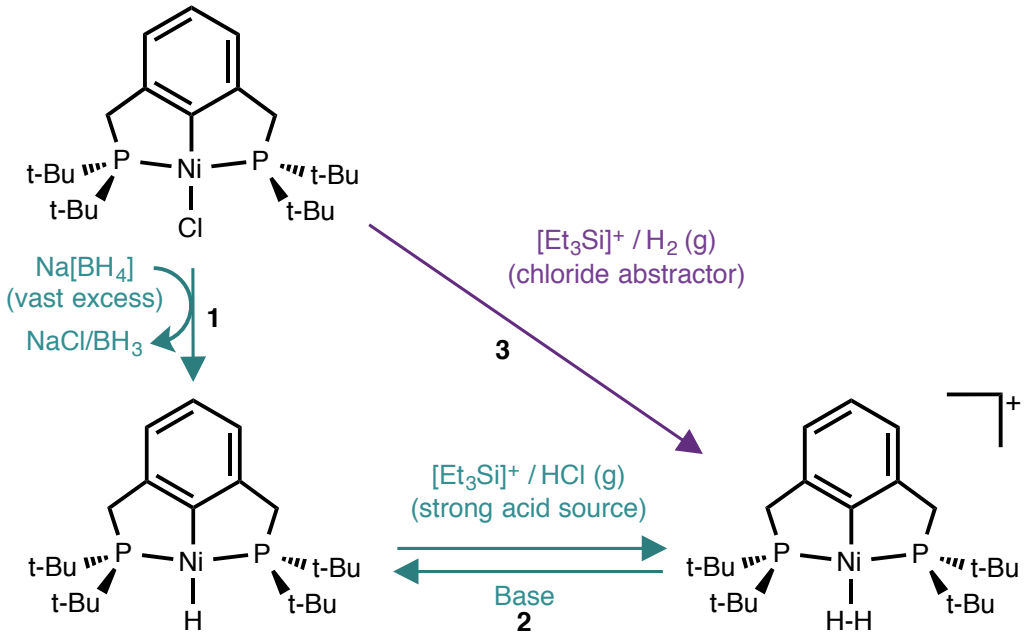

Scheme 3-5. Proposed synthetic routes to $[(^{tBu}PCP)Ni(H_2)]^+$. Steps 1 & 2 (shown in aqua) show conversion to $(^{tBu}PCP)NiH$, followed by protonation. Reaction 1 did not go to completion, resulting in multiple possible reaction pathways for the reagents in Step 2. Step 3 (shown in violet) shows chloride abstraction with the silylium ion (discussed in Chapter 2), followed by reaction with H_2. Step 3 is the pathway used successfully in this report.

We postulated that we could improve the thermal stability of Caulton's nickel dihydrogen complex by removing the basic site from the backbone of the ligand, preventing deprotonation of the dihydrogen complex. Initially, low temperature protonation of the metal hydride was undertaken. However, because first row metal hydrides are susceptible to conversion to chlorides in dichloromethane,[19] and the preparation of the metal hydride gave incomplete conversion in our hands, the reaction between the silylium cation-generated super acid and nickel hydride was never clean. To circumvent these issues, the chloride-abstraction route was used (Scheme 3-5).

3.4.2 Synthesis. Combination of solid (^{tBu}PCP)NiCl (**3-1**) and $[(Et_3Si)_2H][B(C_6F_5)_4]$ (**2-1**) in fluorobenzene under hydrogen afforded Et_3SiCl, Et_3SiH, and $[(^{tBu}PCP)Ni(H_2)][B(C_6F_5)_4]$ (**3-2**) (Scheme 3-6). A new signal is apparent in the $^{31}P\{^1H\}$ NMR spectrum at 103 ppm.

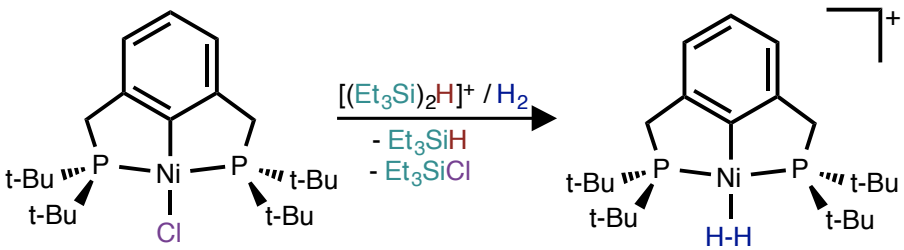

3-1 **3-2**

Scheme 3-6. Synthetic preparation of $[(^{tBu}PCP)Ni(H_2)][B(C_6F_5)_4]$ (**3-2**). Reaction was carried out in fluorobenzene solvent.

3.4.3 Structure. Layering a solution of **3-2** in fluorobenzene with alkane solvent precipitated X-ray quality crystals. The structure of the cation is shown in Figure 3-6. The d_{HH} apparent from the diffraction data is obviously too short (as is often the case from X-ray structures) (0.55 Å vs. 0.74 Å in free H_2). Solution NMR spectroscopic methods were employed to confirm the dihydrogen ligand and determine d_{HH}.

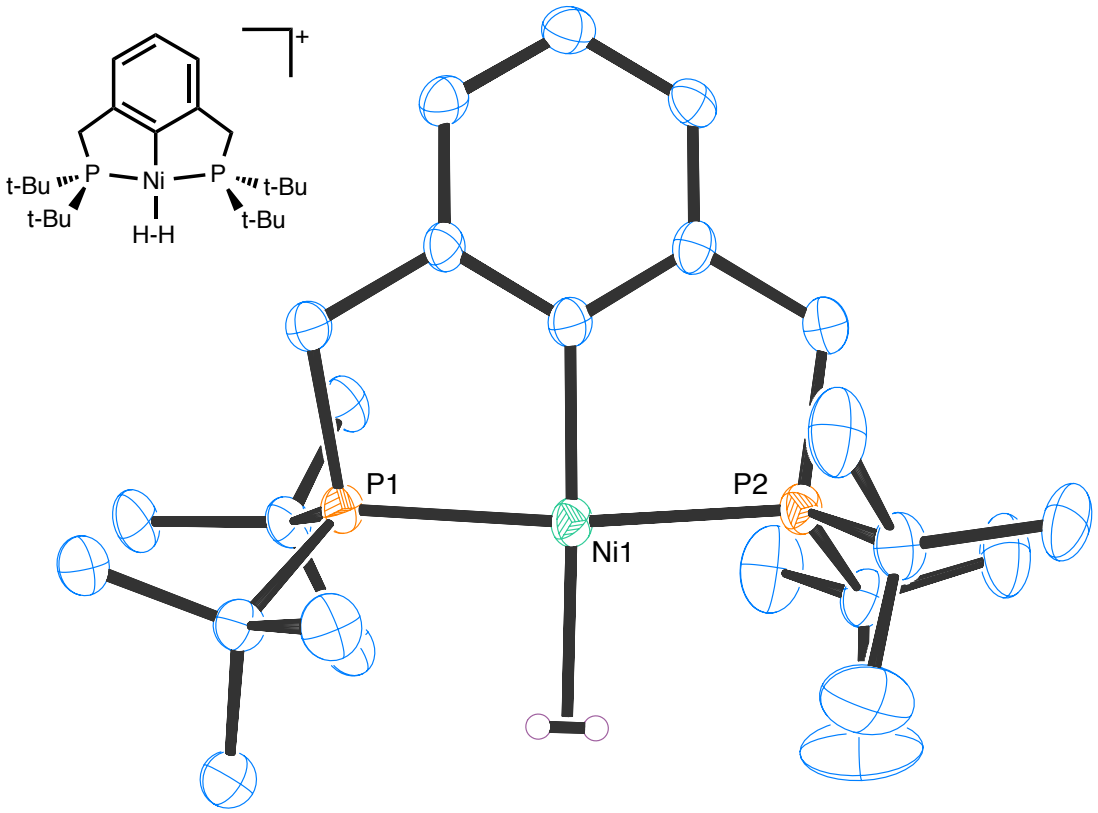

Figure 3-6. ORTEP[20] of [(^{tBu}PCP)Ni(H_2)][B(C_6F_5)$_4$] (**3-2**). Probability ellipsoids are set to the 50% level. Pincer ligand hydrogen atoms and the anion have been omitted for clarity. There are two cations, two anions, and 2 pentane molecules in the unit cell. File: Heinekey/Amanda/AZ0135.

3.4.4 Characterization of the Dihydrogen Ligand in [(^{tBu}PCP)Ni(H_2)][B(C_6F_5)$_4$].

3.4.4a Measurement of T_1. The ^{1}H NMR spectrum of **3-2** features a broad singlet at -3.21 ppm. Inversion-recovery (180-tau-90) experiments (described in Chapter 1.4.3a) indicate that the T_1 relaxation time constant for this resonance is 13 ms at 298 K and decreases to 8 ms at 240 K (See data for all recorded temperatures in Table 3-1). Lower temperatures were not accessible, as the freezing point of fluorobenzene is 233 K. The minimum T_1 could not be confirmed (Figure 3-7), but it is anticipated to be near the shortest observed value. Using T_1 (240K) = 8 ms, it can be estimated that d_{HH} is less than 0.92 Å.

Table 3-1. T_1 data for the H_2 ligand in [(^{tBu}PCP)Ni(H_2)][B(C_6F_5)$_4$] (**3-2**) in C_6H_5F at 500 MHz.

Temperature (K)	Tau$_0$ (ms)	T_1 (ms)
298	9.2	13.3
280	7.4	10.7
260	5.8	8.4
240	5.6	8.1

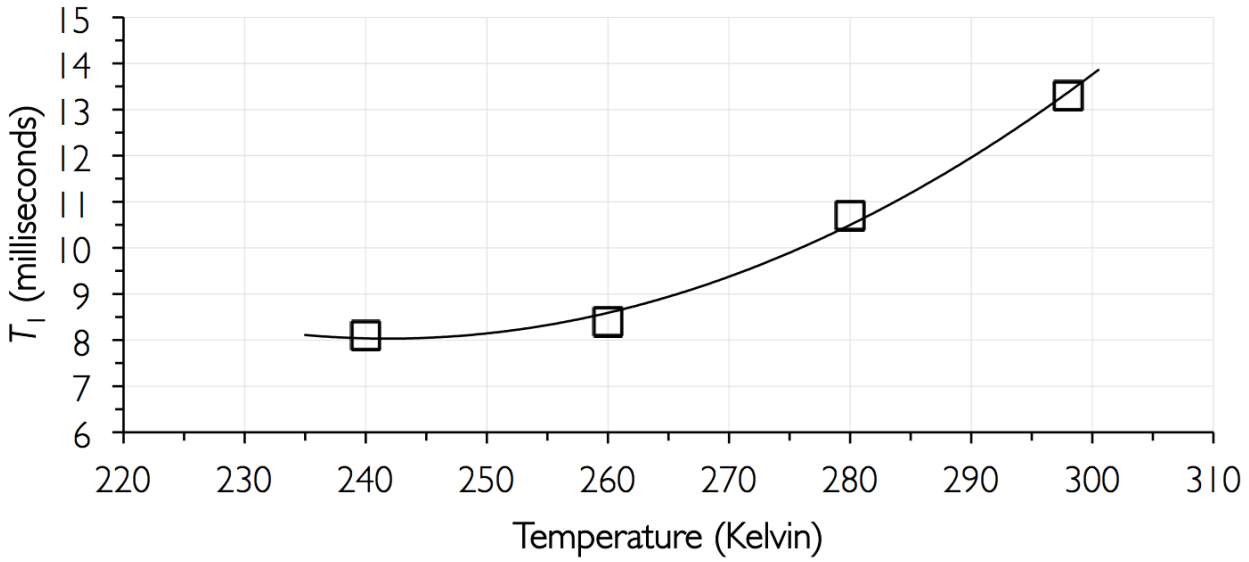

Figure 3-7. T_1 data for the H_2 ligand in [(^{tBu}PCP)Ni(H_2)][B(C_6F_5)$_4$] (**3-2**) in C_6H_5F at 500 MHz.

3.4.4b Observation of $^1J_{HD}$. The short d_{HH} was confirmed by measuring the $^1J_{HD}$. In a partially deuterated sample, [(^{tBu}PCP)Ni(HD)][B(C_6F_5)$_4$] (**3-2-d_1**), $^1J_{HD}$ could be observed at 285 K to be 34 ± 1 Hz (Figure 3-8). As outlined in Chapter 1, this $^1J_{HD}$ corresponds to a d_{HH} of 0.86 ± 0.02 Angstroms.

The fact that the resonance for ligated HD in **3-2-d_1** is too broad to observe any coupling at 298 K suggests that the HD is exchanging rapidly with the small amount of free HD in solution (Figure 3-9). The species in smaller concentration experiences greater broadening, such that the low concentration of free HD in the low temperature spectra is not observable at 4.5 ppm.

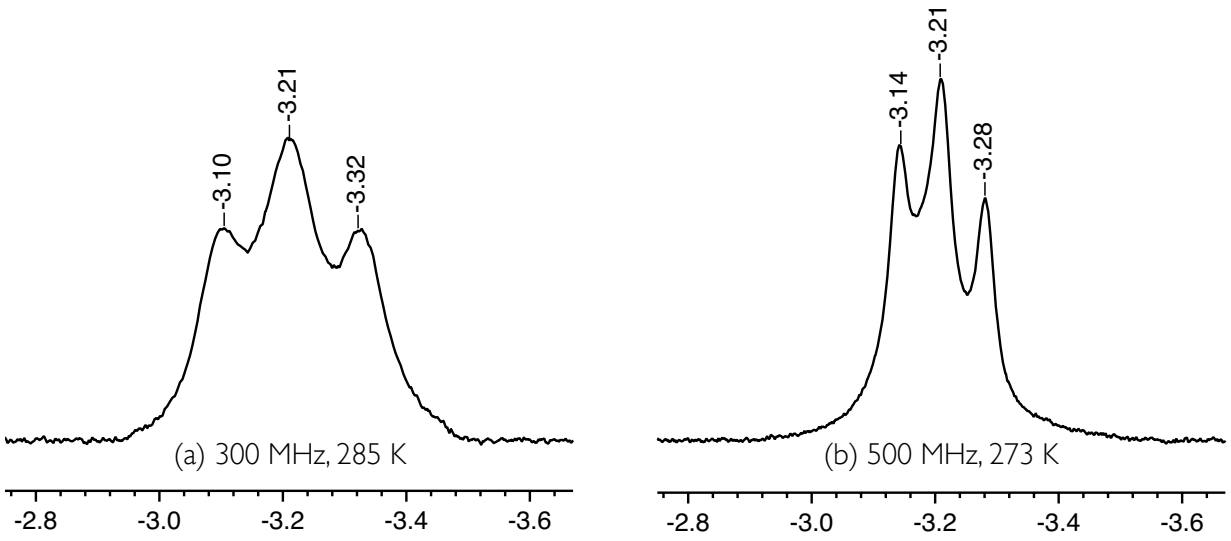

Figure 3-8. ^{1}H NMR spectra of [(^{tBu}PCP)Ni(*H*D)][B(C_6F_5)$_4$] (**3-2-d_1**) in C_6H_5F. (a) 300 MHz, 285 K. (b) 500 MHz, 273 K. Some residual H_2 complex is observed to be overlapping with these signals (distortion from 1:1:1 triplet expected for HD). $^1J_{HD}$ is determined to be 34 ± 1 Hz, corresponding to a d_{HH} of 0.856 ± 0.015 Å. (a) Data from sjconnel/300/SJC4_051412_3/Experiment 3 (b) Data from sjconnel/500/SJC4_060812_1/Experiment 4.

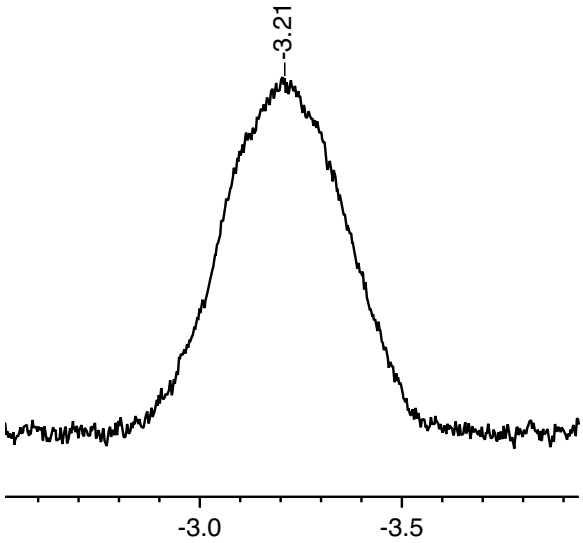

Figure 3-9. ^{1}H NMR Spectrum of [(^{tBu}PCP)Ni(*H*D)][B(C_6F_5)$_4$] in C_6H_5F, 300 MHz, 298 K. At room temperature, the signal is broadened such that the HD coupling is not observable (relative to that observed in Figure 3-8 at 285 K). Cooling the sample slows down the exchange between free and complexed HD gas, such that the $^1J_{HD}$ is observable. Data from sjconnel/300/SJC4_051412_3/Experiment 2.

3.5 [(^{tBu}POCOP)Ni(H_2)][$B(C_6F_5)_4$] (Complex 3-5).

3.5.1 Synthesis. As above for **3-2**, the metal chloride was combined with a chloride-abstracting reagent in inert solvent under an atmosphere of H_2 gas to afford the dihydrogen complex. Yellow (^{tBu}POCOP)NiCl (**3-3**) ((^{tBu}POCOP) = κ^3-1,3-bis[(di-tert-butylphosphinito)]phenyl) and colorless $[(Et_3Si)_2H][B(C_6F_5)_4]$ (**2-1**) were combined in equimolar quantities. Upon dissolution in fluorobenzene, a dark-colored solution was obtained (Intermediate **3-4** (discussed in Ch. 4), which paled to yellow upon addition of H_2 gas (Scheme 3-7). The resulting solution contained Et_3SiH, Et_3SiCl, and the desired product, [(^{tBu}POCOP)Ni(H_2)][$B(C_6F_5)_4$] (**3-5**). The ^{1}H NMR spectrum contained a resonance for the dihydrogen ligand at -2.64 ppm, and a new signal at 220 ppm was observed in the ^{31}P{^{1}H} NMR spectrum.

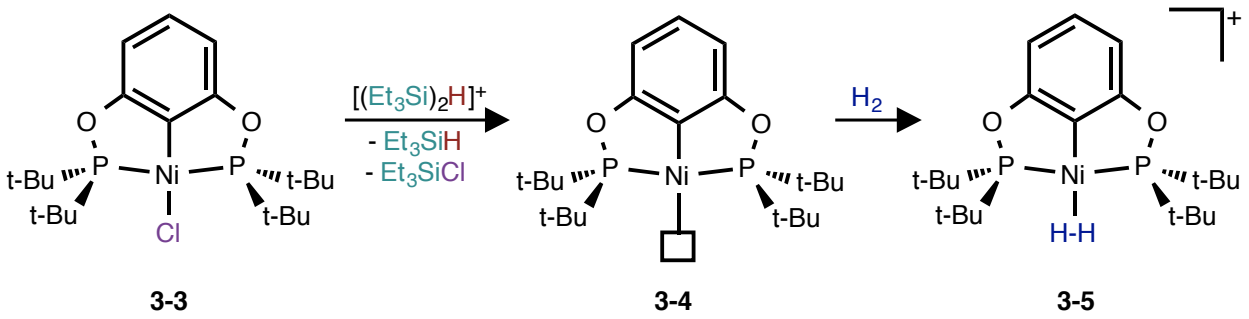

Scheme 3-7. Synthesis of [(^{tBu}POCOP)Ni(H_2)][$B(C_6F_5)_4$] (Complex **3-5**). The triethylsilylium species (**2-1**) was employed as a chloride-abstracting reagent to generate an open coordination site at the metal. Intermediate **3-4** and hypotheses of its identity will be discussed further in Chapter 5. Addition of hydrogen gas resulted in formation of complex **3-5**.

3.5.2 Structure. Layering a solution of **3-5** with alkane solvent precipitated X-ray quality crystals. The asymmetric unit contains two nickel cations, their corresponding $B(C_6F_5)_4$ anions, and a disordered fluorobenzene and pentane solvent molecule. Upon refinement, the R_{int} value = 0.0832 indicated the structure was of slightly less than average quality. The cation of **3-5** is shown in Figure 3-10.

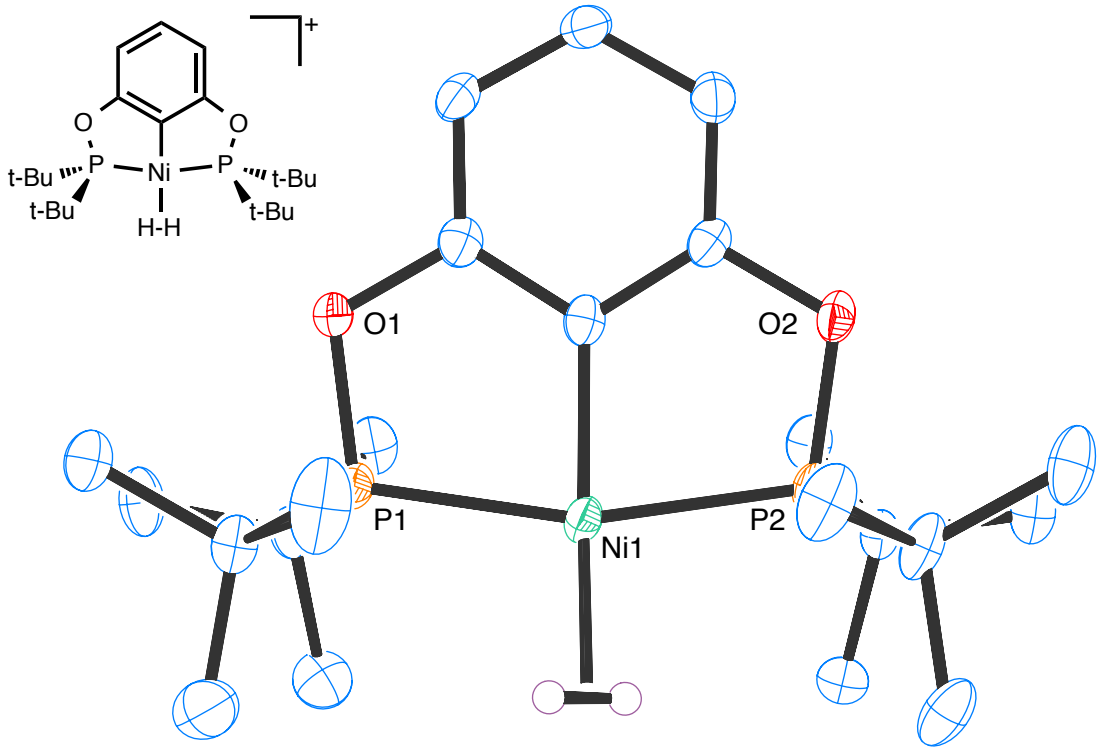

Figure 3-10. ORTEP[20] of the cation of [(^{tBu}POCOP)Ni(H_2)][B(C_6F_5)$_4$] (**3-5**). Ellipsoids are set at the 50% probability level. Anion, fluorobenzene/pentane solvent molecules, and protons on the pincer ligand have been omitted for clarity. Data taken from Heinekey/Samantha/sjc13.

3.5.3 Determination of d_{HH}. To confirm the presence of the dihydrogen ligand, NMR spectroscopic experiments were employed.

3.5.3a. Measurement of T_1. The ^{1}H NMR signal for the H_2 ligand of **3-5** was observed at -2.64 ppm. At 298 K and 500 MHz, the T_1 of the resonance was found to be 16 ± 1 milliseconds, confirming the characterization as a dihydrogen complex. The T_1 was then recorded at decreasing temperature until the freezing point of the solvent was reached. Data was recorded on both 500 and 700 MHz spectrometers. The minimum value at 500 MHz (9.7 ± 1 ms) was recorded at 260 K, and the T_1 value was observed to be increasing as the temperature was lowered further. The T_1(minimum) recorded on the 700 MHz spectrometer was 13 ± 1 ms, recorded at 268 K. These values were included in Equation 1-5 to find d_{HH} = 0.95 ± 0.015 Angstroms (This is consistent with both datasets). The data is plotted in Figure 3-11. As was discussed in Chapter 1.4.3a, the minimum T_1 value is found at a higher temperature at higher field.

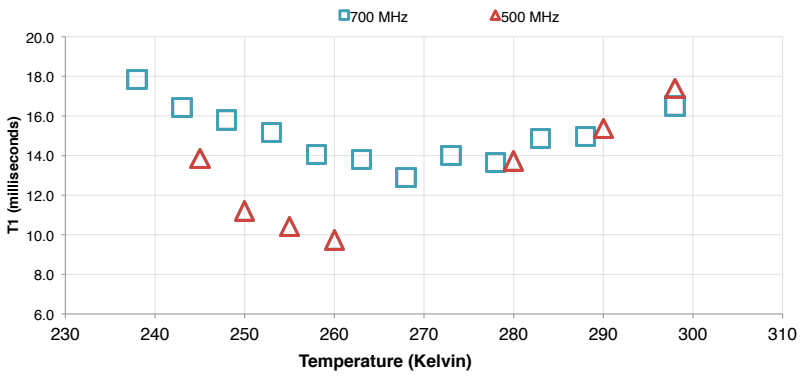

Figure 3-11. Plot of T_1 values recorded on 500 and 700 MHz spectrometers at various temperatures for [(^{tBu}POCOP)Ni(H_2)][$B(C_6F_5)_4$] (**3-5**) in fluorobenzene-H_5. Aqua squares represent the data points from the 700 MHz spectrometer. Red triangles represent data points recorded on the 500 MHz spectrometer. As is discussed in Chapter 1, T_1 (minimum) occurs at a higher temperature at higher field. Data from 700/sjconnel/SJC5_072713_1, 700/sjconnel/SJC5_071813_5, and 500/sjconnel/SJC5_073013_1.

3.5.3b. Observation of $^1J_{HD}$. The presence of an H_2 ligand was confirmed through observation of HD coupling in the partially deuterated ligand. The ^{1}H NMR spectrum of [(^{tBu}POCOP)Ni(HD)][$B(C_6F_5)_4$] (**3-5-d_1**) shows a 1:1:1 triplet at -2.66 ppm (Figure 3-12) with $^1J_{HD}$ = 35 ± 1 Hz. A smaller coupling to ^{31}P atoms in the pincer ligand is also observable. Using Equation 1-8, d_{HH} is estimated to be 0.84 ± 0.02 Angstroms.

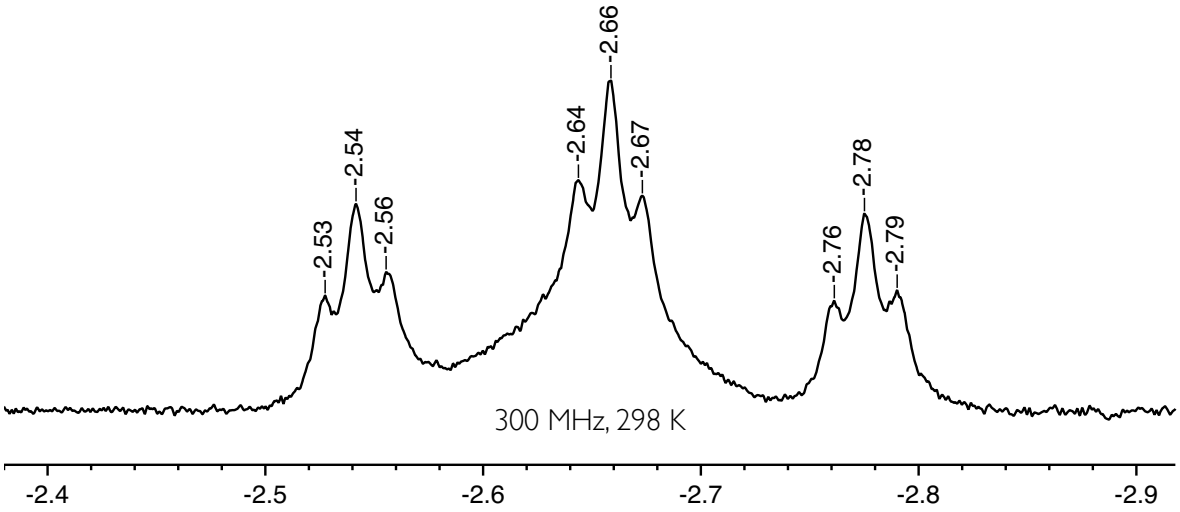

Figure 3-12. ^{1}H NMR Spectrum of [(^{tBu}POCOP)Ni(HD)][$B(C_6F_5)_4$] (**3-5-d_1**) in fluorobenzene-H_5. Spectrum was recorded at 300 MHz and 298 K. Some residual H_2 contributes to the broadness and intensity of the central line of the spectrum. The smaller coupling is to the phosphorous atoms of the ligand. The spectrum shows $^1J_{HD}$ = 35 ± 1 Hz, suggesting that d_{HH} = 0.84 ± 0.02 Angstroms. Data taken from 301/sjconnel/SJC5_101912_1.

3.5.4 Discussion of the "Fast-Spinning" Regime. The d_{HH} found from the T_1(minimum) data presented above (0.95 ± 0.01 Angstroms) is substantially different from that determined from the $^1J_{HD}$ (0.84 ± 0.02 Angstroms). There has been extensive discussion of error in the T_1 relationship due to fast rotation and hopping motions of the H_2 ligand.[21] If we anticipate that the ligand was spinning (like a propeller) at an intermediate rate, then the two measurements could be considered to be in agreement. Based on the solid state structures, the ^{tBu}POCOP ligand is "pulled back" slightly further from the fourth coordination site at the metal relative to ^{tBu}PCP, perhaps lowering the energy barrier for rotation of the dihydrogen ligand (Figure 3-13).

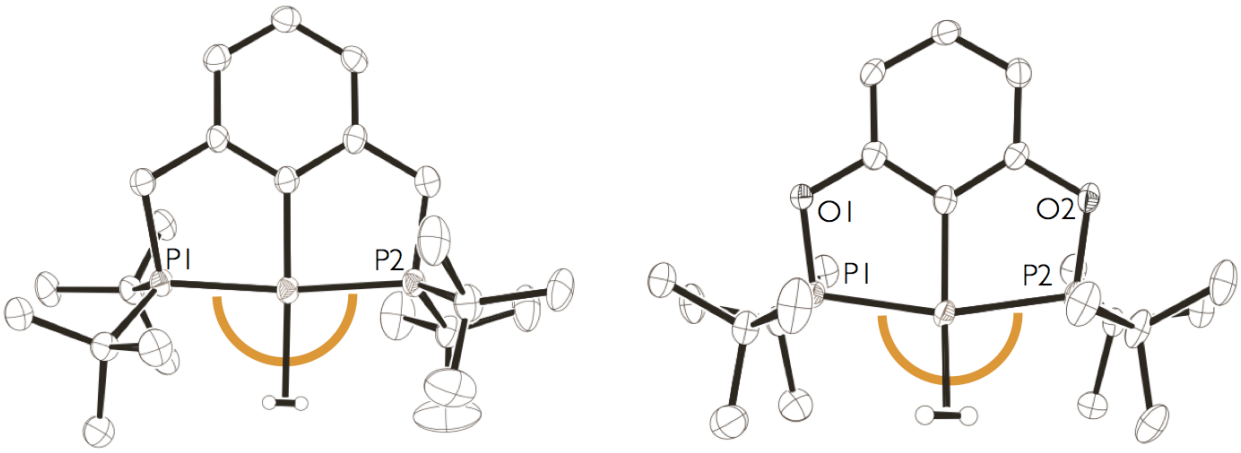

Figure 3-13. Comparison of P-Ni-P angles in [(^{tBu}PCP)Ni(H_2)]$^+$ (**3-2**) and [(^{tBu}POCOP)Ni(H_2)]+ (**3-5**). The POCOP ligand has a smaller bite angle on the nickel, leaving the fourth coordination site slightly more exposed. If this leads to a smaller barrier to H_2 rotation, it could explain the disparity between the T_1- and $^1J_{HD}$- predicted d_{HH} values for **3-5**.

3.5.5 Isotope Shift in $^{31}P\{^1H\}$ NMR Spectra. The partially deuterated sample (**3-5-d_1**) was prepared by introduction of HD gas to the dark colored solution resulting from dissolution of (^{tBu}POCOP)NiCl (**3-3**) and $[(Et_3Si)_2H][B(C_6F_5)_4]$ **2-1** in fluorobenzene. An independent sample of HD confirmed the gas was less than 10% H_2, and contained almost no D_2. Following the reaction with [(^{tBu}POCOP)Ni][$B(C_6F_5)_4$] (**3-4**), the sample quickly (within 15 minutes) reached a statistical distribution of hydrogen and deuterium atoms (25% H_2, 50% HD, 25% D_2). It is likely that this HD scrambling is catalyzed by small amounts of acid or base present in solution. The distribution is apparent in the ^1H spectrum (free H_2/HD) and can be observed in the $^{31}P\{^1H\}$ NMR spectrum as well (Figure 3-14). In the

$^{31}P\{^{1}H\}$ NMR spectrum, a 50 ppb isotope shift is observed between a smaller signal and a larger signal. While three signals are not observed for the three species, the integrations suggest that the larger signal actually contains two signals. The isotope shift results from slightly different phosphorus environments depending on whether the pincer ligand has a H_2, HD, or D_2 coligand. Isotope shifts of this size are precedented.[22] While often additive, isotope shifts are not strictly linear.[23]

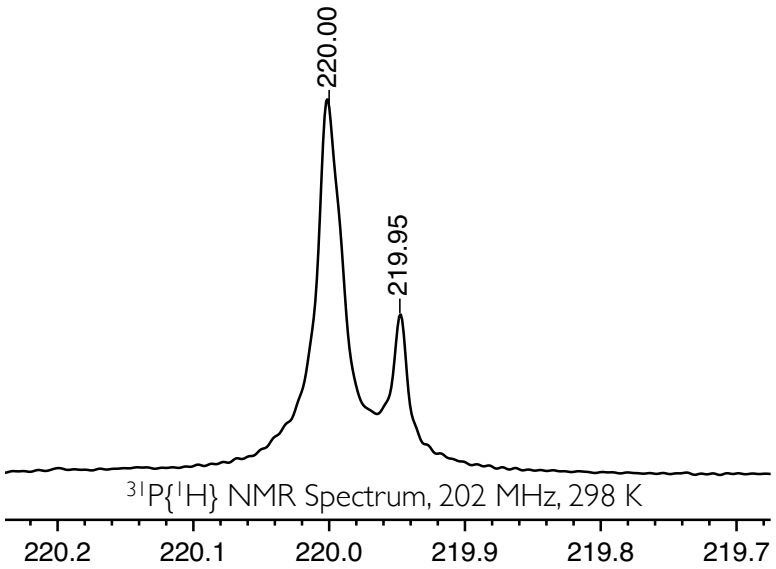

Figure 3-14. $^{31}P\{^{1}H\}$ NMR spectrum of [(^{tBu}POCOP)Ni(H_2)]$^+$ (202 MHz, 298 K, C_6H_5F). The H_2 ligand is a mixture of H_2, HD, and D_2. The ^{1}H NMR spectrum indicates statistical distribution of the isotopes. In this spectrum, the integration of the signals is approximately 3:1, suggesting that the larger signal masks a third signal. Data from Experiment 2 in sjconnel/499/SJC5_101912_3.

3.6 Comparison of Complexes. This chapter covers the synthesis of two nickel dihydrogen complexes, (^{tBu}PCP)Ni(H_2)]$^+$ (**3-2**) and (^{tBu}POCOP)Ni(H_2)]$^+$ (**3-5**). Both have nearly planar, four-coordinate geometry around the metal. The P-Ni-P angles differ slightly, as was shown in Figure 3-13. As is the case in the metal chloride compounds, the tBuPOCOP ligand is "pulled back" from the fourth coordination site, increasing the access to the metal by almost 10°.

The ^{tBu}POCOP ligand is also more electron-withdrawing than the ^{tBu}PCP ligand, as evidenced by the difference in the CO stretching frequencies. When the ligands are coordinated to iridium to give (pincer)Ir(CO) complexes, ^{tBu}POCOP has a CO stretching frequency over 20 cm^{-1} higher than the analogous ^{tBu}PCP complex.[24] The change in electron-density at the metal, however, is not carried into the degree of activation of the dihydrogen ligand on nickel. Coordination of H_2 to the metal increases the bond length from 0.74 Angstroms in free H_2 to 0.86 ± 0.02 Angstroms

(273 K) (**3-2**) and 0.84 ± 0.02 Angstroms (**3-5**). These values were determined from the decrease in the $^{1}J_{HD}$ coupling constant in the partially deuterated species: 34 ± 1 Hz Hz (**3-2**) and 35 ± 1 Hz (**3-5**), and are the same within error.

The only major difference noted between the two complexes in regards to hydrogen coordination is the rate of exchange between the ligand and free HD. In **3-2**, at room temperature, the exchange is occurring at a rate fast enough to broaden the HD signal, such that no HD coupling is observable, and the signal for free HD in solution is broadened into the baseline. In contrast, the HD coupling is observable, and a small signal for free HD is apparent in a solution of **3-5** at room temperature.

3.7 Experimental Details.

General Considerations. All experiments were carried out under argon using Schlenk and glove box techniques unless otherwise noted. Solvents were dried and vacuum transferred immediately prior to use. N,O-bistrimethylsilylacetamide was refluxed in glassware to silylate the surface prior to use with $[(Et_3Si)_2H][B(C_6F_5)_4]$. $[(Et_3Si)_2H][B(C_6F_5)_4]$ (**2-2**) was prepared as described in Chapter 2.

NMR spectra were recorded at 298 K (unless otherwise noted) on Bruker AV300, AV500, DRX500, or AV700 spectrometers. ^{1}H NMR chemical shifts are reported relative to residual resonances of the solvent: C_6D_5H (δ = 7.16), C_6D_4HF (δ = 6.96, 6.99, 7.17), $CDHCl_2$ (δ = 5.32). Some ^{1}H NMR spectra were recorded in *protio*-fluorobenzene using a solvent suppression pulse program or acquisition of several hundred scans. $^{31}P\{^1H\}$ NMR chemical shifts were externally referenced to H_3PO_4 (85% in H_2O) (δ = 0.00).

The neutral alumina used for purification of the pincer metal chloride compounds was Alumina Neutral Super I, Catalog # 04589-25, Dynamic Adsorbants, Norcross, GA. It should be noted that the pincer metal chlorides synthesized here are completely stable to H_2O. They can be purified, handled, and stored in air.

HD gas synthesis.

HD gas was synthesized in a manner similar to the preparation described by Wender, *et al.*[25] A Schlenk flask containing $LiAlH_4$ (6.5 g, 170 mmol) and a stir bar was immersed in an ice bath (controls reaction rate). D_2O (2 mL, 100 mmol) was added via syringe through the septum. The reaction readily evolves HD gas, which is transferred through a vacuum manifold to a gas storage flask. **Caution**: calculations should be carried out so as not to generate more than ~4 atm of gas in the gas storage flask. Cooling the coconut charcoal-filled finger in liquid nitrogen promotes adsorption of the gas. Since the reaction is carried out with a deficiency of D_2O, the $LiAlH_4$ dries the generated gas.

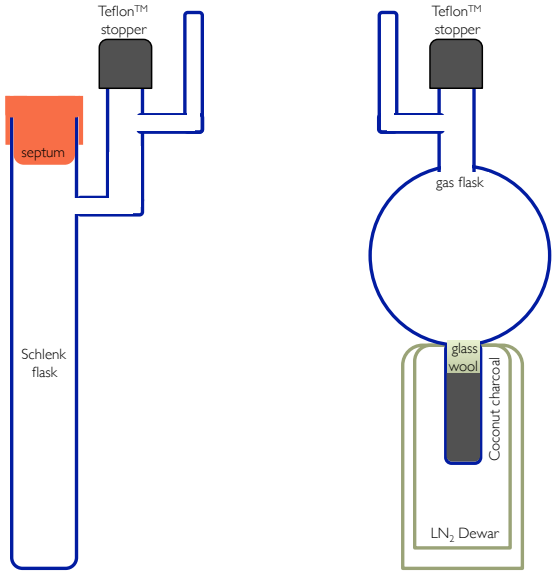

(^{tBu}PCP)NiCl (3-1).

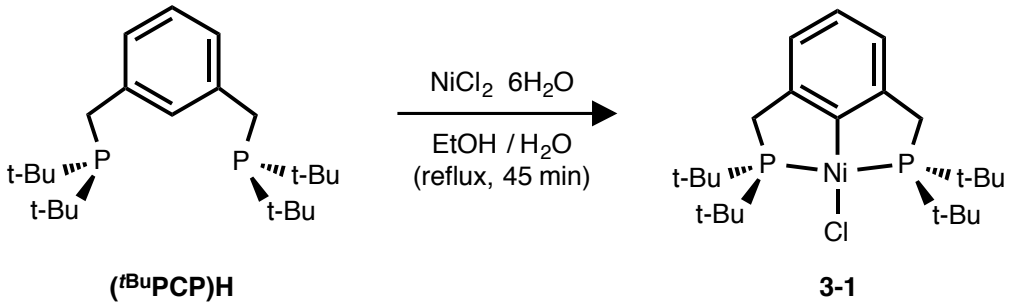

(^{tBu}PCP)H **3-1**

The following preparation was only slightly modified from those published by Moulton & Shaw[17] and Boro, *et al.*[26] Reference 26b contains the crystal structure of this species.

(^{tBu}PCP)H (Aldrich) (0.300 g, 394.55 g/mol, 0.76 mmol) was dissolved in degassed ethanol (5 mL). A solution of $NiCl_2$•$6H_2O$ (0.181 g, 237.69 g/mol, 0.76 mmol) in degassed water (1 mL) was added to the reaction mixture by cannula. The reaction was heated to reflux for 45 minutes, and then cooled in an ice bath. Yellow crystalline needles were precipitated.

The supernatant was removed by cannula, and the yellow crystals were dissolved in ethanol. The yellow solution was filtered through neutral alumina, which removed $NiCl_2$•$6H_2O$, as well as unreacted ligand. The solvent was removed *in vacuo*, and a yellow solid was collected (0.170 g, 487.69 g/mol, 0.35 mmol, 46 % yield). In general, reproducible yields were between 40-55%.

If the product appeared at all green after being exposed to vacuum, the solid was dissolved and filtered through alumina a second time to remove all $NiCl_2$•$6H_2O$. Crystalline product was obtained from a concentrated solution in alkane cooled to - 25 °C.

CAS #	60426-33-7	
^{1}H NMR	(C_6D_6, 500 MHz, 298 K) :	1.41 ppm (vt, 36H, ^{t}Bu-CH_3); 2.91 ppm (vt, 4H, CH_2) 6.85 ppm (d, 2H, aromatic); 7.01 ppm (t, 1H, aromatic)
^{31}P{^{1}H} NMR	(C_6D_6, 202 MHz, 298 K):	67.4 ppm

NMR Data from sjconnel/500/SJC4_042412_1/ Expts 2 & 3

Crystal structure reported by Boro, *et al.*[26b]

[(^{tBu}PCP)Ni(H_2)][$B(C_6F_5)_4$] (3-2).

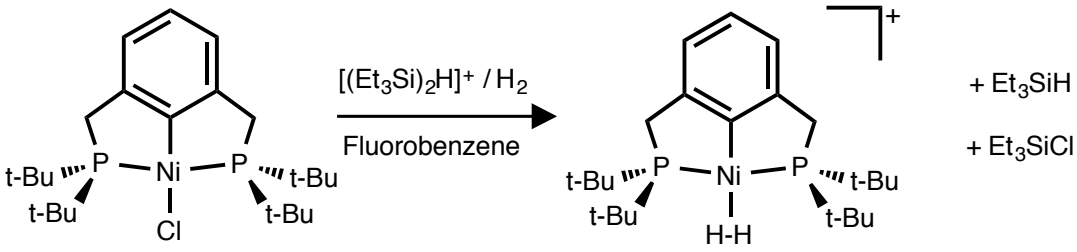

3-1 **3-2**

(^{tBu}PCP)NiCl (50 mg, 487.69 g/mol, 0.10 mmol) was combined with $[(Et_3Si)_2H][B(C_6F_5)_4]$ (92 mg, 910.58 g/mol, 0.11 mmol) in a silylated glass vessel with a magnetic stir bar. Fluorobenzene (~3 mL) was added by vacuum transfer, and a dark red-brown solution resulted. The solution was frozen (liquid nitrogen), the head space evacuated, and H_2 gas (1 atm) was introduced. Upon thawing, the solution became yellow-green with stirring. The solution was again frozen, the head space evacuated, and pentane (~25 mL) was added by vacuum transfer. A solid precipitated. After the precipitate settled, the solution was removed by cannula, and the solid was dried *in vacuo*. Isolated (crude): 55 mg, 48% yield.

CAS #	1417797-53-5	
^{1}H NMR	(C_6H_5F, 500 MHz, 298 K):	1.05 ppm (vt, 36H, ^{t}Bu-CH_3); 3.13 ppm (s, 4H, CH_2) -3.21 ppm (br, 2H, H_2); (aromatics coincident with protio-solvent signals)
^{31}P{^{1}H} NMR	(C_6H_5F, 202 MHz, 298 K):	103 ppm

NMR data from sjconnel/500/SJC4_062512_2 / Expts 1 & 3.

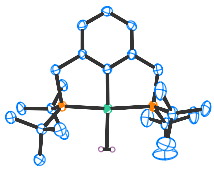

X-ray structural details available from the CCDC: Structure # 891930. Included here as Figure 3-6. Data from Heinekey/Amanda/AZ0135.

(^{tBu}POCOP)H (Ligand).

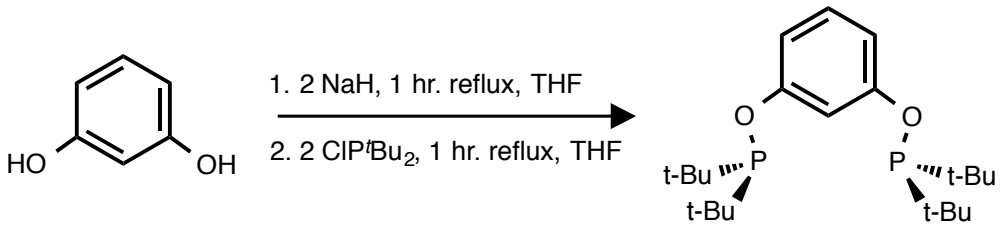

(^{tBu}POCOP)H

Synthesis was modified from the preparation originally reported for iridium complexes.[27] A solution of NaH (0.24 grams, 24 g/mol, 10 mmol) in THF (~10 mL) was added to a solution of resorcinol (0.500 grams, 110.1 g/mol, 4.5 mmol) in THF (~ 20 mL). The reaction mixture was brought to reflux for 1 hour, cooled, and then ClPtBu2 () was added via syringe. The reaction was refluxed for an additional hour. After cooling to room temperature, the reaction mixture was filtered through Celite to remove NaCl, and then the solvent was removed *in vacuo*. The product is an oily white solid that can be carried directly into the metallation reaction. Reproducible yields were approximately 90%.

CAS # 33880-20-7

^{1}H NMR (C_6D_6, 300 MHz, 298 K): 1.14 ppm (vt, 36H, ^{t}Bu-CH_3)

^{31}P{^{1}H} NMR (C_6D_6, 122 MHz, 298 K): 150 ppm

NMR data from sjconnel/300/SJC4_091212_1/Expts 1 & 2.

(^{tBu}POCOP)NiCl (3-3).

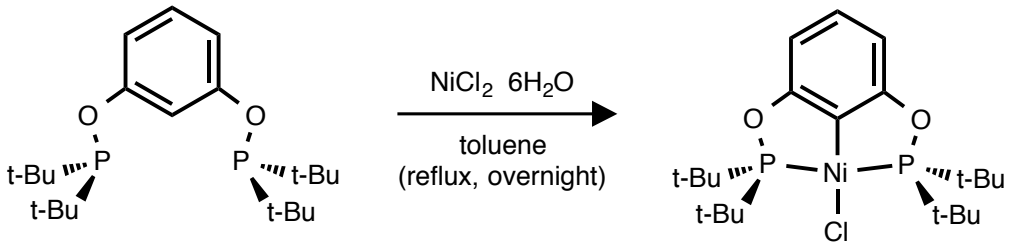

(^{tBu}POCOP)H **3-3**

The following preparation was only slightly modified from that published previously.[28] (^{tBu}POCOP)H (0.250 g, 398.50 g/mol, 0.63 mmol) was dissolved in toluene (~ 20 mL). This solution was added to a suspension of $NiCl_2$ (both the hexahydrate and the anhydrous compound were used in various preparations of this compound) (1 equivalent) in toluene (~10 mL). The mixture was refluxed overnight. The resulting suspension was filtered through Celite. Removing the solvent on a rotary evaporator produced a dark yellow solid. This product was further purified by dissolution in ethanol, filtering through neutral alumina, and removing the solvent *in vacuo* to produce a yellow solid. Reproducibly isolated clean product in approximately 50-60% yield.

CAS #	1108747-38-1	
^{1}H NMR	($CDCl_3$, 300 MHz, 298K):	1.49 ppm (vt, 36H, ^{t}Bu-CH_3); 6.38 ppm (d, 2H, Ar); 6.92 ppm (t, 1H, Ar)
$^{31}P\{^{1}H\}$ NMR	($CDCl_3$, 122 MHz, 298 K):	187 ppm

NMR Data from sjconnel/300/SJC4_091812_2/Expts 1 & 2

Crystal structure reported by Chakraborty, Krause, and Guan.[28]

[(^{tBu}POCOP)Ni(H_2)][$B(C_6F_5)_4$] (3-5).

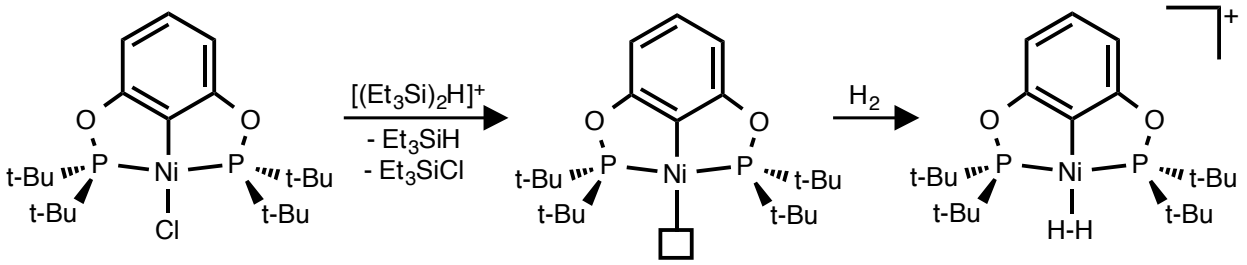

(^{tBu}POCOP)NiCl (50 mg, g/mol, mmol) was combined with [$(Et_3Si)_2H$][$B(C_6F_5)_4$] (92 mg, 910.58 g/mol, 0.11 mmol) in a silylated glass vessel with a magnetic stir bar. Fluorobenzene (~3 mL) was added by vacuum transfer, and a dark red-brown solution resulted. The solution was frozen (liquid nitrogen), the head space evacuated, and H_2 gas (1 atm) was introduced. Upon thawing, the solution became yellow with stirring. The solution was again frozen, the head space evacuated, and pentane (~25 mL) was added by vacuum transfer. A solid precipitated. After the precipitate settled, the solution was removed by cannula, and the solid was dried *in vacuo*. Isolated (crude): 55 mg, 48% yield.

^{1}H NMR (C_6H_5F, 500 MHz, 298 K): 1.10 ppm (vt, 36H, ^{t}Bu-CH_3);
-2.62 ppm (br, 2H, H_2); (aromatics coincident with protio-solvent signals)
^{31}P{^{1}H} NMR (C_6H_5F, 202 MHz, 298 K): 220 ppm

NMR data from sjconnel/499/SJC4_091712_5 / Expts 1 & 2.

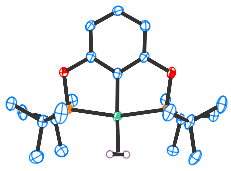

X-ray structure included here as Figure 3-10. Data from Heinekey/Samantha/sjc13.

References

[1] J. C. Gordon, G. J. Kubas *Organometallics* **2010**, *29*, 4682-4701.

[2] D. M. Heinekey *J. Organomet. Chem.* **2009**, *694*, 2671-2680.

[3] (a) Y. Nicolet, C. Piras, P. Legrand, C. E. Hatchkian, J.C. Fontecilla-Camps *Structure* **1999**, *7*, 13-23.

(b) J. W. Peters, W. N. Lanzilotta, B. J. Lemon, L. C. Seefeldt *Science* **1998**, *282*, 1853-1858.

[4] These references are by no means comprehensive, but instead, provide some recent highlights:

(a) F. Gloaguen, T. B. Rauchfuss *Chem. Soc. Rev.* **2009**, *38*, 100-108.

(b) J. M. Camara, T. B. Rauchfuss *Nature Chem.* **2012**, *4*, 26-30.

(c) E. J. Lyon, I. P. Georgakaki, J. H. Reibenspies, M. Y. Darensbourg *Angew. Chem. Int. Ed.* **2012**, *38*, 3178-3180.

(d) S. L. Matthews, D. M. Heinekey *Inorg. Chem.* **2010**, *49*, 9746-9748.

[5] A. Volbeda, E. Garcin, C. Piras, A. L. de Lacey, V. M. Fernandez, E. C. Hatchikian, M. Frey, J. C. Fontecilla-Camps *J. Am. Chem. Soc.* **1996**, *118*, 12989-12996.

[6] (a) D. W. Mulder, E. M. Shepard, J. E. Meuser, N. Joshi, P. W. King, M. C. Posewitz, J. B. Broderick, J. W. Peters *Structure* **2011**, *19*, 1038-1052.

(b) J. C. Fontecilla-Camps, A. Volbeda, C. Cavazza, Y. Nicolet *Chem. Rev.* **2007**, *107*, 4273-4303.

(c) I. Sumner, G. A. Voth *J. Phys. Chem. B* **2012**, *116*, 2917-2926.

[7] H. Ogata, W. Lubitz, Y. Higuchi *Dalton Trans.* **2009**, *37*, 7577-7587.

[8] (a) M. Rakowski DuBois, D. L. DuBois *Chem. Soc. Rev.* **2009**, *38*, 62-72.

(b) M. Rakowski DuBois, D. L. DuBois *Acc. Chem. Res.* **2009**, *42*, 1974–1982.

(c) J. Y. Yang, R. M. Bullock, M. Rakowski DuBois, D. L. DuBois *MRS Bulletin* **2011**, *36*, 39-47.

[9] J. Y. Yang, R. M. Bullock, W. J. Shaw, B. Twamley, K. Fraze, M. Rakowski DuBois, D. L. DuBois *J. Am. Chem. Soc.* **2009**, *131*, 5935-5945.

[10] Includes a crystal structure of a manganese hydride with a protonate amine in the ligand: E. B. Hulley, K. D. Welch, A. M. Appel, D. L. DuBois, R. M. Bullock *J. Am. Chem. Soc.* **2013**, *135*, 11736-11739.

[11] ^{15}N-labelled species allowed spectroscopic observation of the movement of protons from the second coordination sphere to the first coordination sphere based on their interaction with the pendant amines (Figure 2 of cited paper). E. S. Wiedner, A. M. Appel, D. L. DuBois, R. M. Bullock *Inorg. Chem.* **2013**, *52*, 14391-14403.

[12] T. He, N. P. Tsvetkov, J. G. Andino, X. Gao, B. C. Fullmer, K. G. Caulton *J. Am. Chem. Soc.* **2010**, *132*, 910-911.

[13] H. Fan, B. C. Fullmer, M. Pink, K. G. Caulton *Angew. Chem. Int. Ed.* **2008**, *47*, 9112-9114.

[14] C. Tsay, J. C. Peters *Chem. Sci.* **2012**, *3*, 1313-1318.

[15] W. H. Harmon, T.-P. Lin, J. C. Peters *Angew. Chem. Int. Ed.* **2014**, *53*, 1081-1086.

[16] O. R. Luca, J. D. Blakemore, S. J. Konezny, J. M. Praetorius, T. J. Schmeier, G. B. Hunsinger, V. S. Batista, G. W. Brudvig, N. Hazari *Inorg. Chem.* **2012**, *51*, 8704-8709.

[17] C. J. Moulton, B. L. Shaw *J. Chem. Soc., Dalton Trans.* **1976**, *11*, 1020-1024.

[18] D. Morales-Morales, C. M. Jensen *The Chemistry of Pincer Compounds* Elsevier Science, **2007**.

[19] D. S. Moore, S. D. Robinson *Chem. Soc. Rev.* **1983**, *12*, 415-452.

[20] ORTEP for Windows 2013. L. J. Farrugia *J. Appl. Cryst.* **2012**, *45*, 849-854.

[21] (a) D. G. Hamilton, R. H. Crabtree *J. Am. Chem. Soc.* **1988**, *110*, 4126-4133.

(b) K. A. Earl, G. Jia, P. A. Maltby, R. H. Morris *J. Am. Chem. Soc.* **1991**, *113*, 3027-3039.

(c) R. H. Morris, R. J. Wittebort *Mag. Res. Chem.* **1997**, *35*, 243-250.

[22] D. M. Heinekey, M. H. Voges, D. M. Barnhart *J. Am. Chem. Soc.* **1996**, *118*, 10792-10802.

[23] R. A. Bernheim, B. J. Lavery *J. Chem. Phys.* **1965**, *42*, 1464.

[24] I. Göttker-Schnetmann, P. White, M. Brookhart *Organometallics* **2004**, *23*, 1766-1776.

[25] I. Wender, R. A. Friedel, M. Orchin *J. Am. Chem. Soc.* **1949**, *71*, 1140.

[26] (a) B. J. Boro, E. N. Duesler, K. I. Goldberg, R. A. Kemp *Inorg. Chem.* **2009**, *48*, 5081-5087.

(b) B. J. Boro, D. A. Dickie, K. I. Goldberg, R. A. Kemp *Acta Cryst.* **2008**, *E64*, m1304.

[27] I. Göttker-Schnetmann, P. White, M. Brookhart *J. Am. Chem. Soc.* **2004**, *126*,1804-1811.

[28] S. Chakraborty, J. A. Krause, H. Guan *Organometallics* **2009**, *28*, 582-586.

Chapter 4. Reactivity of Nickel Pincer Complexes.

4.1 Introduction. Throughout our studies of the nickel dihydrogen complexes discussed in Chapter 3, we investigated several other nickel pincer complexes. This chapter will provide a summary of the reactivity of the dihydrogen complexes and the characterization data for a few novel compounds.

Nickel pincer complexes have been of increasing interest for homogeneous catalysis. Employing an earth-abundant, inexpensive first-row metal is desirable. Additionally, the pincer ligands provide thermal stability to the catalyst. Further, functionalization of the backbone of the ligand provides a possible molecular tether.[1] In addition to the hydrogen production work discussed in Chapter 3.4,[2] Guan and co-workers have recently developed systems for the hydrosilylation of aldehydes and ketones,[3] as well as CO_2 reduction using Ni pincer complexes.[4]

4.2 Heterolytic Cleavage of the H_2 ligand. The interaction between a dihydrogen molecule and a transition metal complex often activates the H_2 toward heterolytic cleavage.[5] The pK_a of free H_2 is around 35 in non-aqueous solvents,[6] but ligation of H_2 to a Lewis acidic metal center can significantly reduce the pK_a. In our studies, we have shown that [(^{tBu}PCP)Ni(H_2)][B(C_6F_5)$_4$] (**3-2**) readily protonates triethylamine (Scheme 4-1), indicating that the complex is more acidic that triethylammonium in fluorobenzene. The neutral nickel hydride complex, (^{tBu}PCP)NiH (**4-1**), was previously synthesized by treatment of (^{tBu}PCP)NiH with 100-fold excess of $NaBH_4$ in refluxing ethanol.[7] Alternatively, deprotonation of dihydrogen complex **3-2** cleanly forms **4-1**, and it can be isolated from the reaction mixture by removing the solvent in vacuo and extracting into pentane. The formation of the hydride species **4-1** was confirmed by ^{31}P{^{1}H} NMR spectroscopy and observation of the signal for the hydride at -10.0 ppm in the ^{1}H NMR spectrum in C_6D_6.

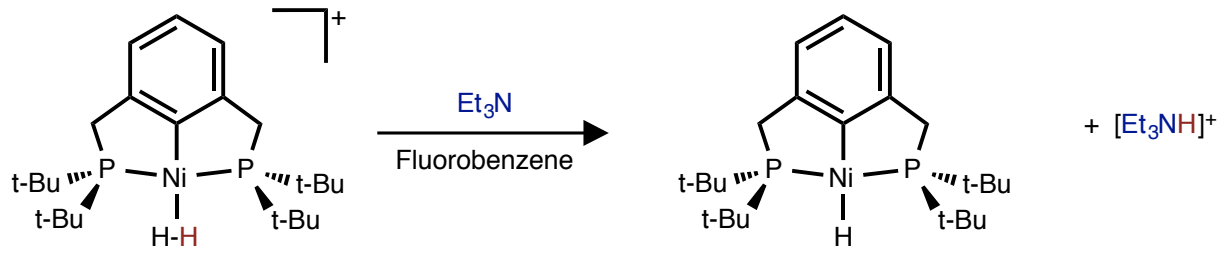

3-2 **4-1**

Scheme 4-1. Heterolytic cleavage of dihydrogen to generate (^{tBu}PCP)NiH. Triethylamine is readily protonated by the dihydrogen complex, indicating that **3-2** is more acidic that $[Et_3NH]^+$.

4.3 Dinitrogen Complexes. Examples of Ni^{II} dinitrogen complexes are rare. The first examples could only be identified *in situ* by IR spectroscopy.[8] Isolable and structurally characterized examples are limited to the tetrapodal cation described by Tsay & Peters in their dihydrogen chemistry[9] and an NNN pincer complex characterized by Budzelaar[10] (Figure 4-1).

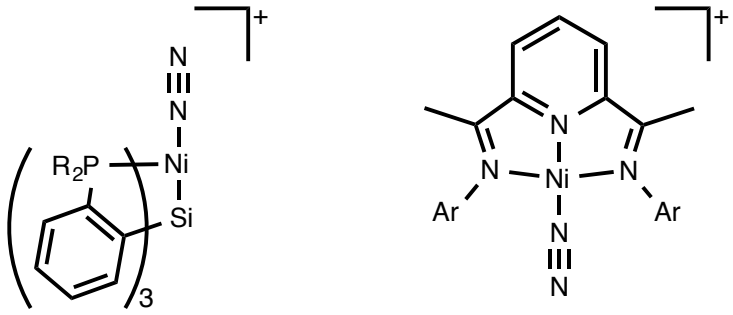

Figure 4-1. Structurally characterized Ni^{II} dinitrogen complexes (a) Peters,[9] R = Ph, ^{i}Pr (b) Budzelaar,[10] Ar = 2,6-diisopropylphenyl.

4.3.1 $[(^{tBu}PCP)Ni(N_2)][B(C_6F_5)_4]$ (4-2).

4.3.1a Synthesis. In the work from Peters' group, the dinitrogen complex is a synthetic intermediate in the dihydrogen complex preparation (Scheme 3-3). As such, we anticipated that treatment of **3-2** with dinitrogen would not displace the hydrogen ligand. Experimentally, a solution of **3-2** was degassed, and one atmosphere dry N_2 was added to the headspace of the NMR tube. A new complex was observed to be in equilibrium with the dihydrogen complex by $^{31}P\{^{1}H\}$ NMR spectroscopy. The new signal at 90 ppm was attributed to $[(^{tBu}PCP)Ni(N_2)][B(C_6F_5)_4]$, (**4-2**). Despite the decrease in the amount of H_2 present in the reaction mixture that resulted from degassing the solution, the solution contained **3-2** and **4-2** in approximately a 2:1 ratio. Figure 4-2 shows the $^{31}P\{^{1}H\}$ NMR spectrum following introduction of 1 atm N_2, and over 24 hours to reach equilibrium.

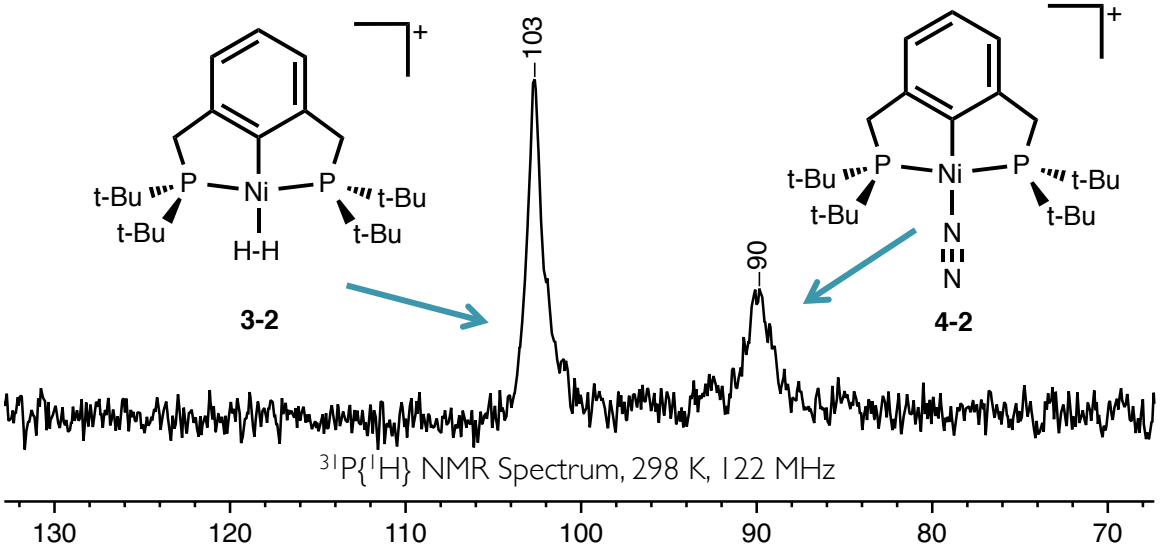

Figure 4-2. $^{31}P\{^{1}H\}$ NMR Spectrum at 298 K and 122 MHz of a fluorobenzene solution containing [(^{tBu}PCP)Ni(H_2)][$B(C_6F_5)_4$] (**3-2**) in equilibrium with [(^{tBu}PCP)Ni(N_2)][$B(C_6F_5)_4$] (**4-2**). The dihydrogen complex is observed at 103 ppm, and the dinitrogen complex is observed at 90 ppm. This sample also contains (^{tBu}PCP)NiCl starting material (not pictured). Data from sjconnel/300/SJC4_042612_1.

Independent synthesis of the dinitrogen complex in a preparation analogous to that employed in the preparation of **3-2** resulted in isolation of complex **4-2** (Scheme 4-2).

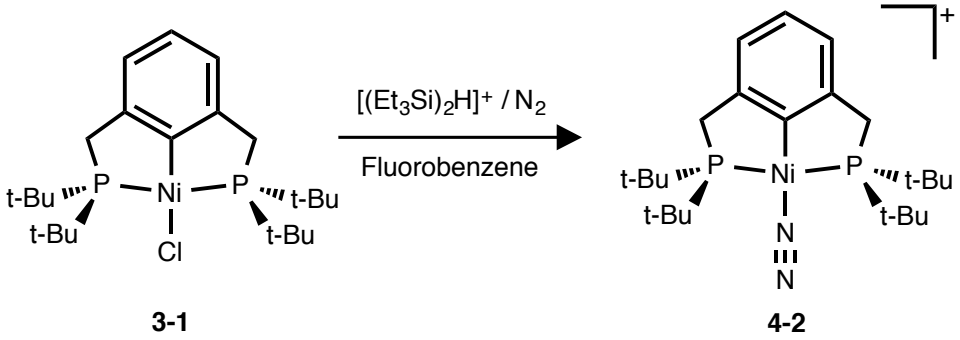

Scheme 4-2. Synthesis of [(^{tBu}PCP)Ni(N_2)][$B(C_6F_5)_4$] (**4-2**).

4.3.1b Structure. A solution of **4-2** in fluorobenzene was layered with alkane solvent, and crystals precipitated. The X-ray structure is shown in Figure 4-3. The dinitrogen ligand maintains a bond length nearly equivalent to that in free N_2. In the absence of H_2 ligand, the $^{31}P\{^{1}H\}$ NMR spectrum contains one sharp resonance at 90 ppm.

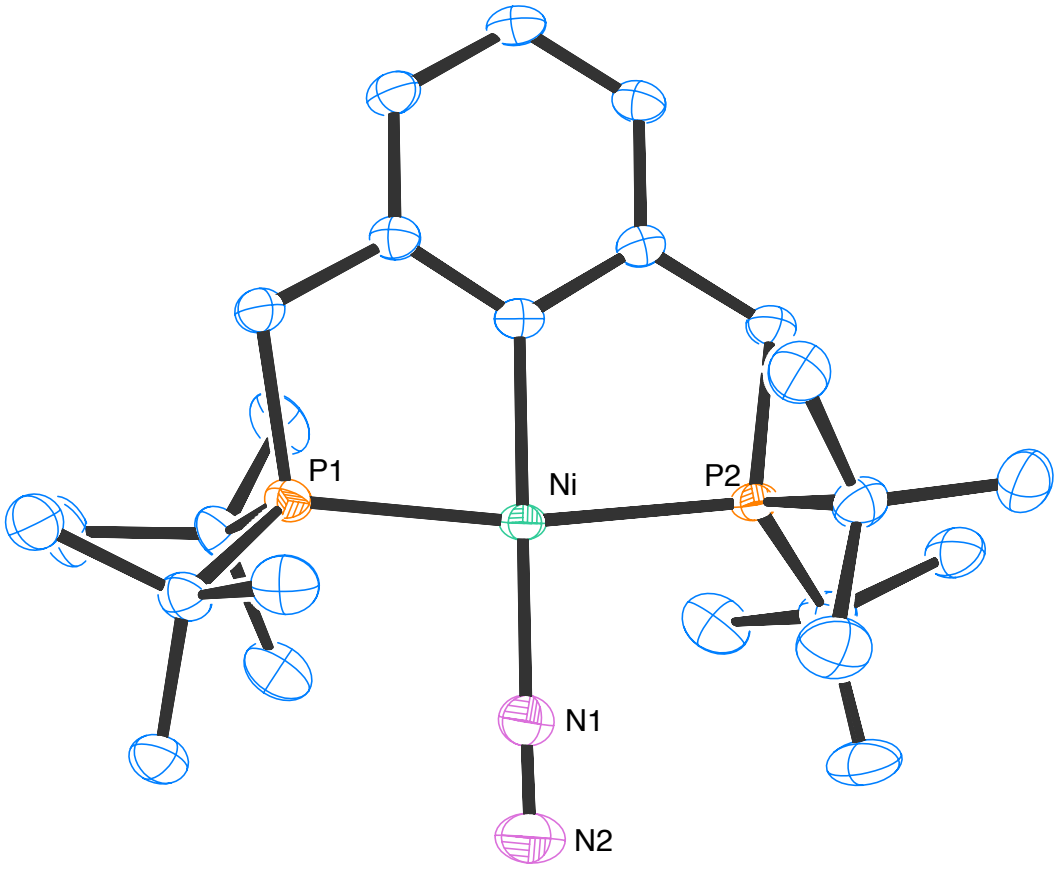

Figure 4-3. ORTEP[11] of [(^{tBu}PCP)Ni(N_2)][$B(C_6F_5)_4$] (**4-2**). The dinitrogen ligand is not activated. The N-N bond length is the same (within error) of free dinitrogen (1.099 Angstroms). Hydrogen atoms, the [$B(C_6F_5)_4$] counteranion, and a disordered pentane solvent molecule have been omitted for clarity. Data from Heinekey/Samantha/sjc07.

4.3.2 [(^{tBu}POCOP)Ni(N_2)][$B(C_6F_5)_4$] (4-3). The procedure was repeated using (^{tBu}POCOP)NiCl (**3-3**) as the starting material. Reaction of [$(Et_3Si)_2H$][$B(C_6F_5)_4$] (**2-2**) with **3-3** in fluorobenzene under one atmosphere dry N_2 (

Scheme 4-3) resulted in the observation of NMR signals associated with a new species. The $^{31}P\{^1H\}$ NMR signal at 205 ppm corresponded to signals for metallated t-butyl groups observed at 1.25 ppm in the ^1H NMR spectrum (as assigned by ^1H-^{31}P HMQC 2D NMR spectroscopy).

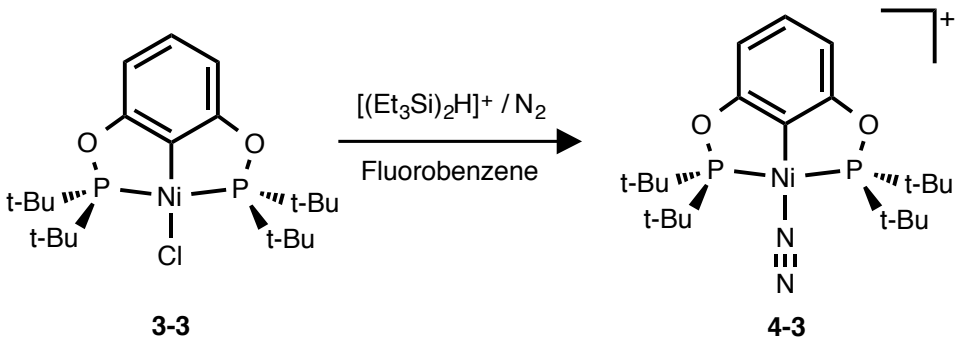

3-3 **4-3**

Scheme 4-3. Synthesis of [(^{tBu}POCOP)Ni(N_2)][$B(C_6F_5)_4$] (**4-3**).

Contrary to that observed for the conversion of [(^{tBu}PCP)Ni(H_2)][$B(C_6F_5)_4$] (**3-2**) to **4-2**, degassing of a solution of **3-5** followed by addition of N_2 results in complete conversion to the dinitrogen species (**4-3**). Despite layering this solution with alkane solvent, no crystalline solid was obtained.

4.4 [(^{tBu}PCP)Ni(CO)][$B(C_6F_5)_4$] (4-4). Moulton & Shaw reported the preparation of [(^{tBu}PCP)Ni(CO)][BPh_4] in 1976.[12] Treatment of an ethanol solution of (^{tBu}PCP)NiCl with carbon monoxide and Na[BPh_4] resulted in the carbonyl complex. We were optimistic that employing Na[BPh_4] as a chloride-abstraction reagent would afford a reactive 3-coordinate intermediate capable of cleanly generating complexes **3-2** and **4-2**, as well as other desired species. Instead, no reaction occurs without CO present, indicating that the reaction proceeds via an associative mechanism.

Addition of one atmosphere of carbon monoxide to the headspace of the reaction vessel rapidly and completely displaces H_2 from **3-2** to form [(^{tBu}PCP)Ni(CO)][$B(C_6F_5)_4$] (**4-4**) (Scheme 4-4). The CO stretching frequency was obtained from a KBr pellet using FT-IR spectroscopy. The stretching frequency was decreased from 2143 cm^{-1} in free CO to 2046 cm^{-1} when ligated.

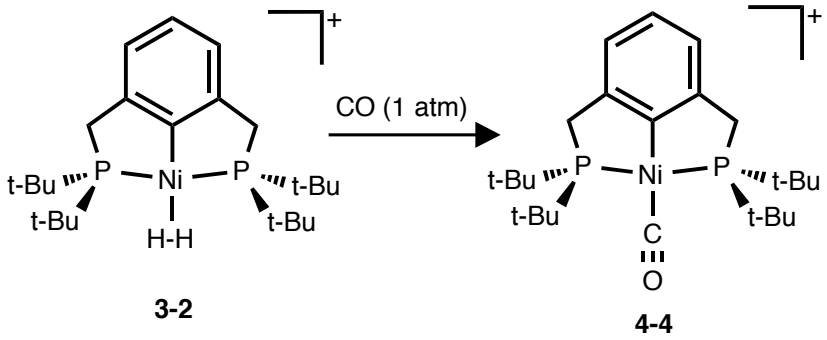

Scheme 4-4. Facile ligand exchange occurs when a solution of **3-2** is exposed to carbon monoxide. The carbonyl complex is observed as the only product.

Dinitrogen and carbonyl stretching frequencies have been used to predict whether the transition metal fragment will bind H_2 as a ligand or promote oxidative addition to generate the dihydride species. Morris & co-workers suggested that the $\nu(N_2)$ for complexes that bind H_2 is between 2060-2150 cm^{-1}, and that the corresponding $\nu(CO)$ is approximately 1860-1960 cm^{-1}.[13] For our complex, the much higher CO stretching frequency (2065 cm^{-1}) suggests back-bonding to the ligand is minimal, which is consisten with the fairly short d_{HH} found in the H_2 complex.

4.5 [(^{tBu}POCOP)Ni]$^+$: Evidence for an Agostic Complex. The interaction between an unsaturated metal center and a covalent C-H bond of its ligand is termed an "agostic" interaction.[14] Many complexes of this nature have been identified by X-ray crystallography, neutron diffraction experiments, and NMR spectroscopy.[15] These complexes often form highly-colored solutions. In addition, the interaction can be characterized by diminished C-H coupling constants. Crystallographically, metal-carbon distances of approximately 2.5 – 3.0 Angstroms can indicate the presence of an agostic interaction.[16]

If no small molecule ligand is introduced following chloride abstraction from (^{tBu}POCOP)NiCl (**3-3**), the solution is very dark red in color. Alternatively, thoroughly degassing a solution of [(^{tBu}POCOP)Ni(H_2)]$^+$ **3-5** results in a similarly dark-colored solution (Scheme 4-5).

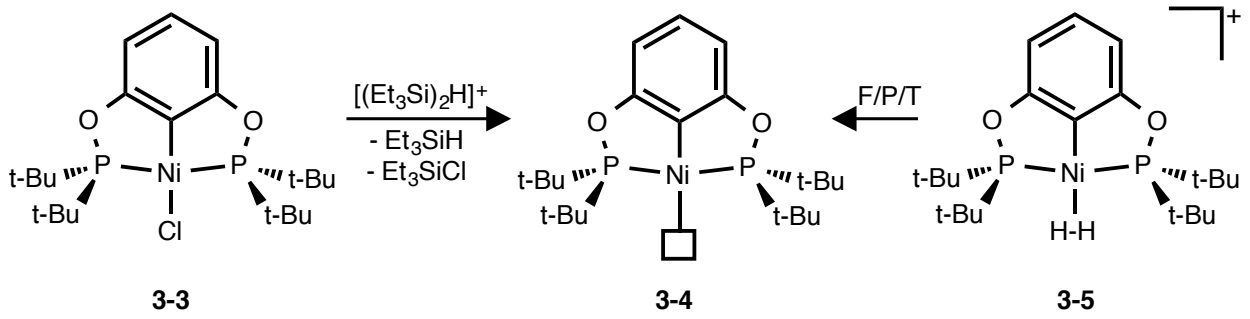

Scheme 4-5. Chloride abstraction from (^{tBu}POCOP)NiCl (**3-3**) or throroughly degassing a solution of [(^{tBu}POCOP)Ni(H_2)]$^+$ (**3-5**) both result in a dark-colored solution with matching $^{31}P\{^1H\}$ NMR spectra. F/P/T = freeze/pump/thaw cycle, a common procedure for degassing solutions.

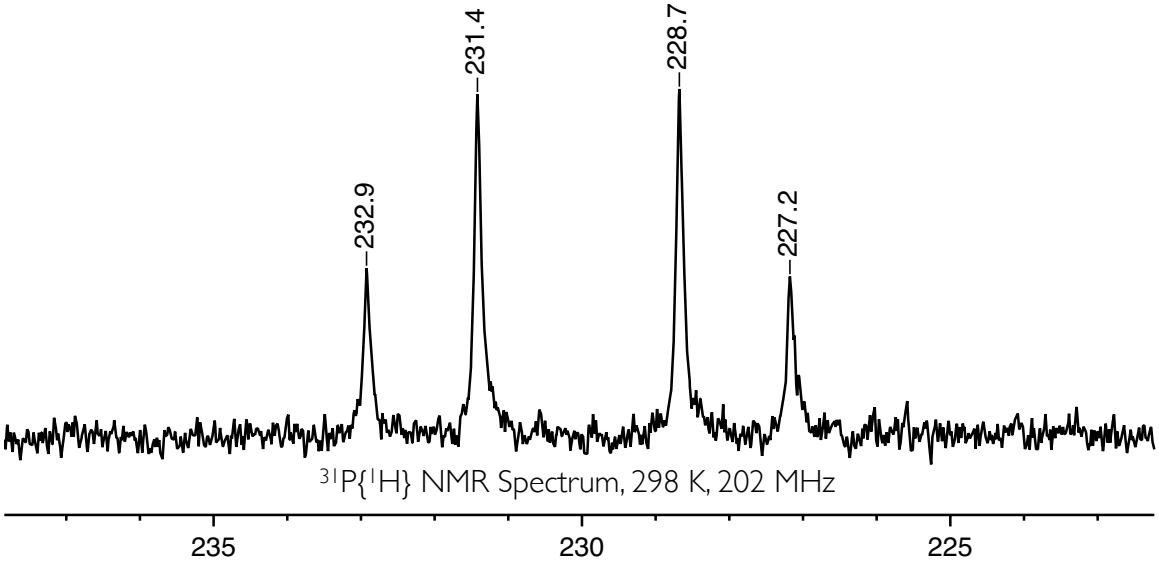

Figure 4-4. $^{31}P\{^1H\}$ NMR spectrum at 298 K (202 MHz) for a reaction mixture containing intermediate **3-4**. Data from sjconnel/499/SJC5_100312_2/Experiment 2. This sample also contains a signal for [(^{tBu}POCOP)Ni(H_2)][$B(C_6F_5)_4$] (**3-5**) (further degassing removed this signal), some (^{tBu}POCOP)NiCl (**3-3**) starting material, and an unidentified $^{31}P\{^1H\}$ NMR signal at 85 ppm. Data from 499/sjconnel/SJC5_100312_3, Experiment 2.

The $^{31}P\{^1H\}$ NMR spectra of these solutions show a second order doublet of doublets (Figure 4-4). This spectrum is attributed to two chemically inequivalent phosphorous atoms coupled to one another. We believe this species to be an agostic complex where a C-H bond of a t-butyl substituent on the ^{tBu}POCOP ligand is interacting with the fourth coordination site of nickel (Figure 4-5).

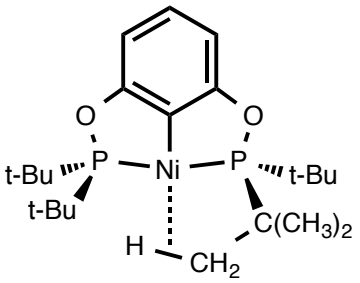

Proposed Structure of 3-4

Figure 4-5. Proposed structure of intermediate **3-4**. To account for the 2 inequivalent phosphorous signals in the $^{31}P\{^{1}H\}$ NMR spectrum, an agostic interaction between the open coordination site at the metal with one set of the t-butyl substituents is proposed. It is anticipated that there is fast (on the NMR time scale) exchange between C-H bonds of the t-butyl substituents, but that exchange from "side to side" between the t-butyl groups is slow on the NMR time scale.

The phosphorous atoms would then be chemically inequivalent (resulting in a different chemical shift), and each would be capable of coupling to the other (resulting in the observed doublet). The spectrum was simulated using gNMR software to determine the actual coupling constant between the two ^{31}P nuclei (J_{PaPb}) is approximately 300 Hz.[17] This suggests the phosphorous atoms remain *trans* to one another. $J_{PP'}$ for phosphorous atoms *cis* to one another are generally much smaller (~ 50 Hz or smaller), but *trans* phosphorous atoms exhibit large coupling constants (> 250 Hz).[18] In the example from Caulton & coworkers, where the pincer ligand distorts to make the phosphorous atoms inequivalent (Figure 4-6), The $J_{PP'}$ coupling constant is diminished to 38 Hz, indicating that the phosphorous arms are no longer *trans* to one another.

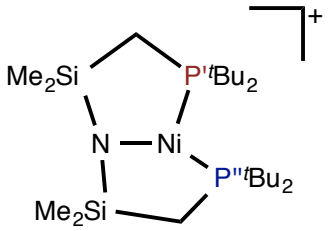

Figure 4-6. Three-coordinate Ni^{II} pincer complex reported by Caulton and co-workers.[18] The two phosphorous atoms have been shown crystallographically to be no longer *trans* to one another, resulting in a decreased $J_{P'P''}$ of 38 Hz. This is much smaller than the > 250 Hz expected if the phosphorous atoms were still *trans* to one another.

H. Mayer & co-workers reported an Ir(pincer) complex which has been crystallographically shown to have a close contact between the metal and C-H bond of the t-butyl substituent (Figure 4-7). By NMR spectroscopy, the phosphorous atoms are chemically inequivalent, but remain mutually *trans* to one another. Similar to our complex, the

^{31}P nuclei couple with $J_{PP'}$ = 350 Hz.[19] Also consistent with our complex, no separate resonances are observed for a proton interacting closely with the metal center. We anticipate this is due to fast exchange between all of the t-butyl protons. There is precedent for C-H agostic complexes of ^{tBu}PCP ligands with exchange so rapid such that the ^{31}P nuclei are equivalent at room temperature.[20]

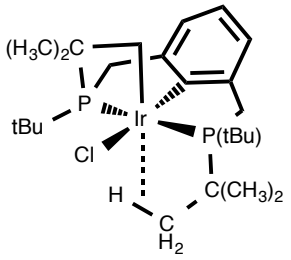

Figure 4-7. Agostic complex reported by H. Mayer & co-workers.[19] One t-butyl substituent cyclometallates to the iridium, but the second just forms an agostic complex, where the C-H bond is not cleaved.

Complex **3-4** was never synthesized in 100% purity. As such, overlapping signals from tBu substituents in impurities were present, and no identification of decreased C-H coupling constants or new signals for C-*H*•••M could be identified by ^{1}H NMR spectroscopy. Crystalline material could not be isolated.

4.6 Experimental Details.

General Considerations. All experiments were carried out under argon by using Schlenk and glove-box techniques. Solvents were dried and vacuum transferred immediately prior to use. Reagents and compounds not synthesized elsewhere in this thesis were obtained from commercial sources and used as received.

NMR spectra were recorded at 298 K (unless otherwise noted) on Bruker AV500 or DRX500 spectrometers. ^{1}H NMR chemical shifts are reported relative to residual resonances of the solvent : C_6D_5H (7.16 ppm), C_6D_4HF (6.96, 6.99, 7.17 ppm). Some ^{1}H NMR spectra were recorded in protiofluorobenzene by using a solvent-suppression pulse program. $^{31}P\{^{1}H\}$ NMR chemical shifts were externally referenced to H_3PO_4 (85 % in H_2O; 0.00 ppm).

(^{tBu}PCP)NiH (4-1).

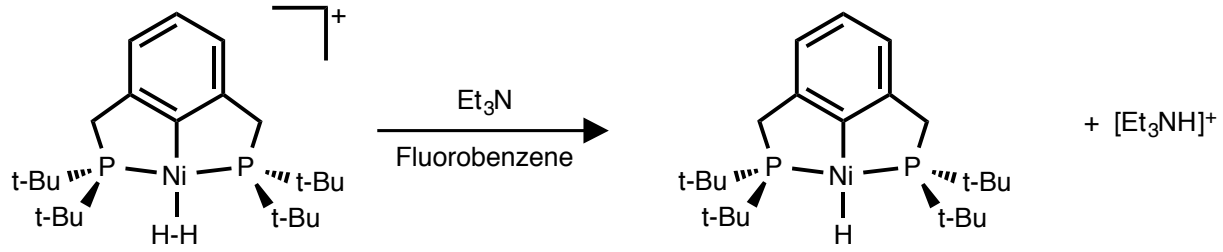

3-2 **4-1**

Compound **4-1** was previously prepared by Boro, et al.[7] The synthetic procedure requires multiple additions of large excesses of $NaBH_4$. Our preparation demonstrated that the dihydrogen ligand is activated toward heterolytic cleavage (relative to free H_2), and gave complete and clean conversion of the dihydrogen complex to **4-1**.

Triethylamine (1 mg, 0.010 mmol, 0.0015 mL) was added to a solution of **3-2** (0.010 g, 0.009 mmol) in fluorobenzene (0.5 mL). The solution paled considerably to a buttery yellow. The solvent was removed *in vacuo*. The resulting solid was extracted with pentane (sonication was required). The solution was isolated from the triethylammonium salt. Removing the pentane *in vacuo* isolated **4-1**.

^{1}H NMR (500 MHz, C_6H_5F, 298 K): 3.38 ppm (s, 4H, CH_2), 1.29 (vt, 36H, *t*Bu-CH_3, apparent J_{PH} = 5Hz), -10.1ppm (t, J_{PH} = 53Hz, 1H, Ni-*H*)

^{31}P{^{1}H} NMR (202 MHz, C_6H_5F; 298 K): 99 ppm

Crystal structure of **4-1** reported by Boro, *et al.*[7]

$[(^{tBu}PCP)Ni(N_2)][B(C_6F_5)_4]$ (4-2).

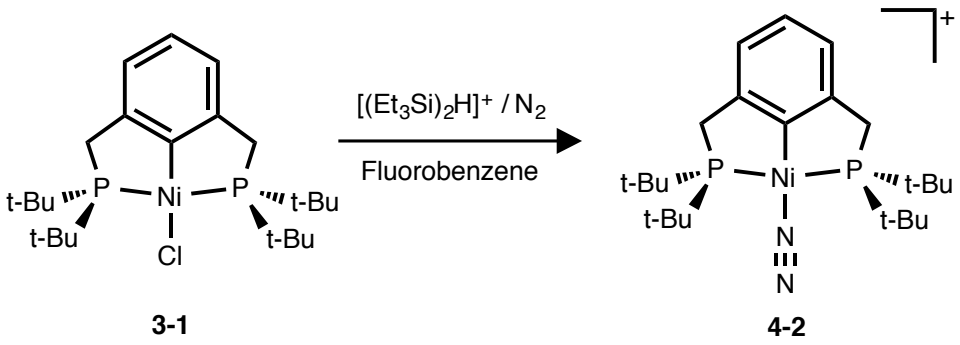

3-1 **4-2**

(^{tBu}PCP)NiCl (**3-1**) (15 mg, 30 mmol) was combined with $[(Et_3Si)_2H][B(C_6F_5)_4]$ (**2-2**) (28 mg, 30 mmol) in a silylated glass vessel. Fluorobenzene (ca. 0.5 mL) was added by vacuum transfer, and a dark red brown solution resulted. The solution was frozen (liquid nitrogen), the headspace evacuated, and N_2 gas (1 atm) was introduced. Upon thawing, the solution became golden yellow. The solution was again frozen, the headspace evacuated, and pentane (ca. 1 mL) was added by vacuum transfer. Block crystals precipitated over 24–48 hours at room temperature. The solution was removed by cannula, and the solid was dried briefly *in vacuo*. Isolated yield (crystalline): 21 mg, 61 %.

^{1}H NMR (500 MHz, C_6H_5F; 298 K): 3.03 ppm (s, 4H, CH_2), 1.14 ppm (vt, 36H, *t*Bu-CH_3)

$^{31}P\{^1H\}$ NMR (202 MHz C_6H_5F; 298 K): 90 ppm

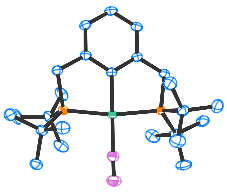

Crystal structure included as Figure 4-3. Data in Heinekey/Samantha/sjc07.

[($^{t\text{Bu}}$POCOP)Ni(N_2)][$B(C_6F_5)_4$] (4-3).

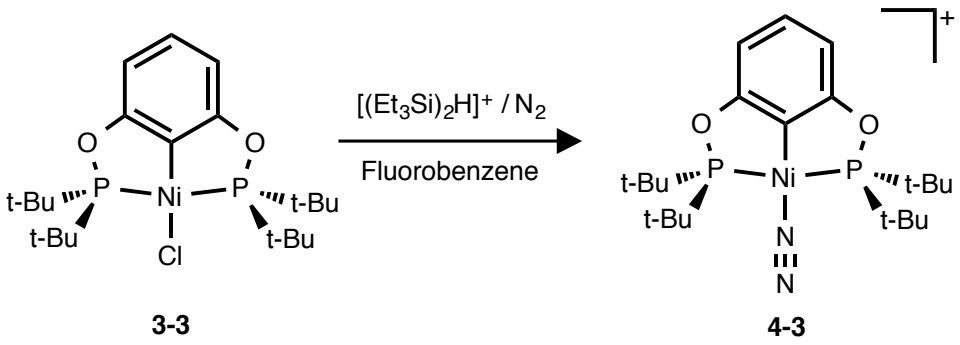

3-3 **4-3**

($^{t\text{Bu}}$POCOP)NiCl (**3-3**) (10 mg, 0.02 mmol) was combined with [$(Et_3Si)_2H$][$B(C_6F_5)_4$] (**2-2**) (18 mg, 0.02 mmol) in a silylated glass vessel. Fluorobenzene (ca. 0.5 mL) was added by vacuum transfer, and a dark red brown solution resulted. The solution was frozen (liquid nitrogen), the headspace evacuated, and N_2 gas (1 atm) was introduced. Upon thawing, the solution became golden yellow. No solid could be isolated from the reaction mixture. Layering with alkane solvent resulted in an oily product.

^{1}H NMR (500 MHz, C_6H_5F; 298 K): 1.25 ppm (vt, 36H, *t*Bu-CH_3), aromatics under solvent signal

$^{31}P\{^1H\}$ NMR (202 MHz C_6H_5F; 298 K): 205 ppm

NMR data from 300/sjconnel/SJC4_092412_1, Experiments 3 & 4

[(^{tBu}PCP)Ni(CO)][B(C_6F_5)$_4$] (4-4).

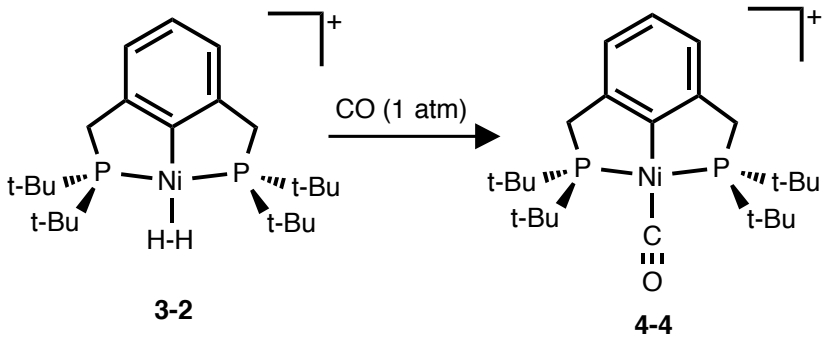

3-2 **4-4**

[(^{tBu}PCP)Ni(H_2)][B(C_6F_5)$_4$] (**3-2**) (15 mg, 13 mmol) was dissolved in fluorobenzene. The solution was frozen, evacuated, and the headspace was filled with CO (1 atm). Upon shaking, the solution paled to light yellow. Addition of alkane solvent with shaking precipitated a pale yellow solid. Isolated yield (crude): 10 mg, 66%.

^{1}H NMR (500 MHz, C_6H_5F, 298 K):	3.25 ppm (s, 4H, CH_2), 1.08 ppm (vt, 36H, *t*Bu-CH_3)
$^{31}P\{^1H\}$ NMR (202 MHz, C_6H_5F, 298 K):	106 ppm
IR (KBr): ν(CO)	2065 cm^{-1}

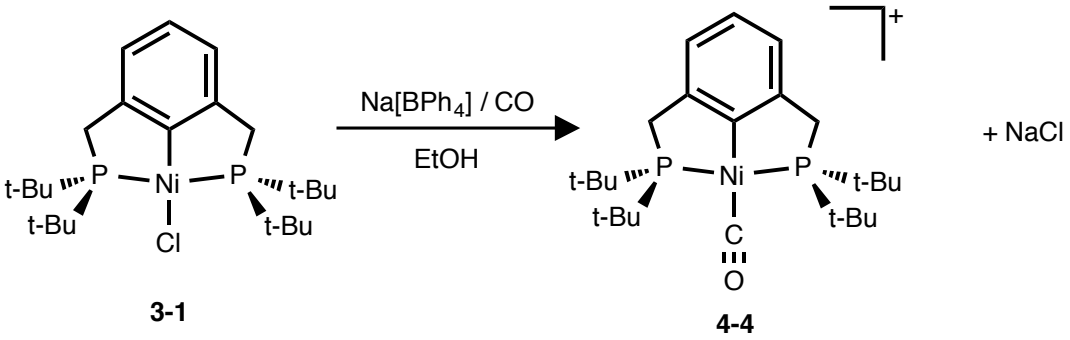

3-1 **4-4**

Alternatively, Moulton & Shaw[12] reported the preparation of cation **4-4** by chloride abstraction from **3-1** with Na[BPh_4] in ethanol. This reaction only proceeds in the presence of carbon monoxide, however, indicating the reaction proceeds *via* an associative mechanism, and that the chloride is not labilized by dissolution in polar solvent alone.

[(^{tBu}POCOP)Ni][$B(C_6F_5)_4$] (3-4).

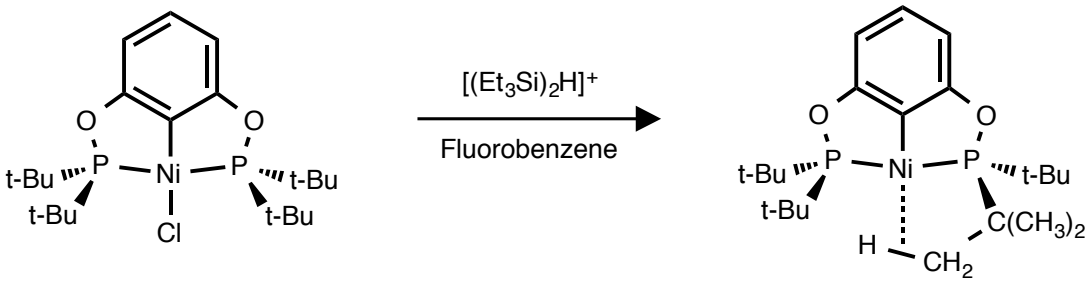

3-3 **Proposed Structure of 3-4**

(^{tBu}PCP)NiCl (**3-1**) (15 mg, 30 mmol) was combined with $[(Et_3Si)_2H][B(C_6F_5)_4]$ (**2-2**) (28 mg, 30 mmol) in a silylated glass vessel. Fluorobenzene (ca. 0.5 mL) was added by vacuum transfer, and a dark red brown solution resulted. The solution freeze/pump/thaw cycled to remove any hydrogen present from decomposition of **2-2**. The solution remained very highly colored.

^{1}H NMR (500 MHz, C_6H_5F; 298 K): (not assigned as ^{1}H NMR showed evidence of an exchange reaction)

^{31}P{^{1}H} NMR (202 MHz C_6H_5F; 298 K): 228 ppm, 232 ppm (roofed pair of doublets, $J_{PP'}$ = 300 Hz)

The same product was observed by ^{31}P{^{1}H} NMR when solutions of either **3-5** or **4-3** were thoroughly degassed. Addition of a small molecule to these reaction mixtures resulted in formation of primarily one ^{31}P{^{1}H} singlet (small impurities present.

References

[1] S. Chakraborty, H. Guan *Dalton Trans.* **2010**, *39*, 7427-7436.

[2] O. R. Luca, J. D. Blakemore, S. J. Konezny, J. M. Praetorius, T. J. Schmeier, G. B. Hunsinger, V. S. Batista, G. W. Brudvig, N. Hazari *Inorg. Chem.* **2012**, *51*, 8704-8709.

[3] S. Chakraborty, J. A. Krause, H. Guan *Organometallics* **2009**, *28*, 582-586.

[4] (a) S. Chakraborty, J. Zhang, J. A. Krause, H. Guan *J. Am. Chem. Soc.* **2010**, *132*, 8872-8873.

(b) F. Huang, C. Zhang, J. Jiang, Z.-X. Wang, H. Guan *Inorg. Chem*. **2011**, *50*, 3816-3825.

[5] G. J. Kubas *Catalysis Lett.* **2005**, *104*, 79-101.

[6] C. A. Kelly, D. R. Rosseinsky *Phys. Chem. Chem. Phys.* **2011**, *3*, 2086-2090. (Section 2.8)

[7] B. J. Boro, E. N. Duesler, K. I. Goldberg, R. A. Kemp *Inorg. Chem.* **2009**, *48*, 5081-5087.

[8] (a) C. W. DeKock, D. A. VanLeirsburg *J. Am. Chem. Soc.* **1972**, *94*, 3235-3237.

(b) H. Huber, E. P. Kündig, M. Moskovits, G. A. Ozin *J. Am. Chem. Soc.* **1973**, *95*, 332-344.

(c) G. A. Ozin, W. E. Kotzbücher *J. Am. Chem. Soc.* **1975**, *97*, 3965-3974.

(d) B. V. Lokshin, I. I. Greenwald *J. Mol. Struct.* **1990**, *222*, 11–20.

(e) A.J. Bridgeman, O. M. Wilkin, N. A. Young *Inorg. Chem. Commun.* **2000**, *3*, 681 – 684.

[9] C. Tsay, J. C. Peters *Chem. Sci.* **2012**, *3*, 1313-1318.

[10] D. Zhu, I. Thapa, I. Korobkov, S. Gambarotta, P. H. M. Budzelaar *Inorg. Chem.* **2011**, *50*, 9879–9887.

[11] ORTEP for Windows 2013. L. J. Farrugia *J. Appl. Cryst.* **2012**, *45*, 849-854.

[12] C. J. Moulton, B. L. Shaw *J. Chem. Soc., Dalton Trans.* **1976**, *11*, 1020-1024.

[13] R. H. Morris, K. A. Earl, R. L. Luck, N. J. Lazarowych, A. Sella *Inorg. Chem.* **1987**, *26*, 2674-2683.

[14] M. Brookhart, M. L. H. Green *J. Organomet. Chem.* **1983**, *250*, 395-408.

[15] Examples of agostic interactions of phosphine ligands:

(a) D. Huang, J. C. Huffman, J. C. Bollinger, O. Eisenstein, K. G. Caulton *J. Am. Chem. Soc.* **1997**, *119*, 7398-7399.

(b) W. Baratta, E. Herdtweck, P. Rigo *Angew. Chem. Int. Ed.* **1999**, *38*, 1629-1631.

(c) G. J. Kubas, R. R. Ryan, B. I. Swanson, P. J. Vergamini, H. J. Wasserman *J. Am. Chem. Soc.* **1984**, *106*, 451-452.

[16] M. Lein *Coord. Chem. Rev.* **2009**, *253*, 625-634.

[17] Simulations were done using *gNMR* software developed by P. H. M. Budzelaar, Version 5.1.

[18] H. Fan, B. C. Fullmer, M. Pink, K. G. Caulton *Angew. Chem. Int. Ed.* **2008**, *47*, 9112 –9114.

[19] H. A. Y. Mohammad, J. C. Grimm, K. Eichele, H.-G. Mack, B. Speiser, F. Novak, M. G. Quintanilla, W. C. Kaska, H. A. Mayer *Organometallics* **2002**, *21*, 5775-5784.

[20] M. E. van der Boom, M. A. Iron, O. Atasoylu, L. J. W. Shimon, H. Rozenberg, Y. Ben-David, L. Konstantinovski, J. M. L. Martin, D. Milstein *Inorg. Chim. Acta* **2004**, *357*, 1854-1864.

Chapter 5: A Dihydrogen Complex of Palladium

5.1 Introduction. Palladium is extensively used in homogeneous catalysis to effect organic transformations. Various phosphine-ligated species are responsible for a seemingly endless collection of cross-coupling reactions.[1] Palladium has been used extensively in hydrogenation catalysis as well. In industrial practices, palladium and platinum are widely employed for hydrogenation and dehydrogenation processes.[2] Despite this, there have been no reports of palladium dihydrogen complexes in the literature. In order to explore the differences in the group 10 metals, we set out to synthesize the palladium analogue of our nickel dihydrogen species.

5.2 The paucity of d^8 dihydrogen complexes. Since Kubas' discovery of the first dihydrogen complex in 1984, the vast majority of complexes studied have been d^6 metal complexes: Cr^0, Mo^0, W^0, Mn^{1+}, Re^{1+}, Fe^{2+}, Ru^{2+}, Rh^{3+}, and Ir^{3+}. These complexes were studied extensively,[3] and it was anticipated that the d^6 electron configuration lent some stability to the dihydrogen complex. The increased electron density of d^8 transition metal complexes was generally found to lead to oxidative addition of the hydrogen ligand to form octahedral d^6 dihydride complexes.[4] At the onset of our research, the d^8 metal dihydrogen complexes in the literature were limited to the following:

5.2.1. Group 9 d^8 Metal Dihydrogen Complexes.

5.2.1a Cobalt(I) Dihydrogen Complexes. Previous work in the Heinekey group by Hebden & St. John reported the first cobalt dihydrogen complex.[5] The complex, (^{tBu}POCOP)Co(H_2), could not be synthesized by simple chloride-abstraction from the metal-halide complex. The synthesis was achieved using a sodium amalgam to abstract the halide from the metal center and reduce the complex. Interestingly this formed a bridging Co-Hg-Co species, identified by X-ray crystallography. Addition of H_2 then resulted in formation of the dihydrogen complex. Increased pressures of hydrogen led to formation of a Co^{III} (d^6) dihydrogen-dihydride complex, stable only at low temperatures (Scheme 5-1).

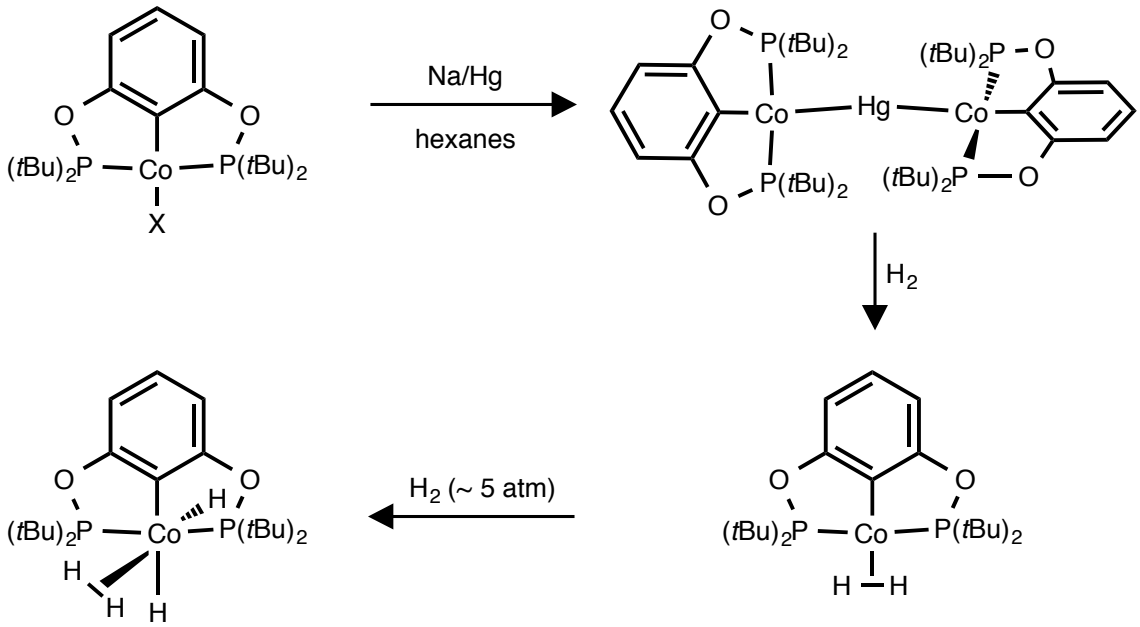

Scheme 5-1. Synthesis of the first reported cobalt dihydrogen complexes. The intermediate species in the preparation is a rare mercury-bridged dimer. Increased pressures of hydrogen result in oxidative addition of the ligand to give a dihydrogen-dihydride species.

Subsequent work by Peters, *et al.* developed cobalt complexes similar to those they reported for nickel (Figure 5-1).[6a] The silyl-ligated complex is diamagnetic and was characterized using standard NMR techniques. In contrast, the boryl-ligated species is paramagnetic. EPR spectroscopy confirmed the identity of the species, and the complex was characterized in the solid state by X-ray crystallography. Additionally, Peters and co-workers have reported hydridoborate complexes of cobalt that may be in equilibrium with dihydrogen-ligated species, as 2 equivalents of hydrogen can be reversibly added to the complex.[6b]

Figure 5-1. Cobalt dihydrogen complexes reported by Peters and coworkers. The silyl-ligated complex is diamagnetic, but the boryl-ligated species is a very rare paramagnetic dihydrogen complex. It was characterized using EPR spectroscopy, observation of the paramagnetic-shifted NMR spectrum, as well as X-ray crystallography.

In 1988, Bianchini and coworkers reported the characterization of a dihydrogen complex.[7] Strong HD coupling was observed, and the system was proposed to be a rapidly equilibrating between a dihydrogen and dihydride complex. Instead, later work by Heinekey & co-workers confirmed that the resulting complex was a dihydride species. T_1(min) for the hydride resonance was near 100 milliseconds.[8] Despite this correction to the literature, later reports by Peters[6a] and Beller[9] both incorrectly identify Bianchini's complex as a dihydrogen complex.

5.2.1b Rhodium (I) Dihydrogen Complexes. Moving down Group 9, there are a handful of rhodium(I) dihydrogen complexes characterized in the literature. A 1983 report from the Kaska and coworkers[10] (prior to Kubas' work) suggests that dihydrogen may be interacting with a rhodium pincer complex, but this was not fully characterized until 1997.[11] The complex, (^{tBu}PCP)Rh(H_2), was definitively assigned to have a dihydrogen ligand by solution NMR spectroscopy. Other examples of rhodium dihydrogen complexes include the cationic [(^{tBu}PNP)Rh(H_2)]$^+$,[12] [(^{tBu}PONOP)Rh(H_2)]$^+$,[13] and a PCP-pincer complex where the *ipso*-carbon atom is sp^3-hybridized, (sp^3-PCP)Rh(H_2)[14] where ^{tBu}PNP = 2,6-bis-[di-t-butylphosphino)methyl]pyridine, ^{tBu}PONOP = 2,6-(tBu$_2$PO)$_2$C$_5$H$_3$N, sp^3-PCP = CH(CH$_2$CH$_2$P(^{t}Bu))$_2$ (Figure 5-2).

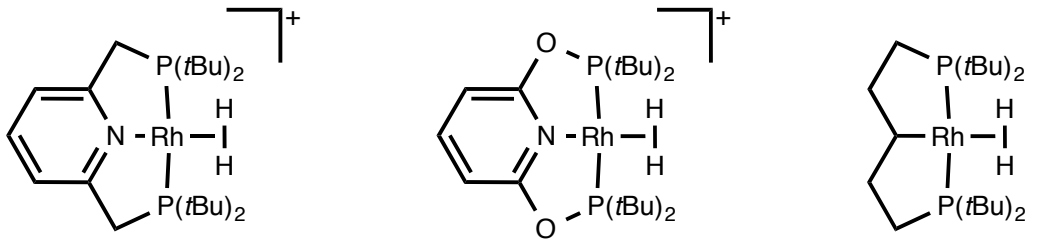

Figure 5-2. Rhodium dihydrogen complexes (of ligands other than ^{tBu}PCP) reported in the literature.

5.2.1c Iridium(I) Dihydrogen Complexes. Iridium(I) dihydrogen complexes are extremely limited. A series of pincer complexes was determined to exist as an equilibrium mixture of the dihydrogen complex and a dihydride-solvent complex in solution.[15] The tBuPOCOP ligands were substituted with electron-withdrawing substituents at the para-position of the phenyl ring. Only the most electron-deficient complex disfavored formation of the dihydride complex (Figure 5-3).

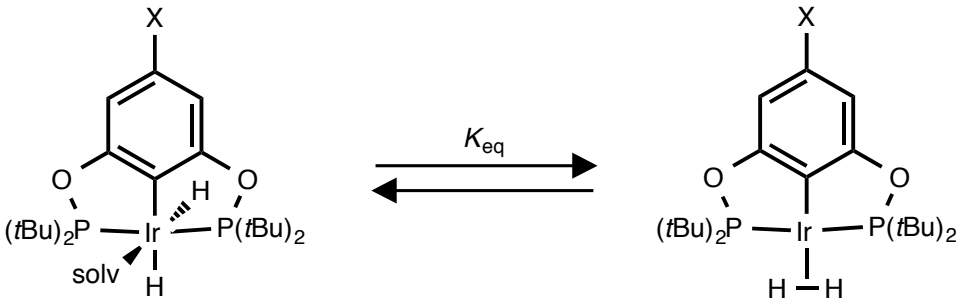

Figure 5-3. The composition of a solution of (^{tBu}POCOP-X)IrH_2 was determined to be solvent and temperature dependent. The species exists as an equilibrium mixture between a dihydride-solvent complex and a dihydrogen complex for X = H, MeO, Me, F, C_6F_5, and 3,5-$(CF_3)_2$-C_6H_3. Only the 3,5-$(CF_3)_2$-C_6H_3-substituted species favored the dihydrogen complex.

5.2.2 Group 10 d^8 Metal Dihydrogen Complexes. As was discussed in Chapter 3, dihydrogen complexes of Group 10 metals were exceedingly rare prior to the start of this work.

5.2.2a Nickel(II) and Palladium(II) Dihydrogen Complexes. Chapter 3 discusses the only nickel dihydrogen complex in the literature prior to 2012,[16] those developed for this thesis,[17] as well as those reported in the past couple of years.[18] This chapter (Chapter 5) will discuss the first dihydrogen complex of palladium, as well as a prior, unsuccessful attempt.

5.2.2b Platinum(II) Dihydrogen Complexes. In the mid- to late- nineties, a few dihydrogen complexes of platinum were reported. These complexes all contained two phosphine ligands and a dihydrogen ligand *trans* to an X-type ligand (hydride,[19,20] methyl,[19b] phenyl[19b]). These complexes are shown in Figure 5-4. $[(Cy_3P)_2PhPt(H_2)]^+$ is closely related to a pincer platinum dihydrogen complex reported in 2002, $[(^{tBu}PCP)Pt(H_2)]^+$.[21] These complexes are compared in Table 5-1.

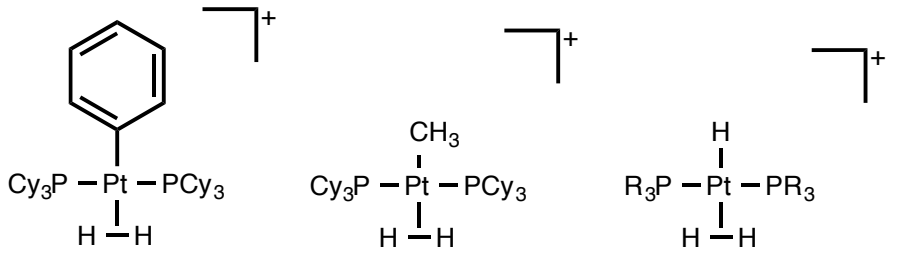

$^1J_{HD}$ = 33.6 Hz

$^1J_{HD}$ = 30.5 Hz

R = Cy, $^1J_{HD}$ = 31 Hz
R = ^{t}Bu, $^1J_{HD}$ = 34.7 Hz
R = ^{i}Pr , $^1J_{HD}$ = 33.7 Hz

Figure 5-4. Non-pincer platinum dihydrogen complexes and their reported $^1J_{HD}$ coupling constants.

Table 5-1. Comparison of pincer and non-pincer dihydrogen complexes of platinum.

	Pincer Platinum Dihydrogen	Non-pincer Platinum Dihydrogen
Cation	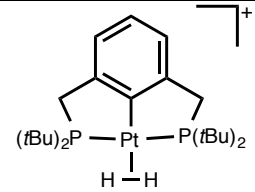	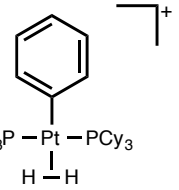
$^1J_{HD}$	33.4 Hz	33.6 Hz
T_1 (minimum)	14 milliseconds (-80 °C)	20 milliseconds (-65 °C)
Chemical Shift of (H_2) ligand resonance	0.18 ppm	-1.9 ppm

The chemical shift of the dihydrogen ligands is somewhat intriguing. Common d^6 metal dihydrogen complexes have chemical shifts significantly upfield of zero, but these group 10 complexes are all close to zero, and, in the cases of $[(^{tBu}PCP)Pt(H_2)]^+$ and $[(^tBu_3P)_2Pt(H_2)H]^+$, are actually downfield of zero. The chemical shifts and $^1J_{HD}$ coupling constants for dihydrogen complexes of Pt and Ni are included in Table 5-2.

Table 5-2. Chemical Shifts of the dihydrogen ligand in selected diphosphine Group 10 complexes.

	Chemical Shift (ppm)	$^1J_{HD}$ (Hz)	Reference
trans-$[(P^tBu_3)_2Pt(H)(H_2)]^+$	1.12	34.7	19a
trans-$[(PCy_3)_2Pt(H)(H_2)]^+$	-0.28	31	19b
trans-$[(PCy_3)_2Pt(Me)(H_2)]^+$	-2.35	30.5	19b
trans-$[(PCy_3)_2Pt(Ph)(H_2)]^+$	-1.9	33.6	19b
$[(^tBuPCP)Pt(H_2)]^+$	0.18	33.4	21
$[(^tBuPCP)Ni(H_2)]^+$	-3.21	35	17a and Chapter 3

5.3 $[(^{tBu}PCP\text{-}H)PdCl]^+$ (5-2). The first palladium pincer complexes were reported in 1976. Despite nearly 40 years of chemistry, the basicity of these species has not been explored. If protonation occurs at the metal, a 5-coordinate, Pd(IV) hydride complex would result. While Pd(IV) hydrides are often cited as intermediate species in catalytic cycles,[22] the only identified palladium(IV) hydrides have been empirically and theoretically predicted in mass spectrometry studies.[23,24] Palladium(IV) compounds number far fewer than their platinum(IV) analogues. Of the known palladium(IV) compounds in the literature, most contain halides, alkyl, or bidentate nitrogen-containing ligands.[25] The phosphine-ligated complexes were primarily characterized by NMR spectroscopy; only a few were stable enough at

room temperature for X-ray crystallographic characterization.[26] Relevant to the pincer chemistry discussed here, Szabó and coworkers have recently proposed that a Heck reaction promoted by [(^{Ph}POCOP)Pd]$^+$ reacts *via* a Pd(IV) intermediate.[27] Similar Pd(IV) transformations have been promoted by NCN pincer ligands[28] and reductive elimination from Pd(IV) ONC pincer ligands has been observed.[29]

5.3.1 Synthesis and structure. (^{tBu}PCP)PdCl (**4-1**) was prepared according to literature procedures. The addition of a strong acid to a solution of **4-1** resulted in a dramatic color change from colorless to orange (Scheme 5-2).

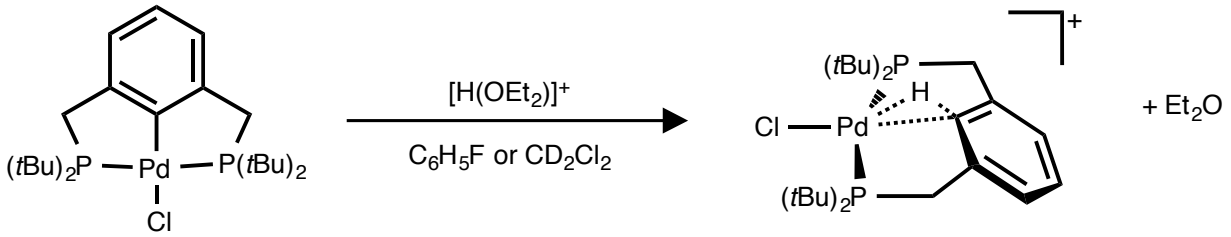

Scheme 5-2. Addition of strong acids to a solution of (^{tBu}PCP)PdCl (**4-1**) resulting in formation of a cationic species.

Layering the orange solution with alkane solvent precipitated crystalline material. The structure was determined by X-ray diffraction (Figure 5-5). The protonation did not occur at the metal, and the formal oxidation state of the metal remains Pd(II). Interestingly, the pincer ligand is no longer planar, and the phenyl rings is bent out of the P-Pd-P plane (Figure 5-6). The *ipso*-carbon atom is observed to be protonated, displaying apparent sp^3-hybridization. The C-H-M distances found in the crystal structure are short, suggesting an agostic interaction between the metal and the C-H bond (agostic interactions were discussed in Chapter 4.5).

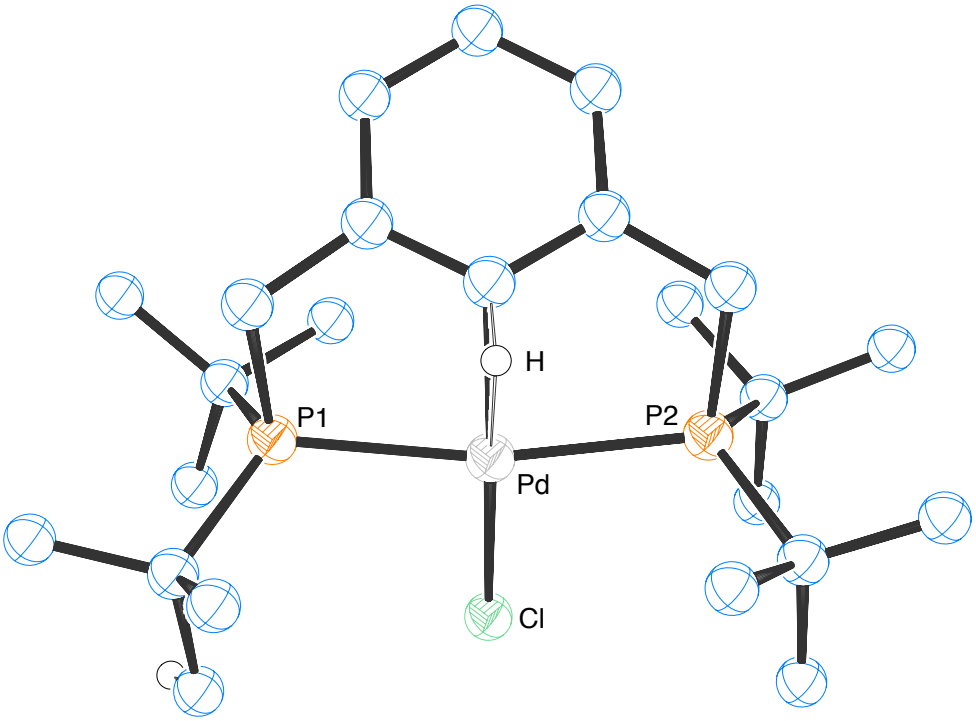

Figure 5-5. ORTEP[30] of [(^{tBu}PCP-H)PdCl][B(C_6F_5)$_4$] (5-2). The counteranion and pincer ligand hydrogen atoms have been omitted for clarity. R = 0.0441. Data from Heinekey/Samantha/sjc16.

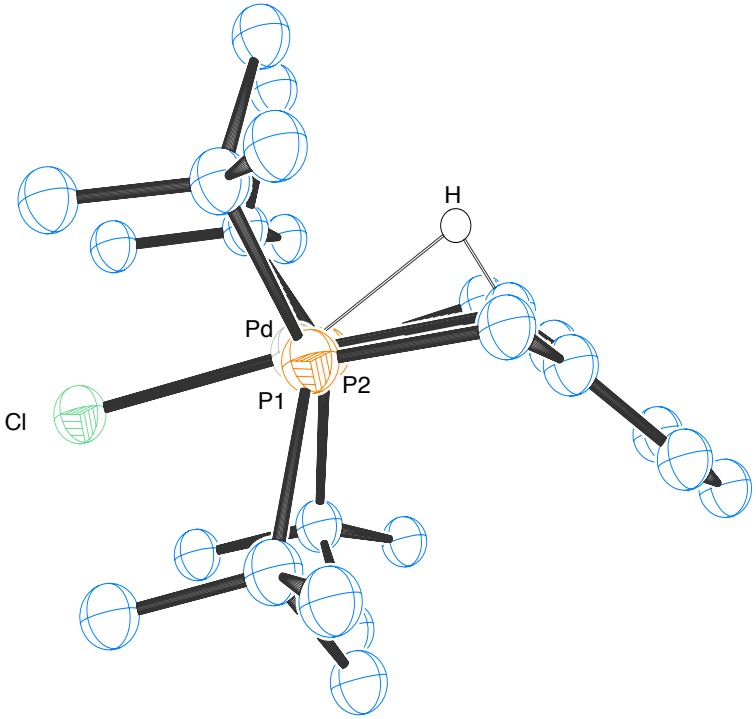

Figure 5-6. ORTEP[30] (Side View) of [(^{tBu}PCP-H)PdCl][B(C_6F_5)$_4$] (**5-2**). Anion and pincer ligand hydrogen atoms have been omitted for clarity.

5.3.2 NMR Spectroscopic Characterization. The NMR spectrum of this complex is interesting because the protonation lowers the symmetry of the molecule. The *tert*-butyl groups and methylene protons on the protonated face of the molecule are chemically inequivalent to those on the opposite face. As a result, two t-butyl signals and two methylene signals are observed in the ^{1}H NMR spectrum (Figure 5-7). In contrast, the phosphorous atoms and methylene carbon atoms remain equivalent and are observed as one resonance each, respectively, in the ^{31}P{^{1}H} and ^{13}C{^{1}H} NMR spectra.

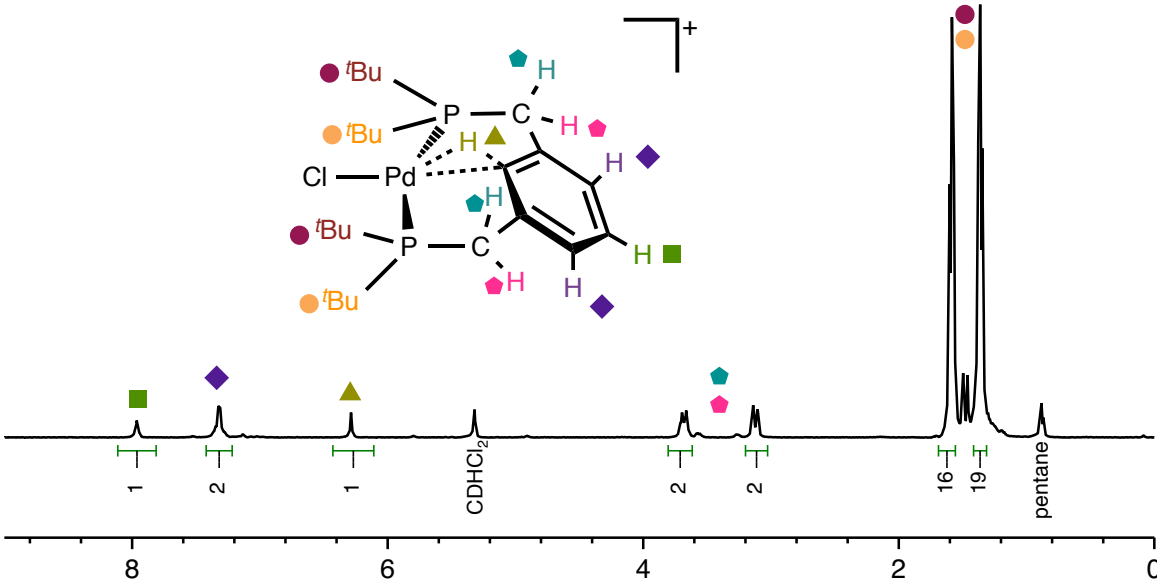

Figure 5-7. ^{1}H NMR Spectrum (500 MHz, 298 K) of [(^{tBu}PCP-H)PdCl][B(C_6F_5)$_4$] in CD_2Cl_2. The protonation of the *ipso*-carbon has resulted in a decrease in the symmetry of the molecule. As such, the methylene and t-butyl resonances have different chemical shifts. It remains unknown which of the two t-butyl virtual triplets and which of the two methylene signals correspond to which face of the molecule. The spectrum is assigned according to color/shape symbol as pictured. Data from sjconnel/499/SJC6_011414_3, Experiment 1.

A ^{13}C-^{1}H HMQC experiment confirms the correlation between the proton observed at 6.3 ppm and the carbon atom observed at 91 ppm (Figure 5-8). The protonation of the *ipso*-carbon has resulted in a dramatic upfield shift in the ^{13}C{^{1}H} signal, away from the chemical shift common to aromatic, sp^2-hybridized carbon atoms, and toward that characteristic of sp^3-hybridized carbon atoms. Additionally, one-bond coupling constants for aromatic carbon-proton species are generally between 150-160 Hz. In this case, the coupling constant is found to be 125 ± 2 Hz. This confirms the bond activation observed in the crystal structure and indicates that this is a C-H agostic complex, where the proton, carbon, and palladium atoms form a 3-center, 2-electron sigma bond.

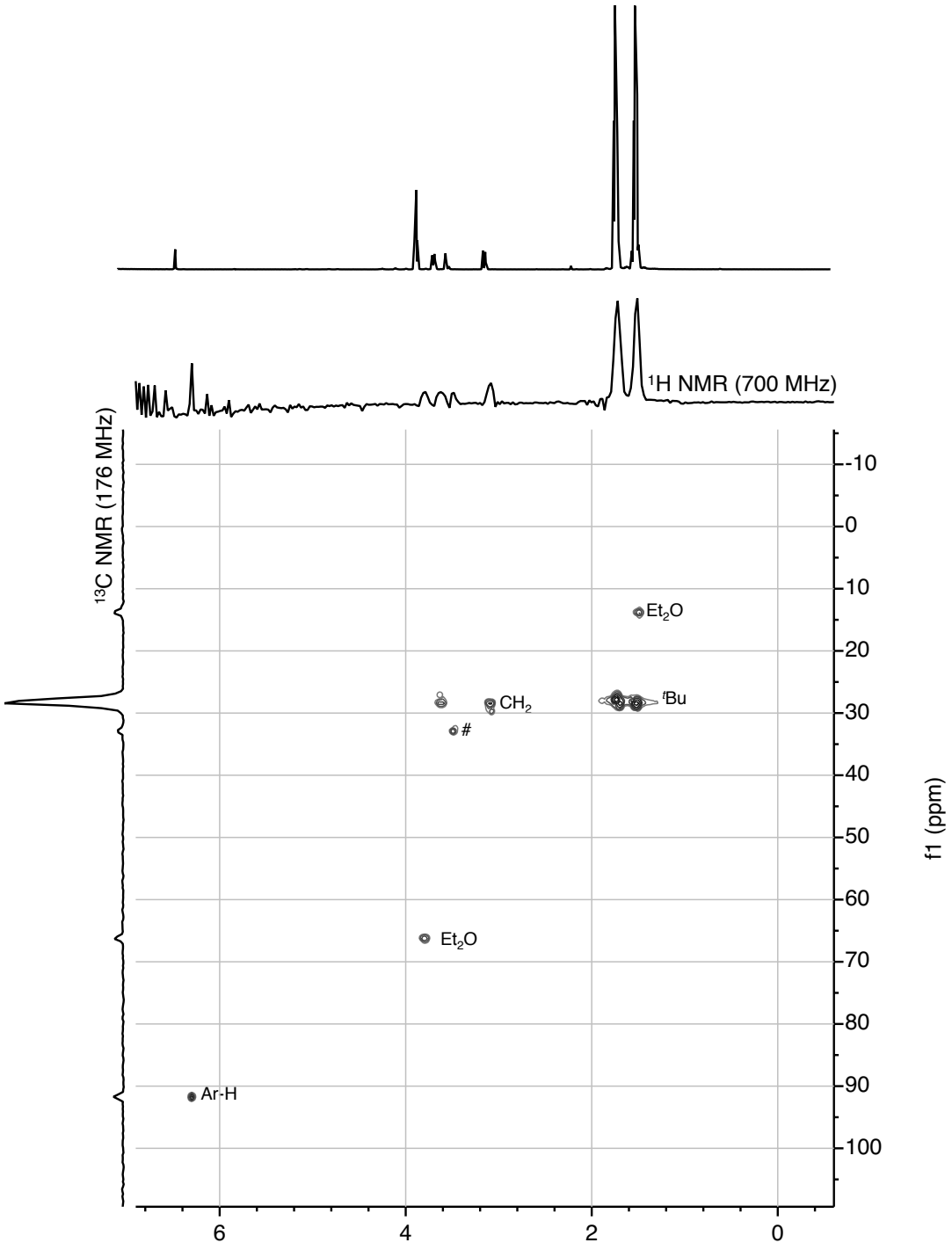

Figure 5-8. ^{1}H - ^{13}C HMQC 2D NMR Experiment, 298 K. Horizontal and vertical traces are internal projections. The upper horizontal trace is the 1D ^{1}H NMR spectrum of the same sample. Aromatic region is removed as the sample was in protiofluorobenzene. Unknown impurity is marked with #. The scalar coupling constant for this experiment was set to 125 Hz.

5.3.3 Comparison to other pincer-H complexes. Pincer ligands are often considered to be innocent ligands in complexes where the metal center facilitates catalysis. Methylene deprotonation (and loss of aromaticity) of PNP ligands are the exception to this, and complexes of this sort have been recently exploited for catalysis.[31] In contrast, there are few examples with structures similar to that in **5-2**.[32] Structurally similar species were achieved *via* arrested metallation of the ligand.[32b-f] A rhodium carbonyl example from Milstein readily metallated following addition of a base. Addition of a strong acid regenerated the agostic complex (Scheme 5-3).[32b] In the metallation of ruthenium bis-pincer complexes, the C-H activation step did not proceed for the second pincer ligand (Scheme 5-4).[32e-f] A report of platinum and iridium sp^3-hybridized PCP complexes also offers structurally similar examples. Further, these species can be obtained from the protonation of the pincer complex (Scheme 5-5).[32a]

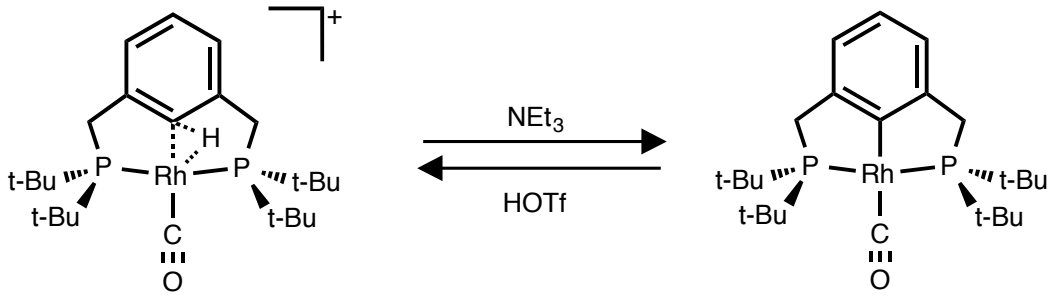

Scheme 5-3. Protonation of the *ipso*-carbon of a pincer ligand reported by Milstein.[32b] The cationic complex was originally obtained following incomplete metallation of the ligand.

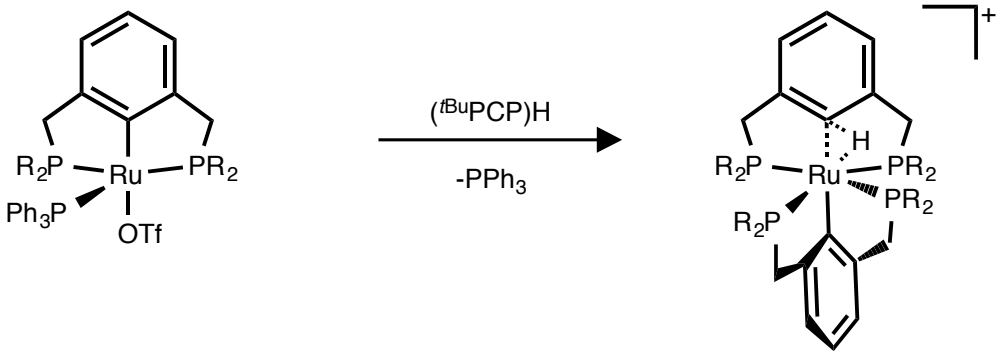

Scheme 5-4. Arrested metallation of a ruthenium bis-pincer complex.

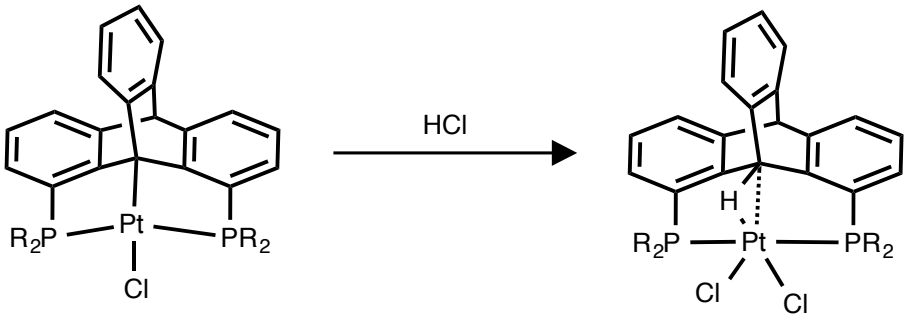

Scheme 5-5. Protonation of a pincer complex results in an agostic interaction between the ipso-carbon-hydrogen bond and the metal center in platinum and iridium examples reported by Gelman.[32a]

The NMR spectra of [(^{tBu}PCP-H)Rh(CO)]$^+$ features a ^{1}H NMR signal for the agostic proton at 4.13 ppm. The doublet (J_{RhH} = 18 Hz) indicates that the proton is interacting with the rhodium metal. The ^{13}C{^{1}H} NMR signal for the *ipso*-carbon is shifted upfield from 131 ppm in the free ligand to 111 ppm. Further, the coupling constant between the *ipso*-carbon and the proton has diminished substantially. Aromatic proton-carbon coupling constants in the ligand are over 160 Hz; but after the interaction with the metal is established, the coupling constant is measured to be 123 Hz. In our complex (**5-2**), the carbon atom is further shifted upfield (90 ppm); whereas the proton experiences a smaller shift (6.3 ppm). The $^1J_{CH}$ coupling constant (125 Hz vs. 123 Hz) is approximately the same between **5-2** and [(^{tBu}PCP-H)Rh(CO)]$^+$.

5.4 [(^{tBu}PCP)Pd(H$_2$)][B(C$_6$F$_5$)$_4$] (Complex 5-3). In order to complete the series of group 10 metal [(^{tBu}PCP)M(H$_2$)]$^+$ complexes, we set out to synthesize the palladium analogue. This complex, [(^{tBu}PCP)Pd(H$_2$)][B(C$_6$F$_5$)$_4$] (Complex **5-3**), is the first reported palladium dihydrogen complex. Its synthesis had been previously attempted by Bullock's group at PNNL, by protonation of the hydride in dichloromethane. Metal hydrides are known to activate carbon-chlorine bonds in dichloromethane, forming the metal chloride.[33] We anticipate that this may have contributed to the difficulty in synthesizing the desired platinum complex. Additionally, the ether molecule released during the reaction may facilitate displacement of the hydrogen ligand.

5.4.1 Synthesis. Our synthesis employed the silylium cation discussed in Chapter 2. Combination of solid [(Et$_3$Si)$_2$H][B(C$_6$F$_5$)$_4$] (**2-2**) and (^{tBu}PCP)PdCl (**5-1**), followed by dissolution in fluorobenzene under an atmosphere of hydrogen afforded Et$_3$SiH, Et$_3$SiCl, and the desired complex, [(^{tBu}PCP)Pd(H$_2$)][B(C$_6$F$_5$)$_4$] (**5-3**) (Scheme 5-6).

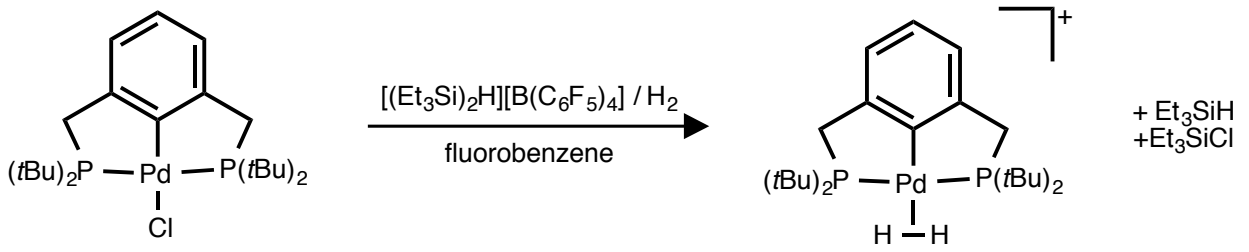

Scheme 5-6. Synthesis of [(^{tBu}PCP)Pd(H_2)][$B(C_6F_5)_4$] (**5-3**).

5.4.2 Determination of d_{HH}. The complex was identified by NMR spectroscopy. The internuclear distance of the hydrogen ligand, d_{HH}, was determined by two solution NMR methods. The measurements confirmed that complex 5-3 is present in solution, and that the dihydrogen ligand is intact.

5.4.2a Measurement of T_1. The resonance for the dihydrogen ligand in the ^{1}H NMR spectrum is shifted downfield of most dihydrogen and metal hydride complexes, in line with observations for other group 10 complexes (Table 5-2). The signal is observed to be a broad line at 1.57 ppm. At room temperature, the T_1 value is short. It continues to decrease as the temperature of the sample is dropped, but the line width increases, making conclusive measurement of T_1(minimum) difficult. The collected data for temperatures 298, 288, 278, and 268 K are shown in Table 5-3. While these values do not allow determination of a T_1(minimum), they are short enough to confirm the presence of a dihydrogen ligand.

Table 5-3. T_1 Data for [(^{tBu}PCP)Pd(H_2)][$B(C_6F_5)_4$] (**5-3**).

Temperature (K)	T_1 (milliseconds)
298	21 ± 1
288	15 ± 3
278	15 ± 5
268	15 ± 5
258 and below	signal too broad

5.4.2b Observation of $^1J_{HD}$. The sample was prepared under HD gas to afford the partially deuterated complex, [(^{tBu}PCP)Pd(HD)][$B(C_6F_5)_4$] (**5-3-d_1**). Within 15 minutes, the scrambling of the HD gas to give 25% H_2, 50% HD, and 25% D_2 had occurred. This is likely catalyzed by adventitious base (Scheme 5-7). The ^{1}H NMR spectrum at

300 MHz distinguishes the H_2 and HD ligands (Figure 5-9). The $^1J_{HD}$ coupling constant is also apparent from the ^2H NMR spectrum at 107 MHz (Figure 5-10). The measured value (37 ± 1 Hz) is one of the largest observed $^1J_{HD}$ coupling constants for any dihydrogen complex, and suggests d_{HH} = 0.81± 0.02 Angstroms. This indicates that the dihydrogen bond is only weakly activated upon coordination to the [(^{tBu}PCP)Pd]$^+$ fragment.

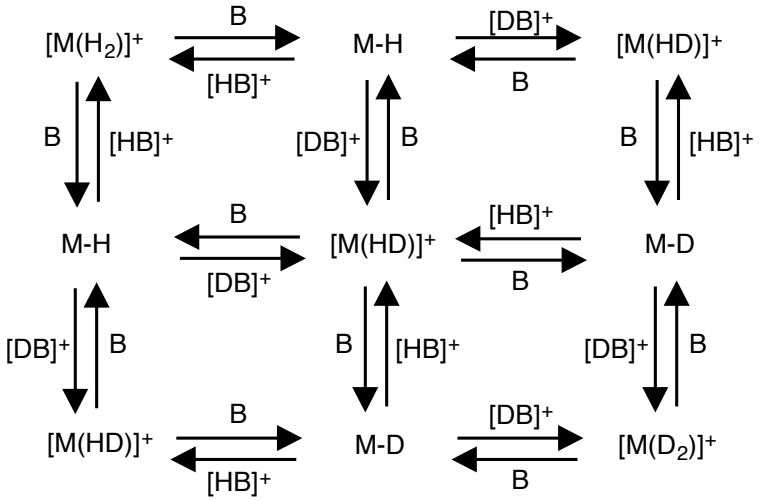

Scheme 5-7. Mechanism of HD scrambling catalyzed by adventitious base.

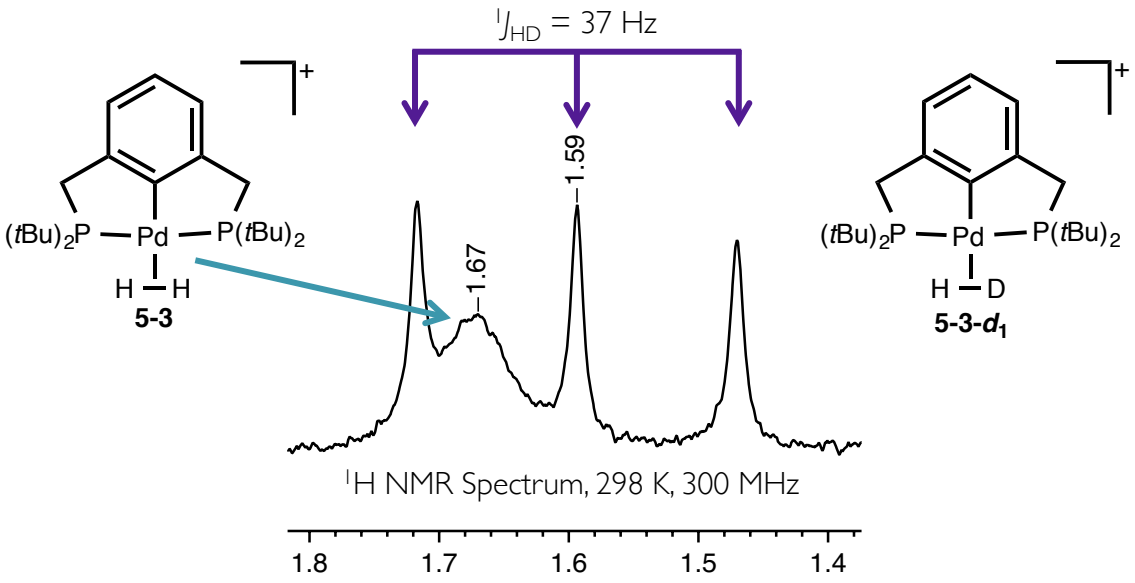

Figure 5-9. ^1H NMR Spectrum (298 K, 300 MHz) of [(^{tBu}PCP)Pd(HD)][B(C_6F_5)4] (**5-3-d_1**). The apparent $^1J_{HD}$ = 37 Hz.

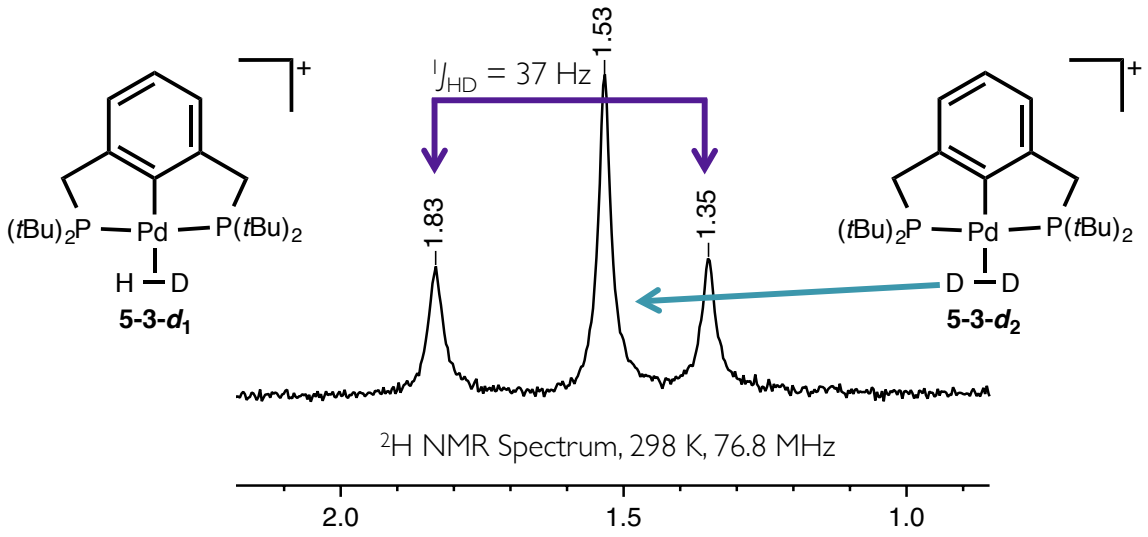

Figure 5-10. ^{2}H NMR Spectrum (298 K, 76.8 MHz) of [(^{tBu}PCP)Pd(HD)][B(C_6F_5)4] (**5-3-d_1**). $^1J_{HD}$ = 37 Hz is confirmed.

5.4.3 Structure. A crystal suitable for an X-ray diffraction experiment was obtained from a solution of **5-3** in fluorobenzene layered with excess triethylsilane and pentane. The structure was of very high quality (R_{int} = 0.0241) and contained two components (A & B). Component A, the major component of the mixture, comprised 83% of the sample. This was the expected dihydrogen complex 5-3. Component B comprised only 17% of the sample, but showed an interesting product.

5.4.3a Major Component. The major component comprised 83% of the sample and was the expected dihydrogen complex (Figure 5-11). As is generally the case, the X-ray diffraction structure underestimated the d_{HH} for the dihydrogen complex.

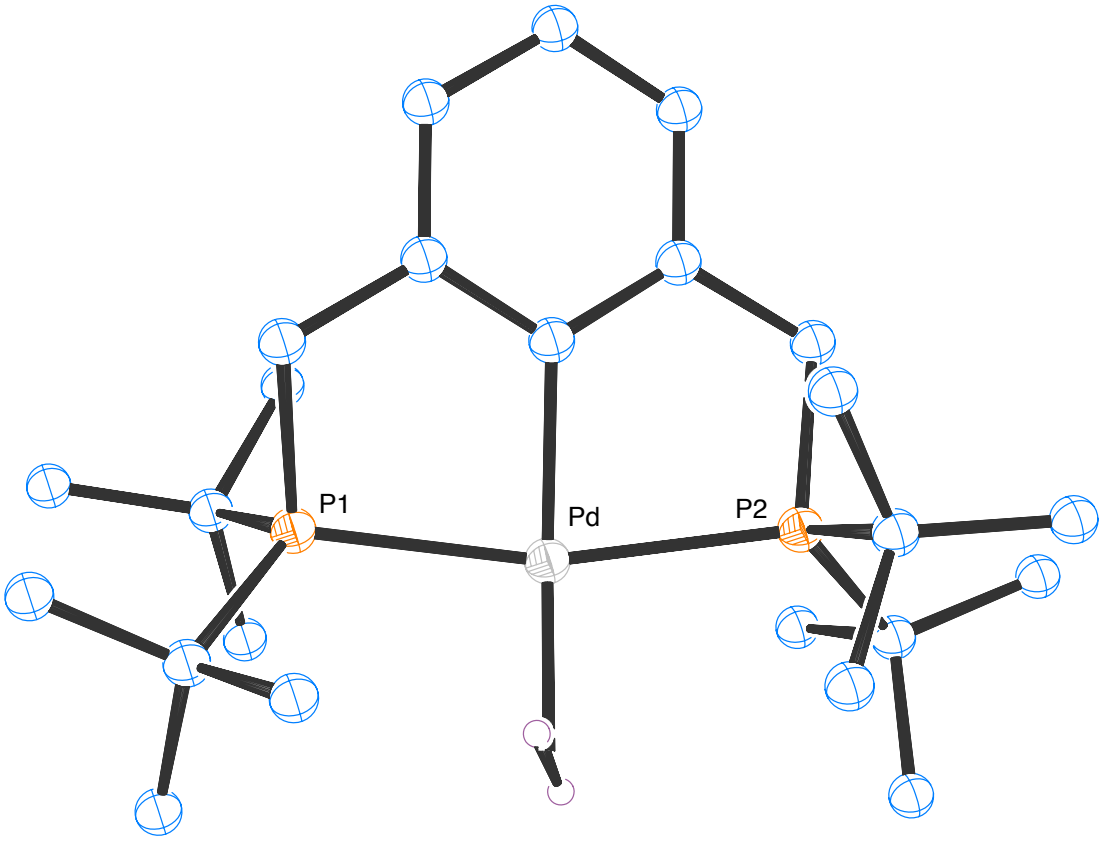

Figure 5-11. ORTEP[30] of [(^{tBu}PCP)Pd(H_2)][B(C_6F_5)$_4$] (Component A) (**5-3**). R = 0.0241. The unit cell contains one cation, one anion, and one disordered fluorobenzene molecule. The anion, solvent molecule, and hydrogen atoms on the pincer ligand have been omitted for clarity. Data from Heinekey/Samantha/sjc15.

5.4.3b Minor Component. The minor component (17% of the sample) showed a metal hydride complex (Figure 5-12). The species appears to have transferred a proton from the dihydrogen ligand to the metal-carbon bond. The "plane" of the pincer ligand has been disrupted, and the phenyl is offset from the P-Pd-P plane (Figure 5-13). Figure 5-14 shows the differences in bond angles and lengths between the major and minor components of the sample. The palladium-carbon bond is lengthened substantially (nearly 0.5 Angstroms) between the two structures, and the bond distances in the "arms" of the pincer ligand have elongated slightly to accommodate the change. The phenyl ring of the ligand remains planar and mostly maintains aromaticity (within error).

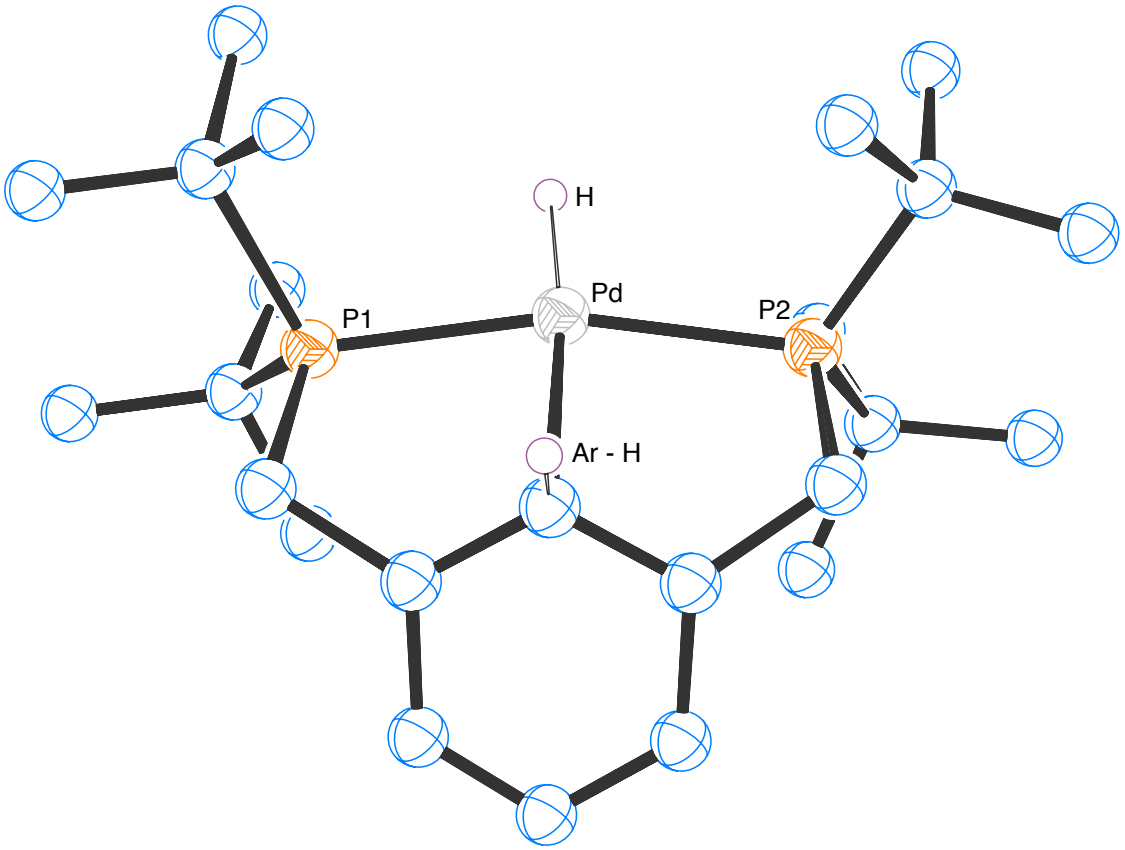

Figure 5-12. ORTEP[30] (Top View) of [(^{tBu}PCP-H)PdH][B(C_6F_5)$_4$] (Minor component). (**5-3**). The anion, solvent molecule, and hydrogen atoms on the pincer ligand have been omitted for clarity. Data from Heinekey/Samantha/sjc15.

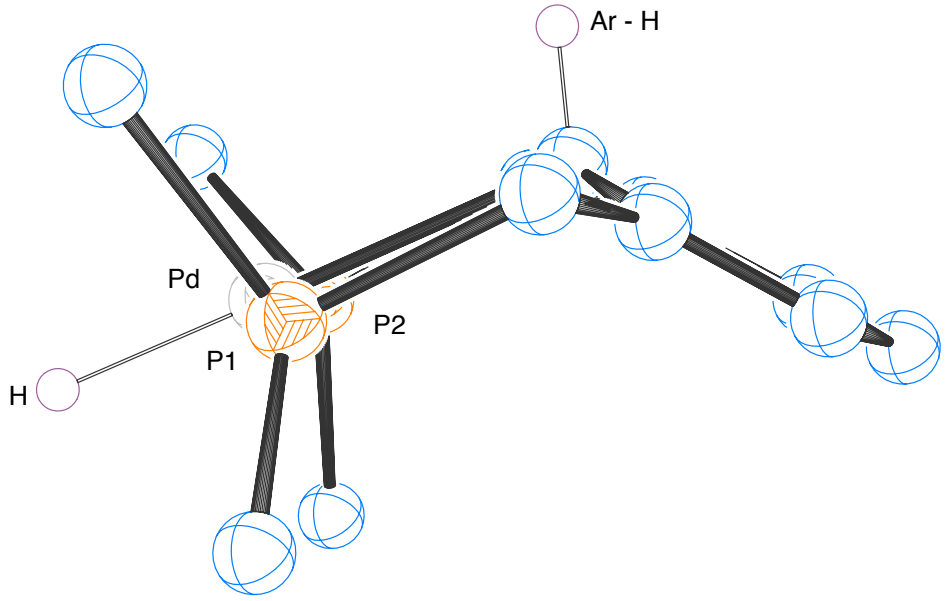

Figure 5-13. ORTEP[30] (Side View) of [(^{tBu}PCP-H)PdH][B(C_6F_5)$_4$] (Minor component). The anion, solvent molecule and pincer ligand hydrogen atoms have been omitted for clarity. Data from Heinekey/Samantha/sjc15.

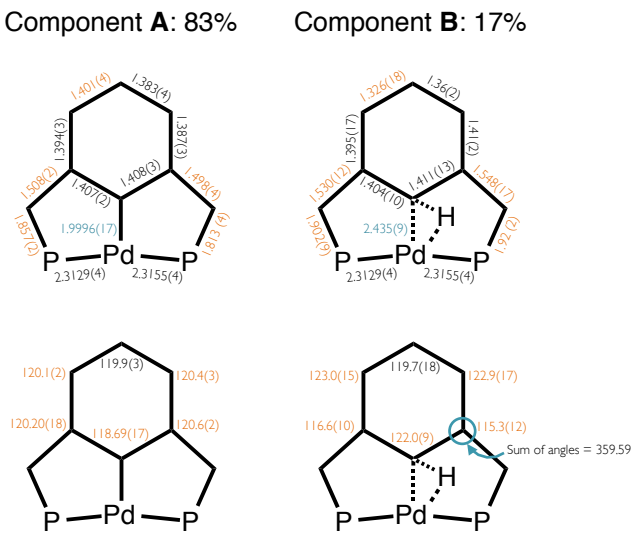

Figure 5-14. Comparison of bond lengths and angles in the major and minor component of the crystals obtained by layering a solution of **4-1** with triethylsilane and pentane. Component A is the dihydrogen complex. Component B shows activation of the dihydrogen ligand to protonate the Pd-C bond. The distances and angles listed in color vary (beyond error) from the distance or angle in the other component.

5.4.3c Comparison between 5-2 and 5-3b. The structure of **5-3b** is remarkably similar to that observed for [(^{tBu}PCP-H)PdCl][B(C_6F_5)$_4$] (**5-2**) (See Figure 5-6 and Figure 5-13). Both phenyl rings are bent substantially out of the plane of the P-Pd-P bond, and the *ipso*-carbon has been protonated. We anticipate that the dihydrogen ligand has sufficient acidity to partially protonate the Pd-C bond, resulting in the formation of species **5-3b**.

To investigate the basicity of these complexes, [H(OEt_2)][B($C_6H_3(CF_3)_2$)$_4$] was combined with (^{tBu}PCP)PdH. As expected, the dihydrogen complex (**5-3**) was observed in solution by NMR. Addition of HD gas readily incorporated deuterium into the structure, and the ^{2}H NMR spectrum closely matches that observed for the HD complex generated by chloride abstraction. Lowering the temperature of these solutions did not result in any changes to the $^1J_{HD}$ coupling constant, and no additional hydride resonances were observed. As such, it is postulated that any **5-3b** in solution is very rapidly equilibrating with **5-3**. **5-3** should be more stable than an HCl complex (the expected analogue in the protonated metal-chloride chemistry), and we anticipate that this is the reason protonation at the *ipso*-carbon of the metal chloride is so readily observed (**5-2**).

5.5 Comparison of Group 10 $[(^{tBu}PCP)M(H_2)]^+$ Complexes. A goal of this project was to synthesize analogous dihydrogen complexes for all of the group 10 metals. Table 5-4 outlines the similarities and differences between these species. In all cases, the metal is in its +2 oxidation state with 8 *d*-electrons. The complexes are all stable for days at room temperature. The dihydrogen ligands are labile (can be exchanged for HD), and there is no clear trend for activation of the dihydrogen ligand. All complexes have short d_{HH} indicated by short T_1 values and strong $^1J_{HD}$ coupling constants.

Table 5-4. Comparison of Group 10 (tBuPCP)M(H2)]+ species. #Reported by Bullock and co-workers.[21]

Metric	$[(^{tBu}PCP)Ni(H_2)]^+$	$[(^{tBu}PCP)Pd(H_2)]^+$	$[(^{tBu}PCP)Pt(H_2)]^{+\#}$
	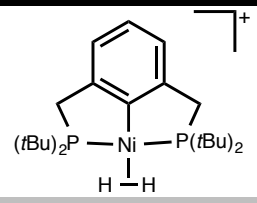	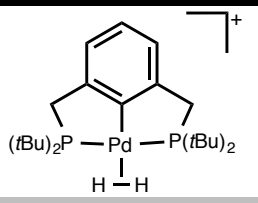	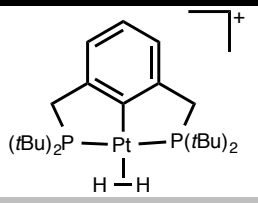
Oxidation State	+2	+2	+2
$^1J_{HD}$ (Hz)	34 ± 1	37 ± 1	33
T_1(minimum) (milliseconds)	< 8	< 15	< 14 ms
Chemical Shift of H_2 ligand (ppm)	-3.21	1.57	0.18

There are remarkably few examples of other complete triads of dihydrogen complexes in the literature available for comparison.[3] The Group 6 triad for the original Kubas complexes, $(PR_3)_2(CO)_3M(H_2)$ where M = Cr, Mo, W, has been completed, with H_2 lability decreasing down the group. The reported d_{HH} values (based on $^1J_{HD}$ = 35, 34, 33.5) steadily increase from 0.84 Angstroms to 0.89 Angstroms, Cr to W. The chemical shifts of these dihydrogen ligands are -7.65 ppm, -3.13 ppm, -14.21 ppm (Cr, Mo, W respectively).[34,35] Similar to that observed in our triad, the dihydrogen ligand on the 2nd row metal is much further downfield-shifted than the other ligand chemical shifts.

5.6 Attempted Syntheses of ^{tBu}POCOP and ^{tBu}PNP Pd Dihydrogen Complexes. Two alternate pincer ligands were employed in an attempt to generate additional palladium dihydrogen complexes for comparison. In both cases, a precipitate resulted from the reaction between $[(Et_3Si)_2H][B(C_6F_5)_4]$ (**2-1**) and the pincer metal chloride in fluorobenzene under H_2 gas (Scheme 5-8). This was somewhat anticipated for the ^{tBu}PNP ligand, as the resulting

dihydrogen complex would be a rare dicationic species. Other solvents will be employed in pursuit of these complexes.

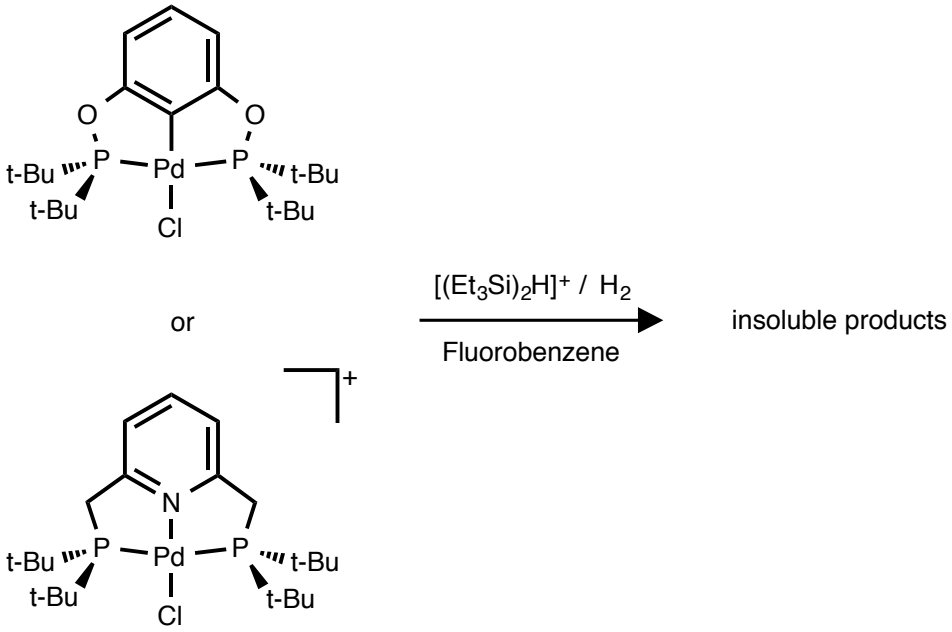

Scheme 5-8. Attempted syntheses of two additional dihydrogen complexes of palladium. Both led to precipitation.

5.7 Experimental Section.

General Considerations. All experiments were carried out under argon using Schlenk and glove box techniques unless otherwise noted. Solvents were dried and vacuum transferred immediately prior to use. N,O-bistrimethylsilylacetamide was refluxed in glassware to silylate the surface prior to use with $[(Et_3Si)_2H][B(C_6F_5)_4]$. $[(Et_3Si)_2H][B(C_6F_5)_4]$ (**2-2**) was prepared as described in Chapter 2. Reagents not synthesized elsewhere in this thesis were commercially available and used as received.

NMR spectra were recorded at 298 K (unless otherwise noted) on Bruker AV300, AV500, DRX500, or AV700 spectrometers. ^{1}H NMR chemical shifts are reported relative to residual resonances of the solvent: C_6D_5H (δ = 7.16), C_6D_4HF (δ = 6.96, 6.99, 7.17), $CDHCl_2$ (δ = 5.32). Some ^{1}H NMR spectra were recorded in *protio*-fluorobenzene using a solvent suppression pulse program or acquisition of several hundred scans. $^{31}P\{^1H\}$ NMR chemical shifts were externally referenced to H_3PO_4 (85% in H_2O) (δ = 0.00).

The neutral alumina used for purification of the pincer metal chloride compounds was Alumina Neutral Super I, Catalog # 04589-25, Dynamic Adsorbants, Norcross, GA. It should be noted that the pincer metal chlorides synthesized here are stable to H_2O and O_2. They can be purified, handled, and stored in air.

(^{tBu}PCP)PdCl (5-1).

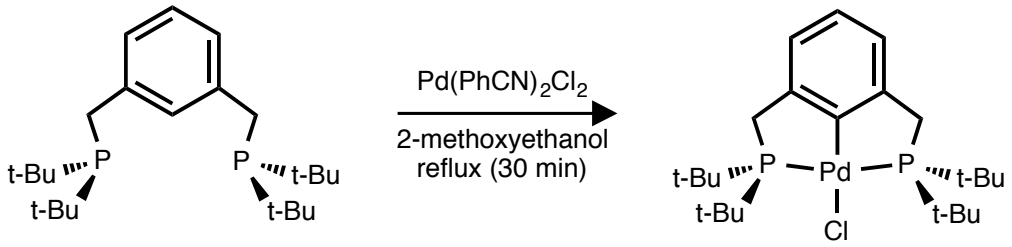

(^{tBu}PCP)H **5-1**

The procedure was slightly modified from that reported by Moulton & Shaw.[36] (^{tBu}PCP)H (Aldrich) 0.250 g, 394.55 g/mol, 0.63 mmol) was suspended in 2-methoxyethanol (15 mL). $Pd(PhCN)_2Cl_2$ (0.243 g, 383.57 g/mol, 0.63 mmol) was added, and the mixture was heated to reflux for 30 minutes. The solvent was removed *in vacuo*, and the precipitate was dissolved in ethanol. The solution was filtered through neutral alumina. The volume of colorless solution was reduced, and cooling the solution to -25 °*C* produced crystalline material. Alternatively, removal of the solvent *in vacuo* left powdered product. Reproducible yields of pure product: ~70%.

^{1}H NMR	(500 MHz, C_6H_5F, 298 K):	1.39 ppm (vt, 36 H, tBu), 3.12 ppm (vt, 4 H, CH_2);
$^{31}P\{^{1}H\}$ NMR	(202 MHz, C_6H_5F, 298 K):	73 ppm

NMR Data from SJC5_081513_1 Experiments 1 & 2.

[($^{t\text{Bu}}$PCP-H)PdCl][B($C_6H_3(CF_3)_2)_4$] (5-2)

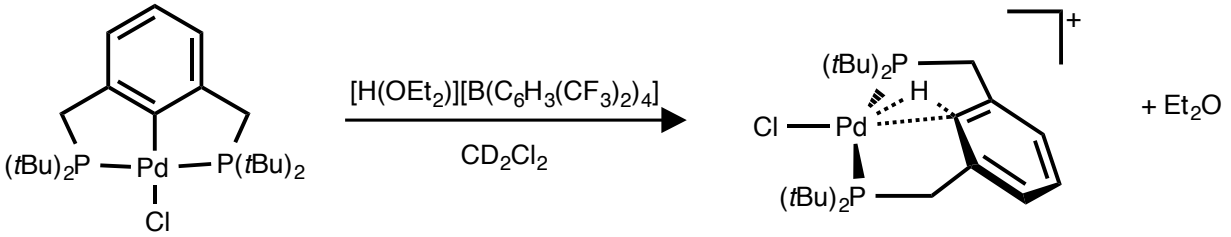

$^{t\text{Bu}}$PCPPdCl (5.8 mg, 535 g/mol, 11 mmol) and [$HOEt_2$][B($C_6H_3(CF_3)_2)_4$] (12.2 mg, 11 mmol) were combined in a Teflon screw-top NMR tube. CD_2Cl_2 was added by vacuum-transfer. Upon thawing, the solution became orange in color. The product could be isolated by layering the solution with alkane to precipitate crystals.

^{1}H NMR	(500 MHz, CD_2Cl_2, 298 K): 1.35, 1.58 ppm (vt, 18 H each, tBu); 3.14, 3.70 (d-vt, 2 H each, CH_2); 6.3 ppm (s, 1H, Pd-H-C); 7.31 (m, 2 H, aromatic); 7.96 (t, 1H, *p-H*)
^{31}P{^{1}H} NMR	(202 MHz, CD_2Cl_2, 298 K): 4.7 ppm

[($^{t\text{Bu}}$PCP-H)PdCl][BF_4] (5-3)

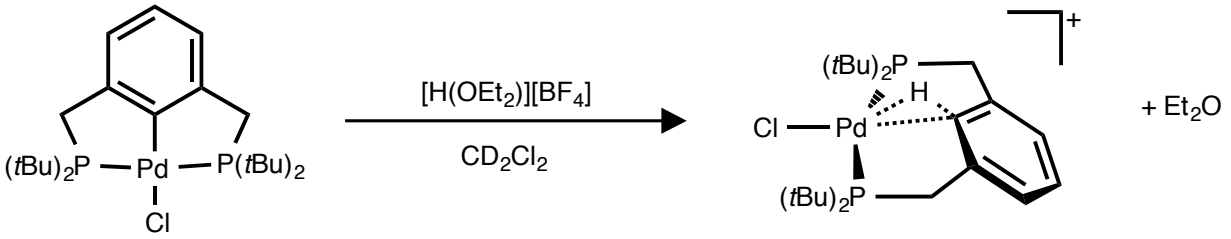

Analogous to the procedure for $^{t\text{Bu}}$PCPPdCl (4.8 mg, 535 g/mol, 9 mmol) was dissolved in CD_2Cl_2, and [$HOEt_2$][BF_4] (85% solution in ether, 9 mmol) was added *via* microliter pipette. Upon thawing, the solution became orange in color. The product could be isolated by layering the solution with alkane to precipitate crystals. The NMR spectra matched that with the BAr^F_4 counterion.

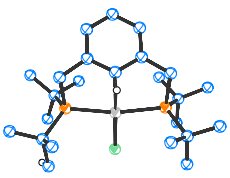

X-ray Structure included here as Figure 5-5. Data from Heinekey/Samantha/sjc16.

[(^{tBu}PCP)Pd(H_2)][$B(C_6F_5)_4$] (5-3).

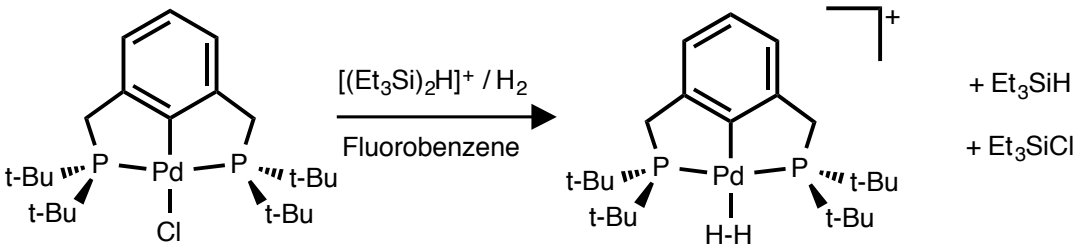

5-1 **5-3**

(^{tBu}PCP)PdCl (8 mg, 535 g/mol, 15 mmol) was combined with [$(Et_3Si)_2H$][$B(C_6F_5)_4$] (14 mg, 910.58 g/mol, 15 mmol) in a silylated NMR tube with Teflon screw top. Fluorobenzene (~0.5 mL) was added by vacuum transfer, and a dark orange solution resulted. The solution was frozen (liquid nitrogen), the head space evacuated, and H_2 gas (1 atm) was introduced. Upon thawing, the solution became lighter orange. The solution was again frozen, the head space evacuated, and pentane (~25 mL) was added by vacuum transfer. A solid precipitated. After the precipitate settled, the solution was removed, and the solid was dried *via* hydrogen purge. Yield by NMR was near quantitative. Isolated (crude): 11 mg, ~50% yield. Isolated (crystalline): 4.5 mg, ~20% yield.

^{1}H NMR (C_6H_5F, 500 MHz, 298 K): 1.03 ppm (vt, 36H, ^{t}Bu-CH_3); 3.08 ppm (s, 4H, CH_2)
1.59 ppm (br, 2H, H_2); (aromatics coincident with protio-solvent signals)

^{31}P{^{1}H} NMR (C_6H_5F, 202 MHz, 298 K): 95 ppm

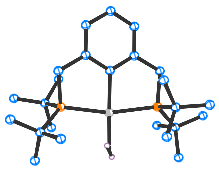

X-ray Structure included here as Figure 5-11. Data from Heinekey/Samantha/sjc15.

References

[1] (a) G. Zeni, R. C. Larock *Chem. Rev.* **2004**, *104*, 2285-2310.

(b) J. M. Mayer, F. E. Michael *Inorg. Chem.* **2007**, DOI: 10.1021/ic700598t.

[2] Greenwood, N. N., Earnshaw. A. *Chemistry of the Elements,* 2nd ed. Oxford, UK: Elsevier, 1997.

[3] Kubas, Gregory. *Metal Dihydrogen and σ-Bond Complexes: Structure, Theory, & Reactivity*. Springer, 2001.

[4] R. H. Crabtree, D. G. Hamilton *Adv. in Organomet. Chem.* **1988**, *28*, 299-338.

[5] T. J. Hebden, A. J. St. John, D. G. Gusev, W. Kaminsky, K. I. Goldberg, D. M. Heinekey *Angew. Chem. Int. Ed.* **2011**, *50*, 1873-1876. This work was highlighted by R. M. Bullock *Angew. Chem. Int. Ed.* **2011**, *50*, 4050-4052.

[6] (a) D.L.M. Suess, C. Tsay, J. Peters *J. Am. Chem. Soc.* **2012**, *134*, 14158-14164.

(b) T.-P. Zin, J. Peters *J. Am. Chem. Soc.* **2013**, *135* 15310–15313.

[7] C. Bianchini, C. Mealli, A. Meli, M. Peruzzini, F. Zanobini *J. Am. Chem. Soc.***1988**, *110*, 8725–8726.

[8] D. M. Heinekey, M. van Roon *J. Am. Chem. Soc.* **1996**, *118,* 12134-12140.

[9] C. Federsel, C. Ziebart, R. Jackstell, W. Baumann, M. Beller *Chem. Eur. J.* **2012**, *18*, 72-75.

[10] S. Nemeh, C. Jensen, E. Binamira-Soriaga, W. C. Kaska *Organometallics* **1983**, *2*, 1442-1447.

[11] W. Xu, G. P. Rosini, M. Gupta, C. M. Jensen, W. Kaska, K. Krogh-Jespersen, A. Goldman *JCS Chem. Comm.* **1997**, 2273-2274.

[12] A. B. Chaplin, A. S. Weller *Organometallics* **2011**, *30*, 4466-4469.

[13] M. Findlater, K. M. Schultz, W. H. Bernskoetter, A. Cartwright-Sykes, D. M. Heinekey, M. Brookhart *Inorg. Chem.* **2012**, *51*, 4672-4678.

[14] A. Vigalor, Y. Ben-David, D. Milstein *Organometallics* **1996**, *15*, 1839-1844.

[15] I. Göttker-Schnetmann, D. M. Heinekey, M. Brookhart *J. Am. Chem. Soc.* **2006**, *128*, 17114-17119.

[16] H. Fan, B. C. Fullmer, M. Pink, K. G. Caulton *Angew. Chem. Int. Ed.* **2008**, *47*, 9112-9114.

[17] (a) S. J. Connelly, A. C. Zimmerman, D. M. Heinekey *Chem. Eur. J.* **2012**, *18*, 15932-15934.

(b) Chapter 3 of this dissertation.

[18] C. Tsay, J. C. Peters *Chem. Sci.* **2012**, *3*, 1313-1318.

[19] (a) G. J. Gusev, J. U. Notheis, J. R. Rambo, B. E. Hauger, O. Eisenstein, K. G. Caulton *J. Am. Chem. Soc.* **1994**, *116*, 7409-7410.

(b) S. S. Stahl, J. A. Labinger, J. E. Bercaw *Inorg. Chem.* **1998**, *37*, 2422-2431.

[20] M. D. Butts, B. L. Scott, G. J. Kubas *J. Am. Chem. Soc.* **1996**, *118*, 11831-11843.

[21] B. F. M. Kimmich, R. M. Bullock *Organometallics* **2002**, *21*, 1504-1507.

[22] N. R. Deprez, M. S. Sanford *Inorg. Chem.* **2007**, *46*, 1924-1935.

[23] P. Sehnal, R. J. K. Taylor, I. J. S. Fairlamb *Chem. Rev.* **2010**, *110*, 824-889.

[24] R. Qian, H. Guo, Y. Liao, H. Wang, X. Zhang, Y. Guo *Rapid Commun. Mass Spectrom.* **2006**, *20*, 589-594.

[25] L.-M. Xu, B.-J. Li, Z. Yang, Z.-J. Shi *Chem. Soc. Rev.*, **2010**, *39*, 712-733.

[26] (a) A. Bayler, A. J. Canty, P. G. Edwards, B. W. Skelton, A. H. White *J. Chem. Soc., Dalton Trans.* **2000**, 3325-3330.

(b) A. J. Canty, J. Patel, M. Pfeffer, B. W. Skelton, A. H. White *Inorganica Chimica Acta*, **2002**, *327*, 20.

[27] J. Aydin, J. M. Larsson, N. Selander, K. J. Szabó *Org. Lett.* **2009**, *11*, 2852-2854.

[28] (a) M.-C. Lagunas, R. A. Gossage, A. L. Spek, G. van Koten *Organometallics* **1998**, *17*, 731.

(b) A. J. Canty, T. Rodemann, B. W. Skelton, A. H. White *Organometallics* **2006**, *25*, 3996.

[29] J. Vicente, A. Arcas, F. Juliá-Hernández, D. Bautista *Chem. Commun.* **2010**, *46*, 7253-7255.

[30] ORTEP for Windows 2013. L. J. Farrugia *J. Appl. Cryst.* **2012**, *45*, 849-854.

[31] (a) J. I. van der Vlugt, J. N. H. Reek *Angew. Chem. Int. Ed.* **2009**, *48*, 8832-8846 and references therein.

(b) W. Bailey, W. Kaminsky, R. Kemp, K. Goldberg **2014**. Submitted.

[32] (a) S. Musa, R. Romm, C. Azerraf, S. Kozuch, D. Gelman *Dalton Trans.* **2011**, *40*, 8760-8763.

(b) A. Vigalok, O. Uzan, L. J. W. Shimon, Y. Ben-David, J. M. L. Martin, D. Milstein *J. Am. Chem. Soc.* **1998**, *120*, 12539-12544.

(c) M. Montag, I. Efremenko, R. Cohen, L. J. W. Shimon, G. Leitus, Y. Diskin-Posner, Y. Ben-David, H. Salem, J. M. L. Martin, D. Milstein *Chem. Eur. J.* **2010**, *16*, 328-353.

(d) A. Vigalok, Y. Ben-David, D. Milstein *Organometallics* **1996**, *15*, 1839-1844.

(e) P. Dani, T. Karlen, R A. Gossage, W. J. J. Smeets, A. L. Spek, G. van Koten *J. Am. Chem. Soc.* **1997**, *119*, 11317-11318.

(f) P. Dani, M. A. M. Toorneman, G. P. M. van Klink, G. van Koten *Organometallics* **2000**, *19*, 5287-5296.

[33] D. S. Moore, S. D. Robinson *Chem. Soc. Rev.* **1983**, *12*, 415-452.

[34] G. J. Kubas, J. E. Nelson, J. C. Bryan, J. Eckert, L. Wisniewski, K. Zilm *Inorg. Chem.* **1994**, *33*, 2954-2960.

[35] G. J. Kubas, C. J. Unkefer, B. I. Swanson, E. Fukushima *J. Am. Chem. Soc.* **1986**, *108*, 7000-7009.

[36] C. J. Moulton, B. L. Shaw *J. Chem. Soc., Dalton Trans.* **1976**, *11*, 1020-1024.

A.1 Abbreviations.

Abbreviation	Long Hand
Me	methyl
Et	ethyl
^{i}Pr	*iso*-propyl
^{t}Bu	*tert*-butyl
Cy	cyclohexyl
Ph	phenyl
Ar	aryl
Mes	mesityl
^{tBu}PCP	1,3-bis-[(di-t-butylphosphino)methyl]phenyl
^{tBu}POCOP	1,3-bis-(di-t-butylphosphinito)phenyl
^{Ph}POCOP	1,3-bis-(di-phenylphosphinito)phenyl
^{tBu}PNP	2,6-bis-[di-t-butylphosphino)methyl]pyridine
^{tBu}PONOP	2,6-bis-(di-t-butylphosphinito)pyridine
F/P/T	freeze/pump/thaw cycle (for degassing solutions)
NMR	Nuclear Magnetic Resonance
FT-IR	Fourier Transform – Infrared
EPR	Electron Paramagnetic Resonance
GC-MS	Gas Chromatography – Mass Spectrometry
ORTEP	Oakridge Thermal Ellipsoid Plot

A.2 Library of Numbered Compounds.

#	Formula	Structure
2-1a	$[Et_3Si(C_7H_8)][B(C_6F_5)_4]$	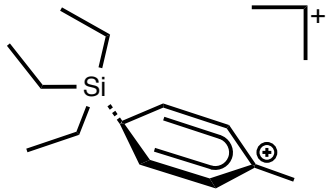
2-1b	$[Et_3Si(C_6H_6)][B(C_6F_5)_4]$	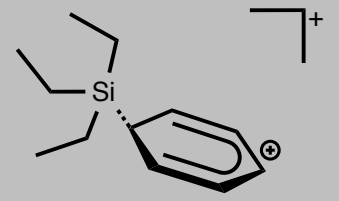
2-1c	$[Et_3Si(C_6H_5Cl)][B(C_6F_5)_4]$	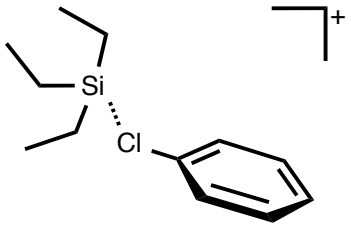
2-2	$[(Et_3Si)_2H][B(C_6F_5)_4]$	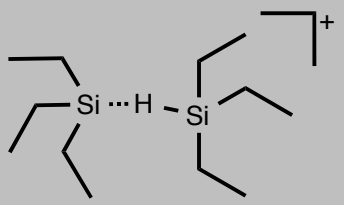
2-3	$F_2B(C_6F_5)$	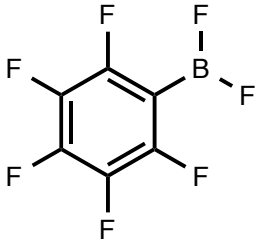

#	Formula	Structure
3-1	(^{tBu}PCP)NiCl	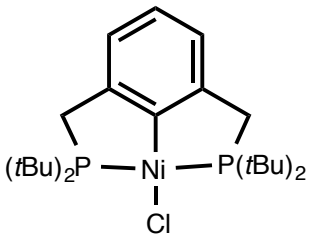
3-2	[(^{tBu}PCP)Ni(H_2)][$B(C_6F_5)_4$]	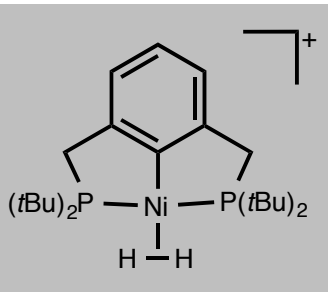
3-3	(^{tBu}POCOP)NiCl	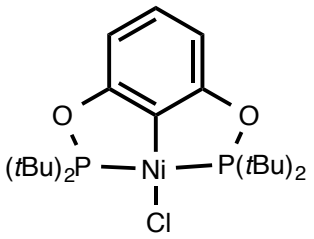
3-4	[(^{tBu}POCOP)Ni][$B(C_6F_5)_4$]	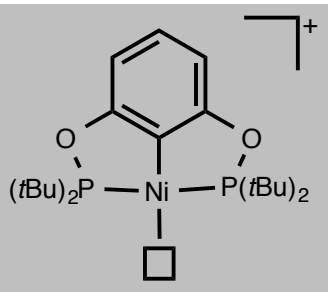
3-5	[(^{tBu}POCOP)Ni(H_2)][$B(C_6F_5)_4$]	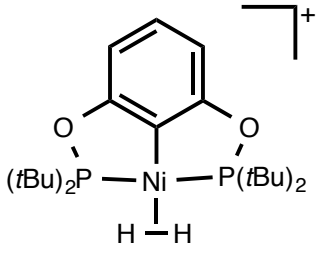

#	Formula	Structure
4-1	(^{tBu}PCP)NiH	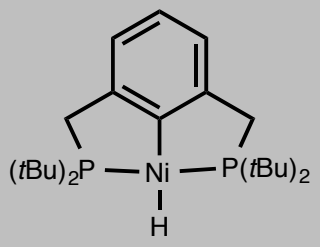
4-2	[(^{tBu}PCP)Ni(N_2)][$B(C_6F_5)_4$]	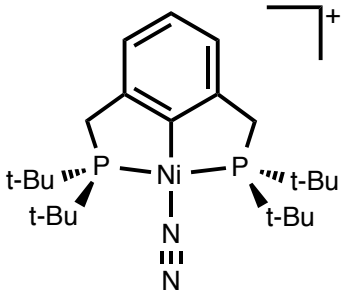
4-3	[(^{tBu}POCOP)Ni(N_2)][$B(C_6F_5)_4$]	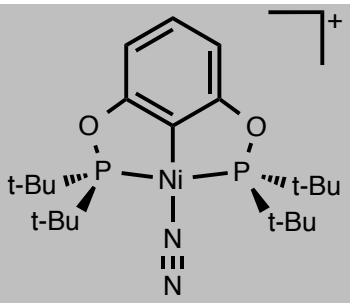
4-4	[(^{tBu}PCP)Ni(CO)][$B(C_6F_5)_4$]	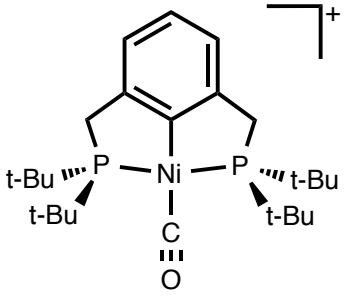

#	Formula	Structure
5-1	(^{tBu}PCP)PdCl	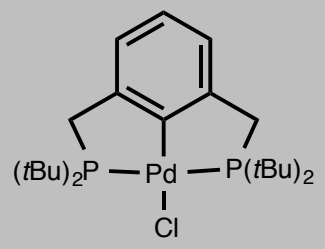
5-2	[(^{tBu}PCP-H)PdCl][$B(C_6F_5)_4$]	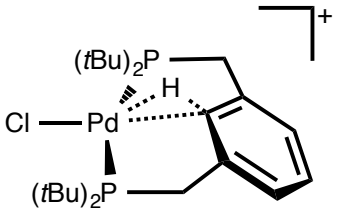
5-3	[(^{tBu}PCP)Pd(H_2)][$B(C_6F_5)_4$]	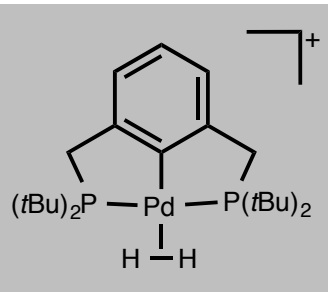
5-3b	[(^{tBu}PCP-H)PdH][$B(C_6F_5)_4$]	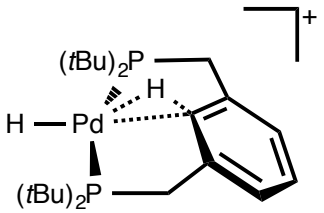

A.3 List of Figures.

Chapter 1.

Chapter 2.

Chapter 3.

Chapter 4.

Chapter 5.

A.4 List of Schemes.

Chapter 2.

Chapter 3.

Chapter 4.

Chapter 5.

A.5 List of Tables.

Chapter 2.

Chapter 3.

Chapter 5.

Bibliography.

Atta-ur-Rahman and Muhammad Iqbal Choudhary. *Solving Problems with NMR Spectroscopy.* San Diego, CA: Academic Press, 1996.

Auner, Norbert and Johann Weis, eds. *Organosilicon Chemistry, From Molecules to Materials.* Weinhem: VCH, 1994.

Bakhmutov, Vladimir. *Practical NMR Relaxation for Chemists.* West Sussex, UK: John Wiley & Sons, Ltd., 2004.

Becker, Edwin. *High Resolution NMR: Theory and Chemical Applications*. New York, NY: Academic Press, 1980.

Crabtree, Robert. *The Organometallic Chemistry of the Transition Metals*, 4th Ed. Hoboken, NJ: John Wiley & Sons, Inc., 2005.

Drago, Russel S. *Physical Methods in Chemistry.* Philadelphia, PA: W. B. Saunders Co., 1977.

Fitzgerald, John J., ed. *Solid-State NMR Spectroscopy of Inorganic Materials*, Chapters 1, 11-12. Washingon, D.C.: ACS Symposium Series, Oxford University Press, 1999.

Greenwood, N. N. and A. Earnshaw. *Chemistry of the Elements,* 2nd ed. Oxford, UK: Elsevier, 1997.

Harris, Robin K. and Brian E. Mann. *NMR and the Periodic Table*, London, UK: Academic Press, Inc., 1978.

Jacobsen, Neil E. *NMR Spectroscopy Explained: Simplified Theory, Applications, and Examples for Organic Chemistry and Structural Biology.* Hoboken, NJ: John Wiley & Sons, Inc., 2007.

Kubas, Gregory. *Metal Dihydrogen and σ-Bond Complexes: Structure, Theory, & Reactivity*. Springer, 2001.

Lewis, J. and R. G. Wilkins, eds. *Modern Coordination Chemistry.* New York, NY, Interscience Publishers, Inc., 1960.

Platz, Mattew S. and Robert A. Moss and Maitland Jones, Jr., eds. *Reviews of Reactive Intermediate Chemistry*. Hoboken, NJ: John Wiley & Sons, Inc., 2007.

Rovnyak, David and Robert Stockland, Jr., eds. *Modern NMR Spectroscopy in Education*, Washington D.C.: ACS Symposium Series, Oxford University Press, 2007.

Shriver, D. F. and M. A. Drezdzon. *The Manipulation of Air-Sensitive Compounds,* 2nd Ed. New York: John Wiley & Sons, 1986.

Vita.

Samantha Jo Connelly was born in Litchfield, Illinois in July 1987 to parents Becky and Gary Connelly. She attended school in Grinnell, Iowa, where she was a member of Grinnell Community Senior High School's Class of 2005. Her undergraduate degree was earned at the University of Iowa in Iowa City, Iowa in May 2009. While there, she studied lanthanide cluster chemistry in the laboratory of Professor Lou Messerle and received her Bachelor of Science degree with Honors in Chemistry. Her most recent work has been under the direction of Professor D. Michael Heinekey at the University of Washington.